# THE STRENGTH OF AGGREGATES FORMED IN FLOCCULATION

A thesis submitted for the degree of
Doctor of Philosophy in the University of London

by

DONALD KENNETH WELDON SMITH

Imperial College of Science and Technology
London S.W.7.

November 1977

## ABSTRACT

The strength of aggregates formed in flocculating suspensions has been investigated. The main factors which control the size to which flocs can grow and remain stable are the strength of the particle — particle bonds and the hydrodynamic conditions to which the flocs are subjected. These factors have been studied separately.

The force of adhesion of spherical glass beads to silica plates in solutions of electrolytes and polymeric flocculants has been measured by gravitational, hydraulic and centrifugal methods. Electrolyte and flocculant concentrations, pH, time and particle size were all found to influence the strength of the particle — particle bonds.

A study of the properties of flocs formed from microscopic glass beads under dynamic conditions has been made using the conventional water treatment "jar test" and with a specially constructed rotating concentric cylinder apparatus to produce well-defined Couette flow. Measurements of floc size distributions were made during floc formation and subsequently during break-down when the shear-rate was increased. The strength of flocs, as indicated by their average size, was found to correlate well with the results for the effect of electrolyte and flocculant concentration on the strength of the inter-particle bond. However, the resistance of the flocs to break-down upon shearing was found to decrease with time, contrary to the adhesion results, indicating the importance of re-formation of bonds in determining the dynamic strength of flocs. For conditions under which floc break-down could be measured, the average floc size was found to depend on the inverse 0.2 power of shear-rate. This result is a lower dependence on shear-rate than has been found for electrolytically coagulating systems and than predicted by a current theoretical model of floc strength.

## ACKNOWLEDGEMENTS

I would like to express my sincere thanks to my supervisor, Dr. J.A. Kitchener, for his encouragement and guidance throughout the course of this work.

The granting of leave of absence and financial assistance by provision of a Study Award by the New Zealand Department of Scientific and Industrial Research is gratefully acknowledged.

I am also grateful to Dr. Jameson for his helpful discussions on hydrodynamics and to all the members of staff of the Department of Mineral Resources Engineering for the generous assistance they have given me.

Finally, I want to give my thanks to all who have helped me during the preparation of this work, especially my wife, Janet, for all her support and patience.

# LIST OF CONTENTS


| | Page |
|---|---|
| ABSTRACT | 1 |
| ACKNOWLEDGEMENTS | 2 |
| LIST OF CONTENTS | 3-5 |
| LIST OF FIGURES | 6-10 |
| LIST OF TABLES | 11-12 |
| LIST OF SYMBOLS USED | 13-15 |
| CHAPTER 1 Flocculation | 16-27 |
| 1.1. Introduction | 16-17 |
| 1.2. Development of the Current Flocculation Model | 17-20 |
| 1.3. The Nature of Modern Flocculants | 20-22 |
| 1.4. Principles of Action | 22-24 |
| 1.5. Characteristics of Flocculation | 24-26 |
| 1.6. Aims of the Project | 26-27 |
| CHAPTER 2 Adhesion | 28-42 |
| 2.1. Introduction | 28 |
| 2.2. Theoretical Considerations | 28-29 |
| 2.3. The Forces Involved in Adhesion | 29-33 |
| 2.4. The Measurement of Adhesive Forces | 33 |
| 2.5. Experimental Studies of Cohesion | 33-34 |
| 2.6. Experimental Studies of Adhesion | 34-40 |
| 2.7. Interpretation of Results | 40-42 |
| CHAPTER 3 Experimental - Adhesion | 43-53 |
| 3.1. Materials | 43-46 |
| 3.2. Detachment of Particles by the Force of Gravity | 46-47 |
| 3.3. Detachment by Hydrodynamic Forces | 48-49 |
| 3.4. Detachment by Centrifugal Force | 49-53 |

| | Page |
|---|---|
| CHAPTER 4 Results and Discussion - Adhesion | 54-71 |
| 4.1. Conditions for Flocculation | 54-55 |
| 4.2. Inversion Experiments: Results | 55-57 |
| 4.3. Flow-through Experiments: Results | 57-59 |
| 4.4. Centrifugal Experiments: Results | 59-67 |
| 4.5. Discussion | 68-71 |
| CHAPTER 5 Hydrodynamics and Floc Models | 72-91 |
| 5.1. Introduction | 72 |
| 5.2. Simple Flow Fields | 73-75 |
| 5.3. Fluid Flow Between Rotating Concentric Cylinders | 75-79 |
| 5.4. Particle Behaviour in Couette Flow | 79-84 |
| 5.5. Floc Models | 84-90 |
| 5.6. Conclusions | 90-91 |
| CHAPTER 6 Experimental - Floc Properties | 92-105 |
| 6.1. Materials | 92 |
| 6.2. "Jar Tests" | 92-94 |
| 6.3. Rotating Concentric Cylinder Apparatus | 94-105 |
| CHAPTER 7 Results and Discussion - Floc Properties | 106-137 |
| 7.1. Jar Tests: Results | 106-111 |
| 7.2. Rotating Concentric Cylinder Apparatus: Results | 111-125 |
| 7.3. Discussion | 125-137 |
| CHAPTER 8 Conclusions | 138-141 |
| CHAPTER 9 References | 141-149 |
| APPENDICES | |
| I The Forces Acting on a Bead in the Inversion Experiments | 150 |
| II The Hydrodynamic Force Acting on a Bead in the Flow-through Experiments | 151-153 |
| III The Force Acting on a Bead being detached by the Centrifugal Method | 154-155 |

Page

IV Adsorption of Polyacrylamide onto Glass Surfaces 156-158

V Tables of Results 159-183

a) Inversion experiments 159-160

b) Flow-through experiments 161-165

c) Centrifugal experiments 166-170

d) Rotating cylinder experiments 171-183

# LIST OF FIGURES


| | | Page |
|---|---|---|
| Figure 1 | Representations of Bridging Flocculation | 19 |
| Figure 2 | The Forces Acting on a Particle on an Inclined Plane | 35 |
| Figure 3 | The Forces Acting on a Sphere at Rest on the Surface in a Boundary Layer | 37 |
| Figure 4 | The Forces Acting on a Sphere Using the "Gravity Method" | 38 |
| Figure 5 | The Forces Acting on a Particle Attached to a Substrate Undergoing Centrifugal Rotation | 40 |
| Figure 6 | Photograph of the Surface of a Ballotini Bead taken by Scanning Electron Microscopy | 45 |
| Figure 7 | Design of the Cartridge used in the Centrifugal Experiments | 50 |
| Figure 8 | Inversion experiments - effect of $MgSO_4$ concentration on the adhesion of 10 $\mu m$ diameter beads | 56 |
| Figure 9 | Inversion experiments - effect of $MgSO_4$ concentration on the adhesion of 30 $\mu m$ diameter beads | 58 |
| Figure 10 | Flow-through experiments - effect of flowrate on adhesion with 0.5 mM $MgSO_4$ at pH 7 | 60 |
| Figure 11 | Flow-through experiments - effect of flowrate on adhesion with 0.5 mM $MgSO_4$ at pH 10 | 61 |
| Figure 12 | Flow-through experiments - effect of flowrate on adhesion with 0.5 p.p.m. Magnafloc 292 at pH 7 | 62 |

| | | Page |
|---|---|---|
| Figure 13 | Centrifugal experiments - water deposition - effect of flocculant concentration on adhesion | 64 |
| Figure 14 | Centrifugal experiments - water deposition - effect of time on adhesion | 65 |
| Figure 15 | Centrifugal experiments - $MgSO_4$ deposition - effect of flocculant concentration on adhesion | 66 |
| Figure 16 | Centrifugal experiments - $MgSO_4$ deposition - effect of time on adhesion | 67 |
| Figure 17 | Couette Flow | 73 |
| Figure 18 | Hyperbolic Flow | 74 |
| Figure 19 | Poiseuille Flow | 75 |
| Figure 20 | Flow Between Rotating Concentric Cylinders | 76 |
| Figure 21 | Transition Reynolds Numbers for the Outer Cylinder Rotating | 78 |
| Figure 22 | Relative Orientations of an Ellipsoid with respect to a Flow Field | 79 |
| Figure 23 | The Stresses Acting on each of the four Quadrants of a Sphere in Couette Flow | 81 |
| Figure 24 | Diagram of horizontal concentric rotating cylinder apparatus | 96 |
| Figure 25 | Photograph of dye test on concentric cylinder apparatus | 98 |
| Figure 26 | Photographs of the distribution of beads caused by secondary flows | 100 |

| | | Page |
|---|---|---|
| Figure 27 | Photograph of rotating cylinder apparatus and ancillary equipment | 102 |
| Figure 28 | Jar Tests - effect of flocculant concentration on floc size | 107 |
| Figure 29 | Jar Tests - effect of $MgSO_4$ concentration on floc size | 107 |
| Figure 30 | Jar Tests - effect of pH on floc size | 108 |
| Figure 31 | Jar Tests - effect of flocculant concentration on floc size at a high $MgSO_4$ concentration | 108 |
| Figure 32 | Jar Tests - effect of bead concentration on floc size | 109 |
| Figure 33 | Jar Tests - effect of bead size on floc size | 109 |
| Figure 34 | Jar Tests - effect of delayed stirring on floc size | 110 |
| Figure 35 | Rotating cylinder experiments - floc formation with 4mM $MgSO_4$ and 2.5 p.p.m. BTI A140 | 112 |
| Figure 36 | Rotating cylinder experiments - floc formation with 4mM $MgSO_4$ and 5 p.p.m. BTI A140 | 113 |
| Figure 37 | Rotating cylinder experiments - floc formation with 6mM $MgSO_4$ and 5 p.p.m. BTI A140 | 114 |
| Figure 38 | Rotating cylinder experiments - floc formation with 8mM $MgSO_4$ and 2.5 p.p.m. BTI A140 | 115 |
| Figure 39 | Rotating cylinder experiments - floc formation with 8mM $MgSO_4$ and 5 p.p.m. BTI A140 | 116 |

| | | Page |
|---|---|---|
| Figure 40 | Rotating cylinder experiments - floc formation with 16mM $MgSO_4$ and 2.5 p.p.m. BTI A140 | 117 |
| Figure 41 | Rotating cylinder experiments - floc break-down with 6mM $MgSO_4$ and 5 p.p.m. BTI A140 | 120 |
| Figure 42 | Rotating cylinder experiments - floc break-down with 8mM $MgSO_4$ and 5 p.p.m. BTI A140 | 121 |
| Figure 43 | Rotating cylinder experiments - floc break-down with 8mM $MgSO_4$ and 5 p.p.m. BTI A140 | 122 |
| Figure 44 | Rotating cylinder experiments - floc formation with a 0.0625% w/v suspension of beads | 124 |
| Figure 45 | Rotating cylinder experiments - floc break-down with 10-16 μm diameter beads | 126 |
| Figure 46 | Rotating cylinder experiments - floc break-down with 32-45 μm diameter beads | 127 |
| Figure 47 | Rotating cylinder experiments - variation of floc size with particle size and shape | 128 |
| Figure 48 | Rotating cylinder experiments - effect of $MgSO_4$ and flocculant concentration on floc size | 130 |
| Figure 49 | Rotating cylinder experiments - variation of floc size with shear rate | 132 |
| Figure 50 | Rotating cylinder experiments - effect of bead size on floc size | 134 |
| Figure 51 | The forces acting on a bead in the inversion experiments | 150 |
| Figure 52 | The hydrodynamic force acting on a sphere at rest on the surface in Couette flow | 151 |

Page

Figure 53 The velocity profile in the flow between parallel plates 151

Figure 54 The force acting on a bead in the centrifuge experiments 154

Figure 55 Adsorption of polyacrylamide onto Ballotini beads in the rotating cylinder experiments 157

# LIST OF TABLES


| | | Page |
|---|---|---|
| Table 1 | Variation of average equilibrium floc sizes | 119 |
| Table 2 | Inversion experiments - adhesion of 10 μm diameter beads | 159 |
| Table 3 | Inversion experiments - adhesion of 30 μm diameter beads | 160 |
| Table 4 | Flow-through experiments - adhesion of 10 μm diameter beads | 161-162 |
| Table 5 | Flow-through experiments - adhesion of 30 μm diameter beads | 163-164 |
| Table 6 | Flow-through experiments - adhesion with a cationic flocculant | 165 |
| Table 7 | Centrifugal experiments - water deposition | 166-167 |
| Table 8 | Centrifugal experiments - $MgSO_4$ deposition | 168-170 |
| Table 9 | Rotating cylinder experiments - floc formation with 0.125% w/v suspensions of 5-40 μm diameter beads | 171-176 |
| Table 10 | Rotating cylinder experiments - floc break-down with 0.125% w/v suspensions of 5-40 μm diameter beads | 177-179 |
| Table 11 | Rotating cylinder experiments - floc formation with 0.0625% w/v suspensions of 5-40 μm diameter beads | 180 |
| Table 12 | Rotating cylinder experiments - floc break-down with 0.125% w/v suspensions of 10-16 μm diameter beads | 181 |

| | | Page |
|---|---|---|
| Table 13 | Rotating cylinder experiments - floc break-down with 0.125% w/v suspensions of 32-45 μm diameter beads | 182 |
| Table 14 | Rotating cylinder experiments - comparison of floc formation with beads and crushed glass | 183 |

## LIST OF SYMBOLS USED

$a$ = sphere radius

$a_1, a_2$ = radius of spheres 1 and 2

$A$ = Hamaker constant

$A_{12}, A_{132}$ = Hamaker constant for materials 1 and 2 in vacuum and immersed in material 3

$A_p$ = area of paddle blades normal to flow

$b$ = sphere diameter

$b_1, b_2$ = length of principal and secondary axes of a spheroid

$C_d$ = drag coefficient

$d$ = distance between surfaces

$d_{av}, d_{max}$ = average and maximum floc diameter

$F$ = force

$F_A, F_B, F_C, F_G, F_H$ = adhesional, buoyancy, centrifugal, gravitational and hydrodynamic force

$g, \tilde{g}$ = gravitational acceleration, gravitational field vector

$h$ = Planck's constant

$H$ = distance between parallel plates

$j_{11}, j_{12}$ = functions of the spheroidal intergrals $\alpha_1$ and $\alpha_2$

$J$ = perpendicular distance of the tangent plane from a point on a spheroid's surface to the centre

$J_{ij}$ = collision frequency of i and j - type particles

$K$ = constant

$L$ = distance of a particle from the axis of rotation

$m$ = particle mass

$n$ = revolutions per minute

$n_i, n_j, n_k$ = concentration of i, j and k - type particles

$P$ = power transmitted to suspension

$P_l$ = axial force between touching spheres in Couette flow

$P_{rr}$ = radial force on a sphere in Couette flow

$Q$ = flow-rate

$r$ = radial distance

$r_p$ = ratio $b_1/b_2$

$r_e$ = equivalent ellipsoidal ratio

$R_o, R_I$ = radii of outer and inner cylinders

$Re, Re_{trans}$ = Reynolds number, transition Reynolds number

$R_{ij}$ = distance between centres of touching i and j - type particles

$S_{rr}, S_{r\phi}$ = radial and tangential stresses on a sphere in Couette flow

$S_{11}, S_{12}$ = shear stresses on an ellipse in a flow field

$t$ = time

$T_A$ = Taylor number

$U$ = defined by $b_1 b_2^2 \alpha_2$

$U_{disp}$ = dispersion free energy

$\bar{v}$ = velocity field (vector)

$V$ = fluid velocity

$V_A$ = fluid velocity at point a if there was no particle present

$\bar{V}, V_{max}$ = average and maximum fluid velocity

$V_1, V_2, V_3$ = components of velocity at point $(X_1, X_2, X_3)$

$V_p$ = mean paddle velocity

$V_R$ = double-layer repulsion energy

$W$ = power dissipated per unit volume

$x$ = distance

$X_1, X_2, X_3$ = co-ordinates of flow field

$X_1^o, X_2^o, X_3^o$ = co-ordinates of axes of an ellipse

$\alpha_1, \alpha_2$ = polarisability of atoms 1 and 2

$\alpha_1, \alpha_2$ = spheroidal integrals

$\gamma, \gamma_{av}$ = velocity gradient, average velocity gradient

$\epsilon_{1,2,3}$ = permittivity of materials 1, 2 and 3

$\eta$ = fluid viscosity

$\theta_1$ = angle between axes of ellipse and flow field

$\kappa$ = Debye-Huckel parameter

$\nu_{1,2}$ = characteristic absorption frequency of atoms 1 and 2

$\rho, \rho_p, \rho_f$ = density of particle and fluid

$\sigma$ = standard deviation

$\phi$ = angle of inclination

$\phi_{1,2}$ = angles between axes of ellipse and flow field

$\psi_{1,2}$ = effective surface potentials of materials 1 and 2

$\omega, \omega_1^o$ = angular velocity, of rotation of a spheroid about its axis of symmetry

$\Omega_o, \Omega_I$ = angular velocity of outer and inner cylinders

# CHAPTER 1

# FLOCCULATION

## 1.1. Introduction

Flocculation is a process of aggregating finely dispersed material in water to make their removal and any subsequent treatment easier. There has been some indecision over the nomenclature of particle aggregation. The terms "coagulation" and "flocculation" have been used indiscriminantly to describe any process in which particle aggregation was promoted by chemical addition. To clarify the situation, LaMer (1) proposed that the process of particle aggregation caused by reducing the electrical double-layer repulsion, by the addition of electrolytes, be called coagulation and that the process in which long-chain polymers or other macro-molecular substances form "bridges" between particles be called flocculation.

There are, however, substances whose actions may be a combination of both methods (e.g. low molecular weight polymers), but such substances have not been used in this work. Although the above distinction has not received universal usage, it is convenient to use the two terms to distinguish between the two principles of action.

Also, a distinction can be made between the aggregates formed by the two processes. Aggregates formed by electrolytic coagulation (e.g. of mineral slurries) are generally too weak for convenience in de-watering processes. Even in a gently stirred slurry, the "coagula" so found are small. However, flocculants act as adhesives and impart a strength

and elasticity to the aggregates. Therefore "flocs" are larger and mutually adhesive when brought together making handling easier (2-4).

Flocculation finds many uses in modern chemical and mineral industries, both in removing unwanted material from water and in recovering material that might otherwise be lost or have to be recovered by more expensive means. Although flocculation has been recognised for many years, little is known at a fundamental level about the nature of floc formation and, in particular, about the strength of the bonding of particles in flocs. The purpose of the research reported in this thesis is to contribute towards an improved understanding of this phenomenon.

## 1.2. Development of the Current Flocculation Model

Flocculation, or sensitisation as it was then known, was discovered by the early colloid chemists when investigating the "protective" action of hydrophilic colloids about the beginning of the century. It was well known that the addition of substances such as gelatin, proteins and gums, in sufficient quantities, would prevent hydrophobic sols from coagulating (or at least substantially protect them from coagulating electrolytes). However, if the hydrophilic colloid was only added in small quantities, it sometimes flocculated the sols or enhanced their susceptibility to coagulation by electrolytes.

This was easy to understand when the hydrophilic colloid was a polyelectrolyte whose charge was

opposite to that of the hydrophobic sol. Then mutual coagulation would occur or at least the sol would be rendered more easily coagulated by electrolytes. However, examples were known of the sensitisation of sols by hydrophilic colloids of the same charge. It was known that protective colloids were adsorbed by the hydrophobic sols and formed a coating over the surface. Freundlich in 1922 (5) suggested that in sensitisation, the particles of hydrophilic colloid were attached to the surface of the hydrophobic particles but not in sufficient quantities to give complete coverage. It was not, however, until polymer science had developed sufficiently for there to be an understanding of the dimensions of macro-molecules in solution and for the availability of synthetic long-chain polymers of very high molecular weight, that the modern bridging mechanisms of flocculation were formulated.

In 1952 Ruehrwein and Ward (6), when studying the flocculation of clays by "soil conditioners", pointed out that flocculant molecules were often comparable in size to the clay particles. They suggested that as the flocculant was strongly and "irreversibly" adsorbed onto the clay particles, it could form bridges between particles. Their illustration of bridging is shown in figure 1(a).

The next development was made by Michaels in 1954 (7) when investigating the flocculation of soils with polyacrylamides. He pointed out that the form of polyelectrolyte molecules in solution changed with the charge density and emphasised the importance of having a long, flexible polymer chain with a moderate

charge density. He represented the polyelectrolyte molecules as long wavy threads attached at each end to different particles. This concept is shown in figure 1(b).

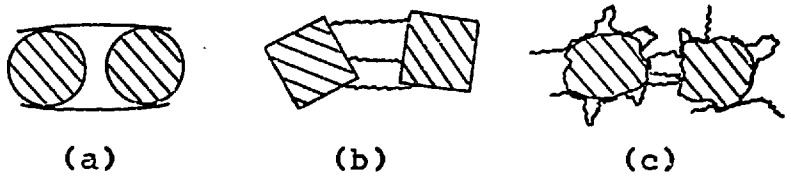



Figure 1. Representations of Bridging Flocculation
a) Ruehrwein and Ward
b) Michaels, and
c) The Current Model

Modern flocculants have very high molecular weights, so even when in the state of a statistical coil they have quite long end-to-end lengths (tenths of a μm). They consist of a large number of monomer units which give them many potential points of attachment to particles. The current concept of polymer adsorption envisages statistically random "loops" as well as end "tails" extending out into solution and being available for bridging. This model is shown in figure 1(c).

The following evidence supports the bridging theory of flocculation:

i) Some non-ionic polymers which act as protection agents if they are of moderate molecular weight, become flocculants at very high molecular weights (e.g. polyethylene oxide).

ii) Flocculation is improved with increasing molecular weight of the flocculant (8)

iii) The calculated end-to-end lengths of the linear flocculants seem long enough to "bridge" the gap between particles even when there is some double-layer repulsion, e.g. some values for $1/\kappa$ for $MgSO_4$ solutions are given below:

| $MgSO_4$ conc. (M) | $10^{-5}$ | $5\times10^{-5}$ | $10^{-4}$ | $5\times10^{-4}$ | $10^{-3}$ | $5\times10^{-3}$ |
|---|---|---|---|---|---|---|
| $1/\kappa$ (nm) | 47 | 21 | 15 | 6.7 | 4.7 | 2.1 |

$\kappa$ is the Debye-Huckel parameter of the solution and has units of reciprocal length. $1/\kappa$ is often considered as indicative of the "thickness" of the double-layer.

iv) Slightly ionized (and therefore expanded) polymers are often more effective than wholely non-ionized ones of the same molecular weight (7).

## 1.3. The Nature of Modern Flocculants

In the 1930's the only application of flocculants was the use of starch in coal preparation and in the early 1950's glue or gelatine was used for treating slurries in South Africa's growing uranium extraction industry. With the growth of the polymer

industry, however, these natural products were supplemented by a wide range of synthetic polymers. Many modern flocculants are based on derivatives of polyacrylamide which is a long-chain polymer that can be produced reproducibly at relatively low cost. Synthetic flocculants have much greater molecular weights (up to $10^7$) than flocculants based on natural products and hence greater chain lengths are available for bridging.

Flocculants are commonly classified according to their ionic characteristics in solution,

a) <u>non-ionic flocculants</u> (or those with only a small proportion of ionic groups present). The most widely used examples of these are:

i) pure polyacrylamide $\left[-\underset{\underset{CONH_2}{|}}{CH} - CH_2-\right]_n$

ii) polyethylene oxide $\left[-CH_2 - CH_2 - O-\right]_n$

iii) polyvinyl alcohol $\left[-CH_2 - \underset{\underset{OH}{|}}{CH}-\right]_n$

b) <u>anionic flocculants</u>. The most common of these is the "partially hydrolysed" polyacrylamide (or copolymer of acrylamide and acrylic acid)

$$\left[-\underset{\underset{CONH_2}{|}}{CH} - CH_2-\right]_x\!\!-\!\!\left[-\underset{\underset{COOH}{|}}{CH} - CH_2-\right]_y$$

The proportion of hydrolysed groups can vary up to 100% (polyacrylic acid) and, of course, this variation greatly alters the flocculant's properties, not only in the groups available for

bonding but also in the configuration the polymer takes in solution, the dimensions expanding to a maximum at fairly high pH ( ∽ 10).

c) cationic flocculants. A great variety of compounds have been developed as cationic flocculants. The three most widely marketed are:

i) polyamines

ii) polythylene imine $\left[-CH_2-CH_2-NH-\right]_n$

iii) products based on copolymers of acrylamide e.g. vinylpyridine and acrylamide.

Some cationic polyelectrolytes of relatively low molecular weight are also widely employed as primary coagulants of clays etc., but this class probably operates by charge neutralisation, not by polymer bridging.

## 1.4. Principles of Action

A review of the principles of action of polymeric flocculants has been made by Kitchener (9). The main points are summarised below:

The simplest form of interaction between a flocculant and a particle would be charge neutralisation, i.e. the flocculation of a negatively charged particle by a cationic polyclectrolyte. This type of interaction, however, even with high molecular weight flocculants, does not promote large floc growth because ionic bonding is very strong and the polymer chains are drawn close to the particle surface, thus reducing the effectiveness of the bridging capabilities of the flocculant.

There are, however, many examples of flocculation by substantially non-ionic flocculants. Fleer and Lyklema (10) used polyvinyl alcohol to flocculate silver iodide sols and Rubio and Kitchener flocculated chrysocolla and malachite with polyethylene oxide (11).

There are also many examples of the adsorption of anionic polyelectrolytes onto negatively charged surfaces. Sarkar and Teot (12) coagulated negatively charged polystyrene latexes with sodium polystyrene sulphonate in the presence of metal ions. O'Gorman and Kitchener (4) were able to flocculate clays with anionic polyacrylamides once the zeta potential had been reduced (but was still negative) by the addition of $MgSO_4$. This type of interaction can promote flocculation because although an individual bond may be weak, multiple attachment of the flocculant to the particle provides a sufficiently strong adsorption and the unattached length of the polymer chain will be free to extend out into the solution, giving a large "bridging distance".

It has been suggested that in the case of clays, that the interaction is between the carboxylate groups and the "positive sites" on the edges of clay platelets formed by aluminium species released from the lattice. Also it has been proposed that there is an interaction between the polymer and the multivalent counterions released from the particles. Similarly, LaMer and Smellie (13) suggested that starches are adsorbed by virtue of their attached phosphate groups. Griot and Kitchener (14) showed that flocculants are capable of adsorption on to silica without intervention of electrostatic bonds and it was concluded that the

formation of hydrogen bonds between the silica and non-ionic polyacrylamide was the principal cause of adsorption. More recently, Rubio and Kitchener (15) have emphasised the additional contribution from hydrophobic association effects in such systems. Evidence included observations of infra-red spectra and the effect of adding "competing" "hydrogen-bond competitors".

## 1.5. Characteristics of Flocculation

Modern synthetic flocculants, because of their high molecular weights, are difficult to dissolve perfectly; considerable time is required to untangle the long chains. On contact with water the grains of flocculant powder swell to form a sticky gel. It is important that strong enough stirring be used to prevent the lumps of gel from sticking together otherwise a large mass may form that would be extremely difficult to dissolve. On the other hand, excessive shearing must be avoided, as it can lead to a break-down of the polymer chain as proved by a fall in the viscosity of highly sheared solutions.

Industrially, the flocculant is usually slowly poured into a vortex created by the stirrer in the flocculant preparation tank or it is added with water through special dispensers supplied by the flocculant manufacturers. For research work, flocculant solutions should be allowed to age for some hours, but long storage is to be avoided because of the possibility of microbial growth.

Two steps are involved in floc formation;

i) diffusion of the flocculant to the particle and its subsequent adsorption onto the surface, and

ii) collisions of the particles resulting in attachment and the build-up of a network of particles to become a floc. The mechanism and kinetics of these processes are difficult to elucidate.

Rapid mixing of the flocculant throughout the suspension to be treated is achieved by the addition of a dilute solution of the flocculant and a period of high-speed stirring. This ensures an even distribution of flocculant throughout the suspension, otherwise zones of "over-dosing" would occur, reducing the efficiency of flocculation. This period of high speed stirring must be short, as excessive stirring at this stage can cause degradation of flocs, possibly with scission of polymer chains.

Once sparse coverage of the particle surfaces by the flocculant has taken place, floc growth from particle collisions will occur by Brownian motion of the colloidal particles. This mechanism of aggregation is called perikinetic flocculation. Collision rates depend only on the temperature and concentration of particles and can be calculated from the classic Smoluchowski theory of coagulation kinetics. Build-up in this way continues until the flocs reach a size at which particle collisions are mainly governed by the hydrodynamic conditions. This is the orthokinetic regime of flocculation. The frequency of orthokinetic particle collisions is a function of the velocity gradient (in fact, it is proportional to it). Hence, the period of rapid mixing is generally followed by

a "conditioning" period of gentle stirring to promote floc growth. The intensity of the stirring is very important at this stage. Increased shearing will result in an increase in particle collisions, but excessive shearing will break flocs.

Thus floc size not only depends on the strength of adsorption of the flocculant to the particle, but also on the hydrodynamic conditions in the pulp. There have been several models of floc structure developed; these are reviewed in Chapter 5.

Suspended solids can be removed from suspension by sedimentation, flotation, sieving, filtration, centrifuging etc. In all these processes flocculation is commonly used to increase particle aggregate size and strength in order to make the operation more efficient and faster. The design of flocculators has developed largely empirically, a particular design being adhered to by a manufacturer because it has been known to "work" in the past, rather than it being designed to fulfil the needs of a well characterised floc. An additional problem is that flocculation is usually carried out as a continuous process whereas the standard water treatment jar test is a batch operation. However, equipment for the laboratory investigation of continuous flocculation is being developed (16).

## 1.6. Aims of the Project

The aim of this study was to investigate the strength of aggregates formed in flocculation. As mentioned earlier, the characteristics of a floc depend on both the strength of the attachment between particles and on the hydrodynamic conditions to which it has

been subjected. It is also recognised that different flocculants, or even one given flocculant in different media, can yield flocs of distinctly different "structure" and mechanical properties.

This study has been approached in two ways. Firstly the strength of the particle-particle bond has been investigated by measuring the force of adhesion of glass beads flocculated to silica plates. The theory of adhesion and a review of the various methods available for making the measurements is presented in Chapter 2. Details of the experimental techniques and the materials used are given in Chapter 3 and the results obtained are listed and discussed in Chapter 4.

The second part of this thesis describes an investigation into the behaviour of flocs when subjected to known shear fields. Chapter 5 reviews the various models proposed of floc structure and growth and the hydrodynamics of the fluid flows that can be used for these studies. A rotating concentric cylinder apparatus designed to produce Couette flow in which to study the behaviour of flocculated glass is described in Chapter 6. The results found are presented and discussed in Chapter 7.

# CHAPTER 2

# ADHESION

## 2.1. Introduction

Measurement of the forces of interaction between small bodies is of prime importance in understanding the behaviour of flocculating systems. This chapter discusses the interaction between small bodies in close contact and describes the various methods for measuring these forces.

In section 2.2. the size and shape of real particles is considered and three model systems for experimental study are mentioned. Section 2.3. discusses the various types of force, both long and short-range, that act on adhering surfaces and the effect of adsorbed molecules is considered.

A review of the many methods developed for measuring these forces of interaction is given in sections 2.4., 2.5., and 2.6. These same methods are suitable for measuring the strength of adhesion of flocculated particles. Section 2.7., discusses the interpretation of adhesion results for non-ideal systems.

## 2.2. Theoretical Considerations

Most particles have complex shapes on a microscopic scale and because surface forces generally have a short "range of action", any interactions between them may be largely confined to those between projecting "peaks". For easier mathematical analysis, these interactions are often approximated by the interaction between a plane surface or between two spheres of equal or unequal radius. Derjaguin(17) developed a theory for the influence of particle form on short-range adhesion

forces for systems in which particle separation is considerably smaller than the size of the particles. He pointed out that if the laws of interaction between parallel plates were known, then the interaction forces between bodies of other geometrical shapes could be calculated. Thus any geometrical model used for an assessment of adhesion can be related to any other. Convenient configurations that have been used experimentally are sphere/plate, sphere/sphere and crossed cylinders.

A convenient size range of particles for study is 1-1000μm diameter. Although the adhesion of particles smaller than this is of interest, very large fields (compared with gravitational forces) are necessary to separate adhering particles. Also, theoretical models are difficult to establish because the particle size may be of the same order as any surface irregularities on the substrate.

For large diameter particles gravitational forces become dominating over any forces of adhesion. However, true adhesional contact may only be made at two or three points of surface irregularity whose diameter is considerably smaller than that of the particle.

## 2.3. The Forces Involved in Adhesion

An extensive review of the theory of adhesion, giving details of the important experimental work up to 1967, has been made by Krupp (18). Kitchener (19) has reviewed the surface forces controlling the deposition of colloidal particles. The forces governing the deposition of small particles are not exactly those required to separate an adhering particle from a

substrate. Once contact has been made, deformation of the particle or substrate may occur, enlargening the interfacial contact area by plastic flow and there is the possibility of chemical bonding or other short-range interactions occurring.

In the absence of adsorbed layers or bridging, the dominating "long range" forces are van der Waals (attractive) forces and (in aqueous media) electrostatic forces (which can be either attractive or repelling).

Van der Waals forces are the fundamental intermolecular attractive forces between small bodies in close contact. Historically two approaches have been used to calculate these forces:

a) The Microscopic Approach of Hamaker (20) uses the interaction between individual atoms (or molecules) and postulates their additivity so that the van der Waals attraction between macroscopic bodies can be calculated by integration over all pairs of atoms in the adjacent bodies. The dispersion free energy between two atoms is given by:

$$U_{disp} = -\frac{3}{2}\frac{h\nu_1\nu_2\alpha_1\alpha_2}{(\nu_1+\nu_2)\ d^6}$$

where $U_{disp}$ = dispersion free energy
$h$ = Planck's constant
$\nu_{1,2}$ = characteristic adsorption frequency of atoms 1 and 2
$\alpha_{1,2}$ = polarisability of atoms 1 and 2
$d$ = gap between atoms.

The van der Waals force between unequal spheres is

$$F = \frac{A_{12}}{6d^2}\left(\frac{a_1\ a_2}{a_1+a_2}\right)$$

where $A_{12}$ = Hamaker constant
$a_1, a_2$ = radii of spheres 1 and 2

For equal spheres this reduces to

$$F = \frac{Aa}{12d^2}$$

The interaction between a sphere and a plate is given by

$$\frac{F}{\text{unit area}} = \frac{Aa}{6d^2}$$

which is twice that between two spheres.

This theory has many short comings especially when predicting the behaviour of dissimilar materials immersed in a liquid. It is now more common to use the second approach if the necessary data are available.

b) The Macroscopic Approach of Lifshitz (21) uses the optical (electromagnetic) properties of interacting macroscopic bodies and calculates their van der Waals attraction from the imaginary parts of their complex dielectric constants. Computation is formidable but approximations are available. Unfortunately, the necessary data are not yet available for all materials.

The Lifshitz expression for the van der Waals force between two spheres of equal size in a third medium

$$F = \frac{ha}{16\pi d^2} \int_0^\infty \left[\frac{\epsilon_1(i\xi)-\epsilon_3(i\xi)}{\epsilon_1(i\xi)+\epsilon_3(i\xi)}\right]\left[\frac{\epsilon_2(i\xi)-\epsilon_3(i\xi)}{\epsilon_2(i\xi)+\epsilon_3(i\xi)}\right] d\xi$$

where $\epsilon_{1,2,3}(i\xi)$ = permittivity of materials 1,2 or 3, a function of the imaginary frequency $i\xi$

This can be related to a Hamaker constant $A_{132}$ for materials 1 and 2 immersed in medium 3 by

$$A_{132} = \frac{3h}{4\pi}\int_0^\infty \left[\frac{\epsilon_1(i\xi)-\epsilon_3(i\xi)}{\epsilon_1(i\xi)+\epsilon_3(i\xi)}\right]\left[\frac{\epsilon_2(i\xi)-\epsilon_3(i\xi)}{\epsilon_2(i\xi)+\epsilon_3(i\xi)}\right] d\xi$$

Electrostatic forces arise from surface charges on the particles - in practice in the form of electrical double layers. These may be attractive if the surfaces are oppositely charged, or repelling if the surfaces have the same sign of charge.

An expression for the double-layer repulsion energy ($V_R$) of two spheres of equal size is

$$V_R = \frac{a\epsilon}{8}\left\{2\psi_1\psi_2 \ln\left[\frac{1+\exp(\kappa d)}{1-\exp(\kappa d)}\right] + (\psi_1^2+\psi_2^2)\ln\left[1-\exp(-2\kappa d)\right]\right\}$$

where $\psi_{1,2}$ = effective surface potential.

The net behaviour of van der Waals and electrical double layer forces has been taken into account in the Derjaguin-Landau-Verwey-Overbeek (DLVO) theory of colloid stability (22). For particles in the size ranges under consideration it is necessary to take into account the retardation effect on the dispersion forces caused at relatively long distances. Approximate corrections are available.

In "clean" systems or systems with only small adsorbed molecules on the surfaces, contact may be sufficiently close for short-range forces to occur. These forces, which are stronger than the van der Waals dispersion forces include hydrogen bonding and the even stronger metallic covalent and ionic bonds. These forces may cause further deformation at the interface, changes which are often slow, so that the strength of adhesion may increase with time.

In many real systems the surfaces of colloidal particles are likely to be contaminated by adsorbed molecules such as surfactants or polymers. It is important to determine the effect that these adsorbed molecules may have on the model adhesion system.

Adsorbed molecules will tend to reduce the adhesion of a particle to a substrate in a number of ways. They may prevent chemical bonding from occurring and any adsorbed layer will affect the van der Waals attraction. In the case of adsorbed macro-molecules the surface separation will be larger, further reducing the van der Waals forces. Adsorbed simple ions will alter the electrical double layer effects. In contrast, the adsorption of a polyelectrolyte in small quantities (as explained in Chapter 1), may allow physical bridging by the molecules between the surfaces. This will provide a new type of attachment, the strength of which is the object of this study.

## 2.4. The Measurement of Adhesive Forces

Many studies have been made of adhesive forces over the past fifty years. Reviews have been given by Böhme et al (23), Krupp (18) and Visser (24). Two approaches have been used - either the cohesion of an ensemble of particles or the adhesion of a single particle to a substrate. The measurement of cohesion will be discussed briefly in section 2.5. and the measurement of adhesion in more detail in section 2.6.

## 2.5. Experimental Studies of Cohesion

Several (non-fundamental) methods have been developed for studying the cohesion of particles. A review of these has been given by Morgan (25) and they are summarised below:

a) Measuring the "angle of repose" of a particle bed.

b) The tensile strength of the particle bed can be measured (26-31).

c) Measuring the minimum aperture size through which an aggregate of particles can pass freely (29,31).

d) Measuring the dispersion of aggregates on impact after a fall from a given height (30).

e) Measuring the dispersion of a particle bed by an air blast (31).

f) Measuring the "internal friction" of a particle bed by using a rotating viscometer (32). (This is not unlike the measurement of the strength of flocculated aggregates described in the second half of this thesis).

g) Measuring the sliding angle of a particle bed over a layer of similar particles deposited on a plane. The plane is tilted and the angle noted (33-4).

Although all these methods give an indication of the relative degree of cohesion, there is no actual measurement of the force of adhesion between particles.

## 2.6. Experimental Studies of Adhesion

This section describes the various methods developed for studying the adhesion of single particles or a number of particles to a substrate. They can be divided into two groups; those experiments which only give an indirect indication of the strength of adhesion and those that give a direct measure of the force necessary to detach a particle normally from a substrate.

Indirect Methods

a) One of the earliest methods used was von Buzagh's method of measuring the angle at which a plane substrate had to be inclined before the majority of the particles adhering to it moved. (35-43). However, what is actually measured is the force ($mg\sin\phi$) required to overcome the sliding friction rather than the force required for normal detachment. (See figure 2)

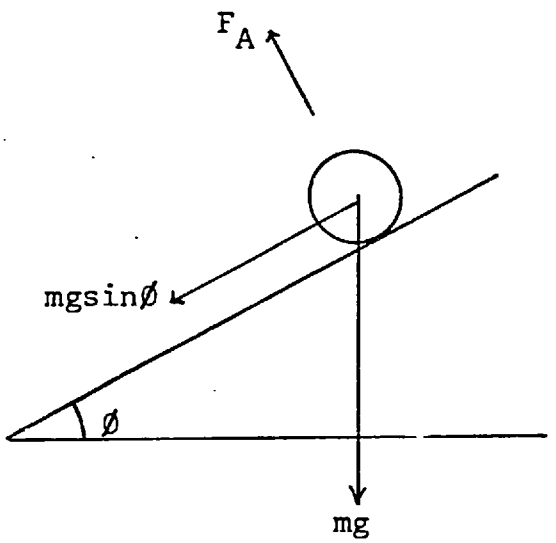



Figure 2 The Forces Acting on a Particle on an Inclined Plane

b) Jordan (43) using a nozzle system measured the adhesion of Quartz and glass particles to a plate as a function of the velocity of an air stream. Gillespie (44) directed an air stream charged with particles towards a cylinder with its axis at right angles to the air current. He determined the

number of adhering particles as a function of their location on the circumference of the cylinder. This type of experiment suffers from the ill-defined aerodynamic conditions, preventing the calculation of the actual forces acting upon the particles. Other examples of this method using air or water streams are given by Larsen, Corn and Silverman and by Zimon (45-7).

c) A "powder bed" method was used by Clayfield and Lumb (48) and Clayfield and Smith (49) to investigate the adhesion of carbon black particles to a packed bed of steel or glass grains. The flow of liquids of different properties through the bed was used to detach the particles. The hydrodynamics of flows through packed beds is complex, hence, the adhesive force could not be calculated directly but a comparison between various sufactants added to the liquid could be made.

d) Another method also using hydrodynamic forces has been developed by Visser (50-1). A turbulent flow of the liquid in the annulus between two concentric cylinders was generated by rotating the inner cylinder. The shearing in the laminar flow of the boundary layer near the cylinder walls was used to detach carbon black and polystyrene particles adhering to a cellophane film attached to the inner cylinder.

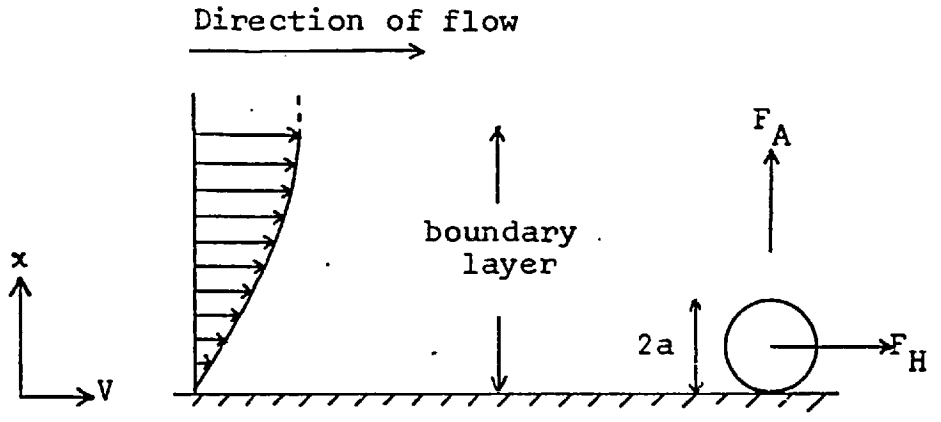



Figure 3. The Forces Acting on a Sphere at Rest on the Surface in a Boundary Layer

As figure 3 shows, the force causing movement is a hydrodynamic force acting horizontally, not a normal force. Visser found an empirical relationship between $F_H$ and $F_A$ by comparing his results with those obtained by a direct centrifugal method for similar particles.

e) Vibration was used by Derjaguin and Zimon (52-3) to measure adhesion. Particles were placed on an acoustic transformer and their separation was measured as a function of the frequency and amplitude of the vibration.

Direct Methods

a) The simplest way to obtain a direct measure of the adhesion of a particle to a substrate is an extension of von Buzagh's sliding angle technique (34). Providing adhesion is strong enough to

prevent sliding, the plane can be slowly inverted, and once the angle of inclination is greater than 90° the force of gravity will act to separate the particles from the substrate. On full inversion to 180° the total weight of the particles will be acting to produce separation and the proportion of particles remaining adhering can be related to the force applied. This is often known as von Buzagh's adhesion number method.

b) A similar method also using gravity as the separating force was used by Stone, Howe et al. and McFarlane and Tabor (54-6).

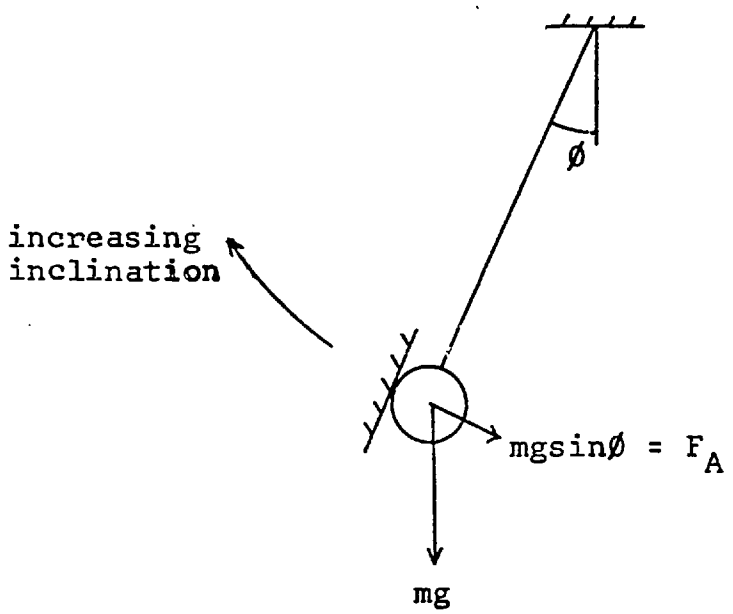



Figure 4. The Forces Acting on a Sphere Using the "Gravity Method"

Figure 4 shows that the component of the force of gravity acting normally from the substrate is mgsinØ. The force increases as the angle of

inclination is increased. This method is only suitable for relatively large particles or weak attachments because very small particles may be retained against their own weight.

c) Bradley (57) used the force supplied by a previously calibrated helical spring to measure the adhesion between two spheres. McFarlane and Tabor (58) suspended a sphere by spring wire and used the deflection of the spring wire to provide the separating force between the sphere and a substrate.

d) The force of adhesion between two crossed filaments has also been measured. When the two filaments are at right angles to each other, this is equivalent to the interaction between a sphere and a plane. Tomlinson (59-60) and Derjaguin et al. (61) measured the deflection of one of the filaments as they were separated from each other. Previous calibrations using weights had been made, hence the force being applied at the moment of separation could be calculated. More recently sensitive microbalances have been used to measure the forces applied as two filaments were separated (62-3).

e) The most widely used method of measuring the force of adhesion is the centrifugal method (23, 52-3, 64-74). The substrate is attached to the rotor of a centrifuge so that it is parallel to the axis of rotation. Upon spinning a centrifugal force will act on the particles adhering to the substrate as is shown in figure 5.

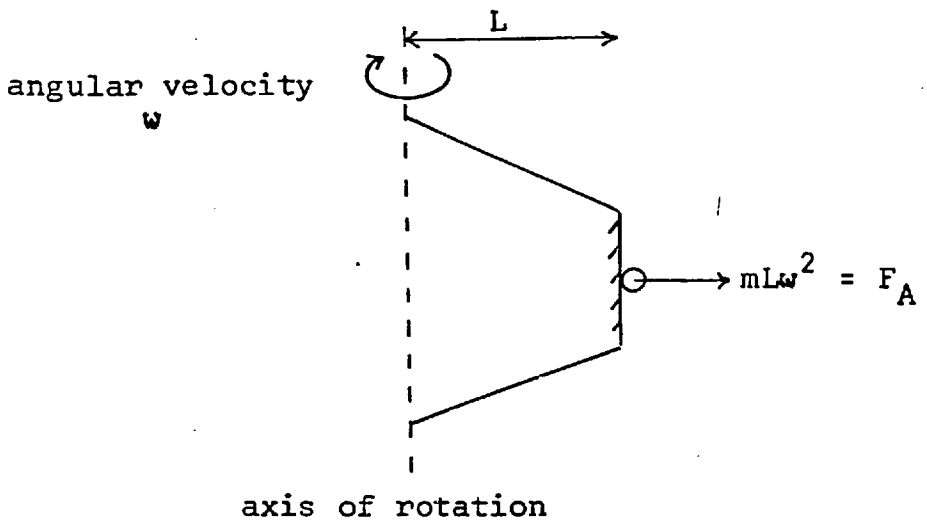



Figure 5. The Centrifugal Force Acting on a Particle Attached to a Substrate Undergoing Centrifugal Rotation

Particles are pre-deposited on a substrate and after photographing or particle counting under a microscope, the substrate is placed in the centrifuge and spun at a determined speed for a given time. Another particle count is made and then the substrate is spun at a higher speed. This treatment is continued until most of the particles have been removed. A graph can then be made of the proportion of particles remaining adhering against the centrifugal force applied. (It is invariably found that there is a wide spread of adhesion values for even a mono-size sample of particles).

This method is suitable for studying adhesion in both a vacuum and in immersed systems and has been extended to very small particles with the use of ultracentrifuges.

## 2.7. Interpretation of Results

The force of adhesion as measured between two spheres or a sphere and a plane substrate is a single result for the two particular sections of surface used. It is important to make a number of measurements and to average them because single results will be influenced by the presence of surface irregularities or contaminants as well as variations in particle size and shape. This also applies for flocculated systems. There may not be an even adsorption coverage of the surfaces and there will be a variation in the strength with which each individual flocculant molecule is attached to the surface.

For the same reasons, when a method is used where the adhesion of a number of particles to a substrate is measured a graph of the proportion of beads remaining (or removed) against the force applied always shows a scatter of results instead of 100% adhesion up to $F_A$ and 0% above it. It is usual to take the force at which 50% of the particles remain adhering as indicative of the average force of adhesion.

It must also be recognised that the contact zones of nominally smooth bodies do not really have the idealised sphere or plane form. There may well be two or three minute areas of contact, and it would be most improbable that all these areas would rupture simultaneously. There seems to be no way of overcoming this imperfection of the experiment. Similarly, the actual rupture of contact may be initiated by uncontrolled vibrations as the conditions of separation are approached.

As the strength of adhesion in flocculated systems was expected to vary greatly with the concentration of flocculant used and with other chemical conditions, three methods of measuring the force of adhesion were chosen that covered a range of magnitudes of applied force. The weakest forces were measured by using a method similar to von Buzagh's adhesion number test (35). The proportion of glass beads deposited on a silica plate that remained attached after inversion was determined. As only a force of one magnitude (that of gravity) could be applied to the attached beads, this method was extended by flowing the flocculating medium past the beads, giving a range of hydrodynamic forces to which the beads could be subjected. An analysis similar to that used by Visser (50) was used to calculate the force acting on the beads. A centrifugal method of detaching the beads was used for the larger forces required at higher flocculant concentrations.

# CHAPTER 3

## EXPERIMENTAL - Adhesion

### 3.1. Materials

Glass was chosen as the material with which to carry out the flocculation experiments because it was possible to obtain commercially, small, perfectly spherical glass beads to small sizes (5μm diameter). The force of gravity acting on beads of this size was sufficiently large to detach weakly adhering beads in the inversion experiments which will be described in the next section. By using polished vitreous silica plates as the substrate, the geometrical requirements for the sphere-plate adhesion model were fulfilled. Silica plates were used because they were available already made up into electrophoresis cells suitable for the inversion and flow-through experiments. (Cells designed for the Rank Brothers Mk III Electrophoresis Apparatus). The Ballotini beads, supplied by Jencons Ltd., consisted of lead glass, of nominal size range 0-60 μm. These were separated into various size fractions by beaker decantation for the smaller sizes and with a "Cyclosizer" ( a set of reverse-flow hydrocyclones) for the larger sizes. After fractionation the beads were prepared for use by leaching in 30% HCl overnight and rinsing thoroughly in doubly-distilled water. This treatment would remove calcium salts (from the water) and other cations from the glass. Acid-leached glass is known to have surface properties very similar to those of vitreous silica (e.g. similar zeta-potential values). The beads were dried at 105°C until they formed a free-running powder and were stored in air-tight containers until use.

In certain experiments where angular particles were required, lead glass was crushed with a porcelain mortar and pestle and sieved to < 100 μm. The product

was then acid-leached and rinsed in the same way as the beads prior to use.

The "plane" surfaces used for model adhesion investigations were obtained from polished silica plates. These were used in a number of experiments and were cleaned before re-use by treatment with ethanol and concentrated $HNO_3$ to remove organic contamination and rinsed with doubly-distilled water.

Under an ordinary optical microscope, the Ballotini beads appeared to be perfectly spherical and their surfaces smooth. The surfaces were further studied by scanning electron microscopy and were found to be covered by circular irregularities of approximately 0.3 μm diameter and estimated height or depth 0.1 μm (see figure 6). The surface of polished silica also contains regular depressions of approximately 300Å diameter and 30Å depth (75). These departures rrom geometrical smooth form are inescapable (at some level or other) and they probably have a profound influence on the adhesion characteristics.

The flocculants used were Magnafloc 292, a cationic polyacrylamide type flocculant supplied by Allied Colloids Ltd., and a range of anionic polyacrylamide type flocculants with varying degrees of hydrolysis supplied by BTI (Bradford) Ltd., (now Cyanamid) under the trade name BTI. 0.1% w/v solutions of the flocculants were prepared weekly, any unused solutions being discarded because of the danger of microbial growth. The freshly mixed solutions were left standing for a few hours and filtered before use and a small amount was diluted, if necessary, immediately prior to use.

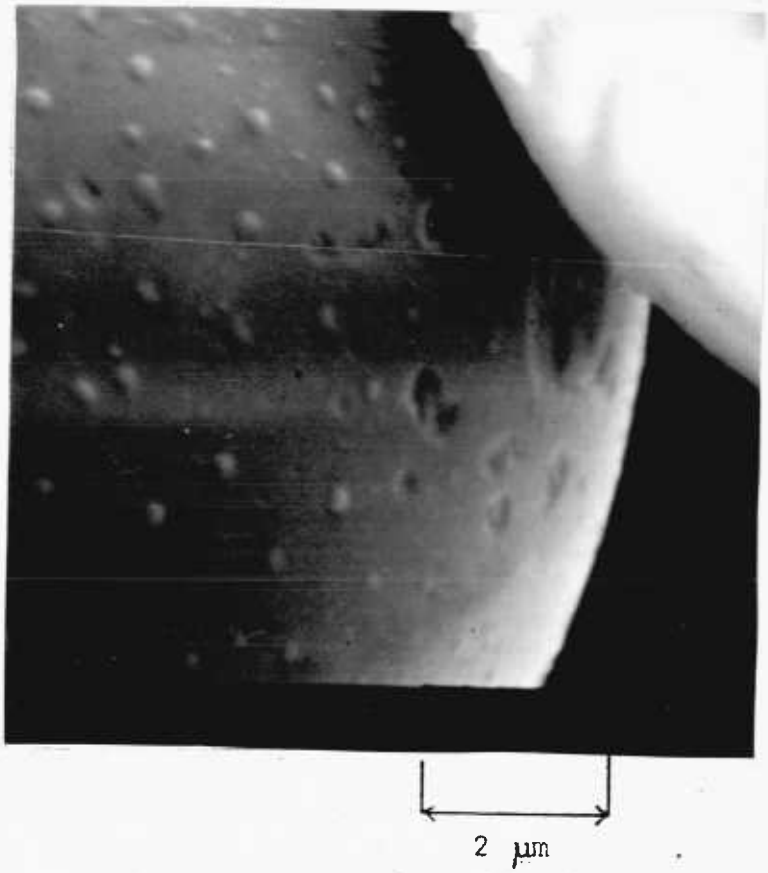



Figure 6 Photograph of the Surface of a Ballotini Bead taken by Scanning Electron Microscopy

The water used in all experiments was double distilled. The second distillation was carried out in an all glass still sealed from the atmosphere after the water had been passed through both an ion-exchange resin and a bed of activated carbon. Any necessary pH adjustments were made with "Analar" HCl or NaOH.

The primary coagulant used (essentially to reduce electrical double layer repulsion) was $MgSO_4$. Stock solutions of 0.15M were prepared and any required dilution was made before each experiment.

3.2. Detachment of Particles by the Force of Gravity (inversion experiments)

This method was similar to von Buzagh's adhesion number experiments (35) in which particles were deposited on a plane surface which was then carefully inverted and the proportion of particles remaining determined. This technique was used for the systems showing the weakest forces (electrolytic coagulation or very low concentrations of flocculant). Two size grades of beads were used in these experiments, average diameters of 10 μm and 30 μm giving forces of gravity of 7pN and 200pN. (See appendix I).

The interior walls of a spectrophotometer cell were used as the substrate. The cell was made of polished vitreous silica and measured 10mm x 1mm in internal cross sectional area and was 35mm long. Prior to each experiment, the cell was cleaned with ethanol and concentrated $HNO_3$ and rinsed thoroughly with distilled water. The cell was mounted on a block of wood which firmly held it so that the surface being used was horizontal and could be positioned under a microscope for counting the number of beads.

A 0.5% w/v suspension of beads was prepared with water previously adjusted to the required pH. 50ml of the suspension was poured into a measuring cylinder and the necessary quantity of $MgSO_4$ added. After gentle inversion of the measuring cylinder to mix in the $MgSO_4$, the coagulating suspension was poured into the cell which was stoppered and laid on its side so that the 35mm x 10mm surfaces were horizontal. The beads were left for 15 minutes to settle and attach firmly before counting them under the microscope.

One eyepiece had a graticule with a grid pattern on it. This was used to help count the number of beads in eight fields of view to give at least 500 beads in all. The cell was then gently inverted and left for a further 15 minutes before counting again in a similar fashion, the number remaining adhering to the face (now upper-most). The proportion of beads remaining adhering could then be calculated.

In the experiments in which a flocculant was used, the bead suspension (with added $MgSO_4$, if any) was gently mixed by inversion for one minute before adding the flocculant. The same adhesion number procedure was then followed.

It was thought that there was a possibility of the beads being removed by slippage as the angle of inclination passed through angles near $90^{\circ}$ rather than by a detachment normal to the surface. In certain experiments the beads were observed as the cell was inverted and although some slippage did occur, most of the beads that were removed were detached as the angle of inclination passed through the range $120^{\circ}$-$150^{\circ}$.

3.3. Detachment by Hydrodynamic Forces (flow-through experiments)

To extend the range of forces to which each bead could be subjected, the cell was connected to ancillary glassware which permitted the supernatant water to flow through the cell at a controlled rate. The flow was controlled by a Teflon stopcock and was uniform. As the glassware immediately up-stream from the plane surfaces of the cell was a smooth cone of decreasing size and the maximum Reynolds number was approximately 50 (see Appendix II), flow was assumed to be laminar. Thus the beads deposited on the surface were subjected to a horizontal shearing force rather than a normal force, which can be calculated from Goldman et al (76) and O'Neil's (77) equation for the force acting on a sphere at rest on the surface in laminar flow

$$F_H = 1.7 \times 6\pi\eta a V_a$$

where $\eta$ = the fluid viscosity

$a$ = the sphere radius

and $V_a$ = the velocity the fluid would have at the sphere centre if the sphere was not there.

The experimental procedure was very similar to that used in the inversion experiments. The beads were deposited on the cell wall in exactly the same way and during the 15 minute interval before counting, the cell was connected to the ancillary flow glassware which was filled with supernatant water prepared with the same concentration of beads and flocculant as for the main experiment. After initial counting, the flow was started and a count made after 5 minutes. The flow-rate was then increased and a further count made after 5 minutes. This procedure was repeated until most of the beads had been removed.

Because there was a danger that bead detachment might sometimes occur by an already moving bead colliding

with another, some experiments were observed as the flow was increased. It was found that detachment first occurred by a bead rolling along the surface and becoming suspended in the flow and being swept away so that collisions were negligible. As the bead rolled, it may have trapped water layers under it, causing it to rise in this way from the surface.

The range of flow-rates used was 0.01 - 0.5 ml/sec giving a range of hydrodynamic forces and moments about the point of contact of 4.8pN - 240pN and $0.024 - 1.2 \times 10^{-12}$ N-m for a 10 μm diameter bead and 4.32pN - 2.16nN and $0.648 - 32.4 \times 10^{-12}$ N-m for a 30 μm diameter bead.

3.4. Detachment by Centrifugal Force (centrifugal experiments)

To further extend the range of forces available for normal detachment of the beads from a silica plate, a centrifugal method was chosen. Special cartridges which held 1 cm diameter disks cut from a polished silica plate in contact with the flocculating medium were designed to fit the laboratory centrifuge. A special bath was also constructed in which to carry out the deposition of the beads onto the disks.

A diagram of a cartridge is given in figure 7. All the components except the disk and seals were machined from brass. The silica disk was held in place in the base by a brass plug and rubber washer. The top surface of the plug was painted black and had a cross scratched into it. This provided a matt background and a reference point for counting the beads. A cover could be placed over the base during flocculant addition. A lid shaped to fit a centrifuge bucket

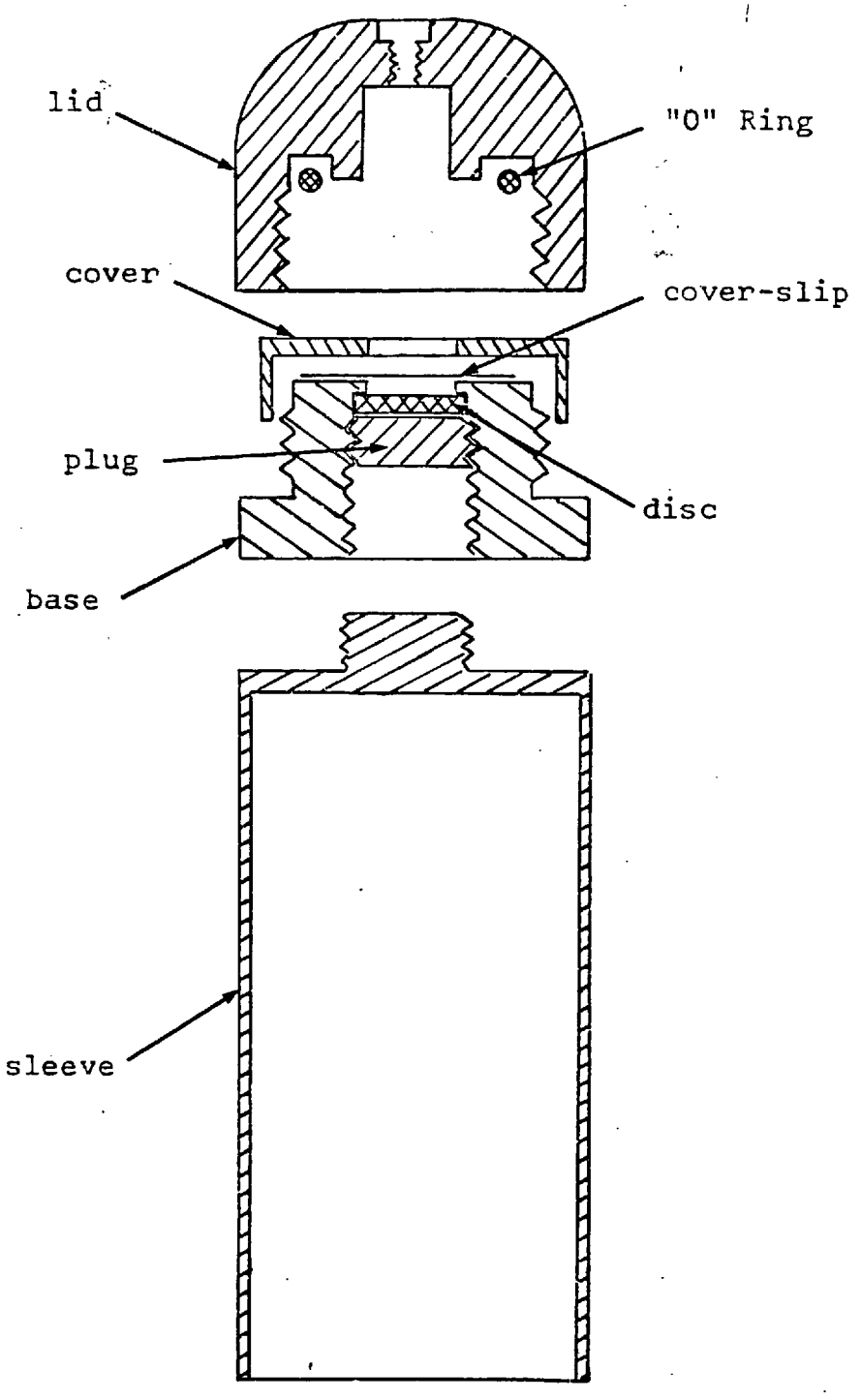



Figure 7 Design of the Cartridge used in the Centrifugal Experiments

could be screwed onto the base and was sealed in place by a rubber O-ring. The lid contained a cavity in which the flocculating medium could be contained in contact with the beads on the disk. A sleeve was screwed into the bottom of the base to prevent the cartridge twisting during spinning.

The bath, which had a volume of 1200 ml, was constructed from Perspex. It held up to four bases at once on brass pins which fitted into slots in the bases, keeping them horizontal. The bath was positioned over a magnetic stirrer and the solutions in it were stirred with a Teflon coated magnetic follower.

The centrifuge employed was a MSE "Super Major" laboratory centrifuge and had a maximum speed of 3600 rpm. An expanded scale voltmeter was connected in series with the centrifuge motor and was calibrated against the drum speed, with the aid of a tachometer.

The distance from the drum axis to the position of the disk during spinning was 20.5 cm, giving a maximum centrifugal field on a bead of 3000 x "g". (Appendix III). With a minimum speed of 500 rpm and a maximum speed of 3600 rpm the range of net forces acting on a 20 μm diameter glass bead in water was 3.53nN to 183nN.

An experiment was commenced by filling the bath with distilled water adjusted to the required pH and with the appropriate quantity, if any, of $MgSO_4$. The bases

containing freshly cleaned disks were placed in the bath, using specially modified tongs. A microscope coverslip was placed on top of each base. The stirrer was set at a high speed (not high enough to create a vortex) and 0.1 g of beads were added. Stirring was continued for one minute and then, 30 seconds after stirring had stopped, the coverslips were removed and the beads allowed to settle for 20 minutes. The covers were then placed on the bases and coverslips on top of them and the solution was drained off and replaced with the flocculating solution. Low speed stirring was commenced and the coverslips were removed. In a test to determine whether flocculant could diffuse to the disk surface, a crystal of $KMnO_4$ was placed on a disk in identical conditions and the immediate steady appearance of colour observed as an indication that diffusion from and hence to the surface could occur.

Stirring continued for 20 minutes, after which the covers were removed, the coverslips replaced and the bath drained so that the bases could be removed to count the beads under the microscope. After counting, the bases were returned to the bath with the flocculating solution to have the lids of the cells fitted. The whole unit was then withdrawn from the bath, the sleeve was screwed on and the cartridge was placed in a centrifuge bucket and spun at the required speed for 15 minutes.

In these experiments, adhesion was strong, so that beads did not slip off during the preparation, or during the acceleration or slowing of the cartridge.

After spinning, the unit was returned to the bath (still upside down) and the top was unscrewed, taking

with it any removed beads. The base was re-inverted for counting. This process was repeated at progressively higher speeds until most of the beads had been removed.

Only one count was made for each disk, but by using the etched lines in the background, the same area could be counted each time. Each area contained at least 150 beads. All experiments were performed in duplicate.

# CHAPTER 4
# RESULTS AND DISCUSSION - Adhesion

## 4.1. Conditions for Flocculation

Initially a range of flocculants and chemical conditions were "screened" to determine the best conditions for obtaining a range of strengths of flocculation. These simple tests were carried out in 50ml measuring cylinders using crushed glass powder; the appearance of any flocs formed, the speed with which they settled and the clarity of the supernatant liquor was noted.

As expected, flocculation of the (negatively charged) glass particles was obtained with certain cationic flocculants. Magnafloc 292 was chosen for further study as it appeared to be the most effective. At pH 7 there was no apparent flocculation when 1 p.p.m. Magnafloc 292 was used; but at 5 p.p.m. very finely-divided weak flocs were formed which left a hazy supernatant. At 10 p.p.m. concentration however, small rapidly settling, flocs were obtained which left a clear supernatant. The same behaviour was found at pH 4 and pH 10.

As this type of flocculation was not expected to produce large, cohesive, elastic flocs (because flocculant chains will be strongly attracted to the particle surface, rather than being available for long inter-particle bridging), it was decided to investigate also the possible flocculation with anionic flocculants. Flocculation could be obtained with various anionic polyacrylamide flocculants providing the electrical double-layer repulsion had been reduced by the addition of $MgSO_4$, and the pH adjusted to 9.5 or beyond. At

pH 10, flocculation was just discernable when the $MgSO_4$ concentration was .4mM and 10 p.p.m. BTI A140 was used (where 1mM means $10^{-3}$ moles per litre). As the $MgSO_4$ concentration was increased to 8mM and beyond flocculation improved, the flocs becoming larger and the supernatant clearer. O'Gorman and Kitchener (4) similarly found optimum flocculation of a negative layer with 5 mM $MgSO_4$ and BTI A130. With 8mM $MgSO_4$ at pH 10 flocculation was observed at 5 p.p.m. flocculant doses, but it was considerably better at 10 p.p.m. and 20 p.p.m. However, at doses of 30 p.p.m. or above, the clarity of the supernatant was reduced, indicating that "overdosing" was occurring. The pH was not increased past 10.5 because of the probability of $Mg(OH)_2$ precipitating.

## 4.2. Inversion Experiments: Results

The results obtained for the adhesion of beads with an average diameter of 10 μm in $MgSO_4$ solutions are given in table 2 and are plotted in figure 8. At $MgSO_4$ concentrations below 0.025mM, no adhesion was detected and at concentrations above 2.0mM there was no detachment of the beads upon inversion.

Taking the value at which 50% of the beads were removed as indicative of the mean force of adhesion, then the force of adhesion of 10 μm diameter beads to the cell in 0.2mM $MgSO_4$ was 7.7pN.

When 10 p.p.m. BTI A140 flocculant was used at pH 10 the adhesion at 0.1mM $MgSO_4$ increased slightly from 33% to 45% and at 0.5mM $MgSO_4$ adhesion increased so that no beads at all were removed. At $MgSO_4$

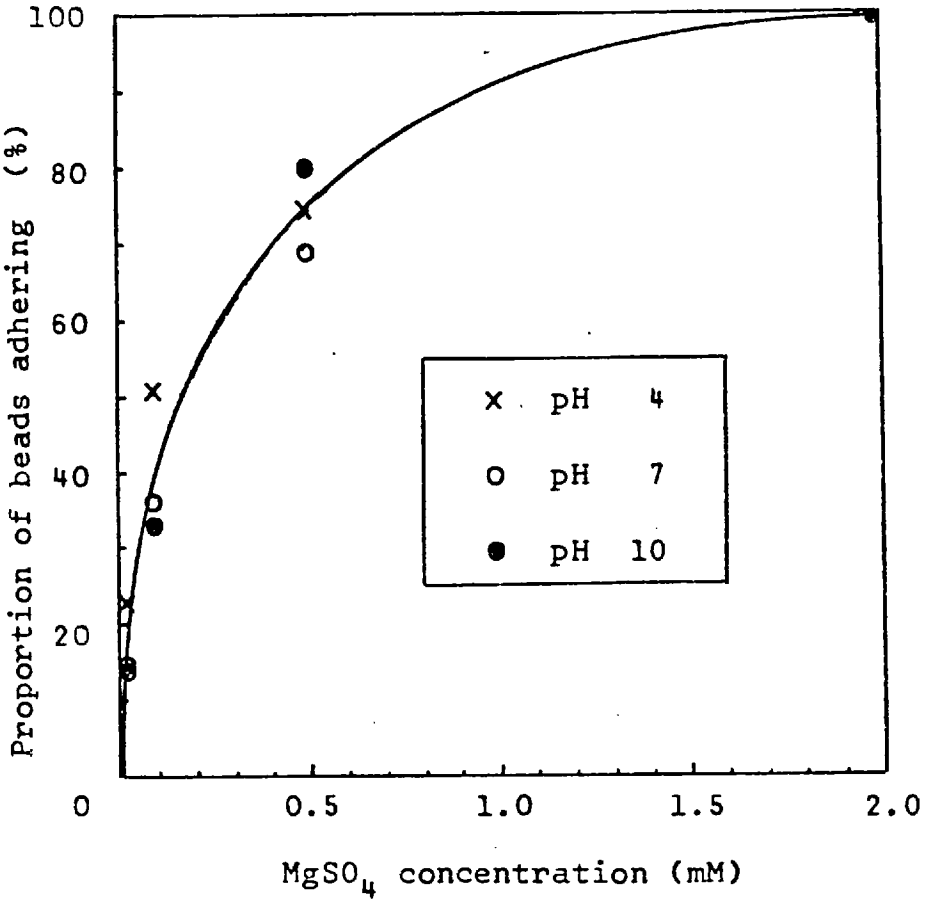



Figure 8 Inversion Experiments - effect of $MgSO_4$ concentration on the adhesion of 10 μm diameter beads.

concentrations below 0.1mM, there was no increase in adhesion with flocculant addition. At all these concentrations there was no visible coagulation or flocculation in the beaker tests.

The results obtained for 30 μm diameter beads are given in table 3 and are plotted in figure 9. The greater force, 208pN resulted in fewer beads adhering for a given $MgSO_4$ concentration, as would be expected as the force of adhesion should increase linearly with bead radius; but the gravitational force increases with the radius cubed. The increase in adhesion with flocculant concentration is evident. Even at concentrations as low as 0.1 p.p.m. there was an increase in adhesion.

Using the convention that the force used applies at the point where 50% of the beads were still adhering, the force of adhesion is 208pN for coagulation with 2.0mM $MgSO_4$ alone and flocculation with 0.3mM $MgSO_4$ + 1.0 p.p.m. flocculant, 0.44mM $MgSO_4$ + 0.5 p.p.m. and 0.7mM $MgSO_4$ + 0.1 p.p.m. flocculant.

Experiments were also carried out using the cationic flocculant Magnafloc 292 at pH 7. It was found that for 10 μm diameter beads, 20% of the beads remained adhering for a flocculant concentration of 0.25 p.p.m. and 50% remained adhering at 0.5 p.p.m. of flocculant. It will be recalled that 1 p.p.m. produced no detectable flocculation.

## 4.3. Flow-Through Experiments: Results

Experiments were carried out with both small and large beads at pH 7 and 10, to determine the adhesion of

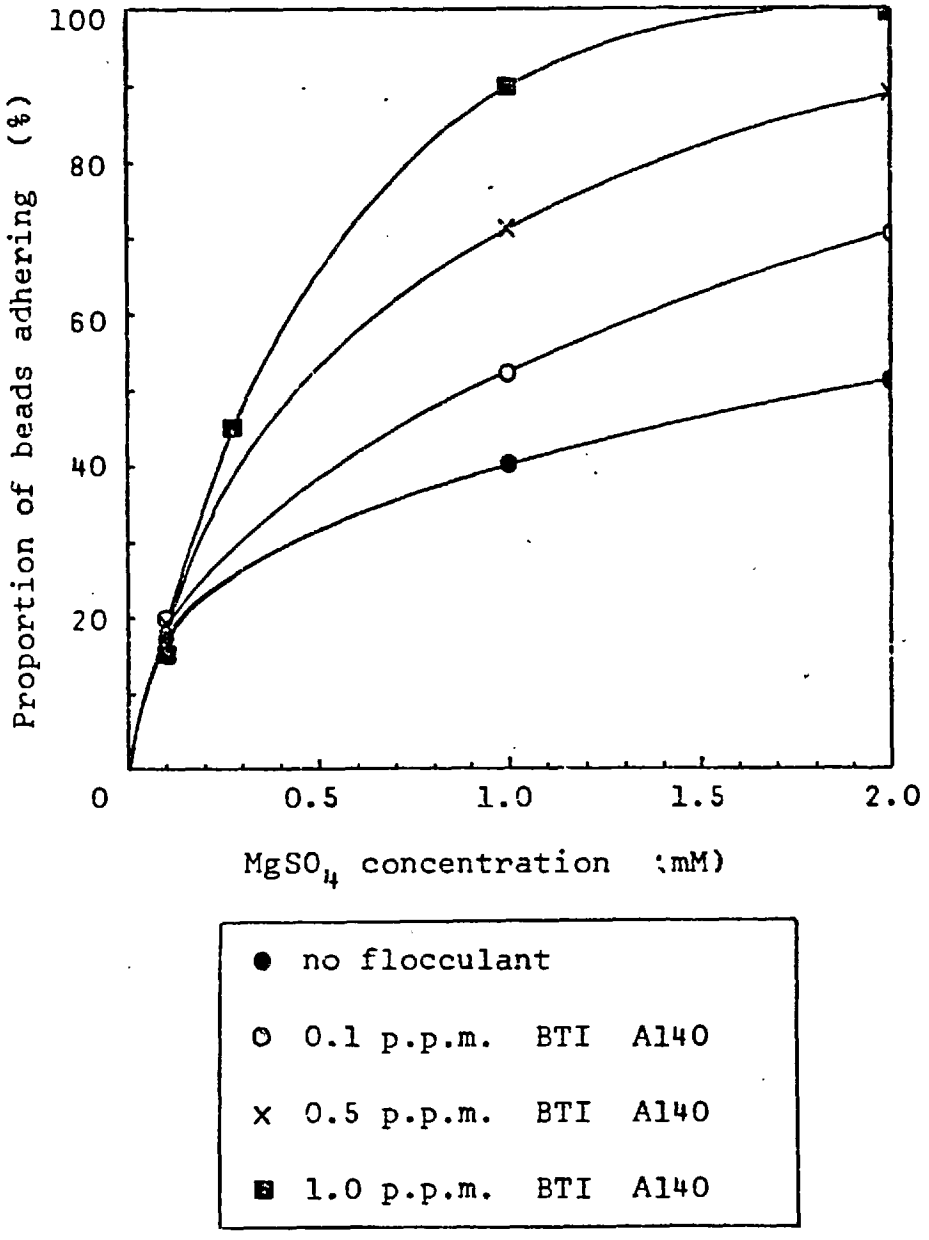



Figure 9 Inversion Experiments - Effect of $MgSO_4$ concentration on the adhesion of 30 μm diameter beads at pH 10.

beads in 0.5mM $MgSO_4$ alone and with 1 p.p.m. BTI A140. The results are shown in tables 4 and 5 and are plotted in figures 10 and 11.

From figure 10 for adhesion in 0.5mM $MgSO_4$ at pH 7, it can be seen that the force required for 50% detachment was 0.19nN for 10 μm diameter beads and 0.43nN for 30 μm beads, a x 2.26 increase in the force of adhesion as the bead radius was trebled. Addition of 1.0 p.p.m. BTI A140 resulted in an increase in adhesion to values of 0.28nN and 1.1nN respectively.

The results for the same concentration at pH 10 (see figure 11) show that the force required for the detachment of 10 μm diameter beads was 0.17nN and for 30 μm diameter beads was 0.86nN a fivefold increase. The increase in adhesion was considerably greater at pH 10 than at pH 7, complete adhesion occurring in the case of 1.0 p.p.m. flocculant with 30 μm diameter beads.

The results for cationic flocculation are given in table 6 and figure 12. The force value for 50% adhesion was 12pN for 10 μm diameter beads and 0.76nN for 30 μm diameter beads, indicating a greater dependence on particle size than predicted by Derjaguin's theory.

## 4.4. Centrifugal Experiments: Results

Deposition of the beads onto the silica disks was carried out in two ways. Firstly, the beads were settled onto the disks in distilled water at pH 10. After 20 minutes the water was drained off and replaced with the flocculating medium of 8mM $MgSO_4$ and flocculant. The results for these experiments are

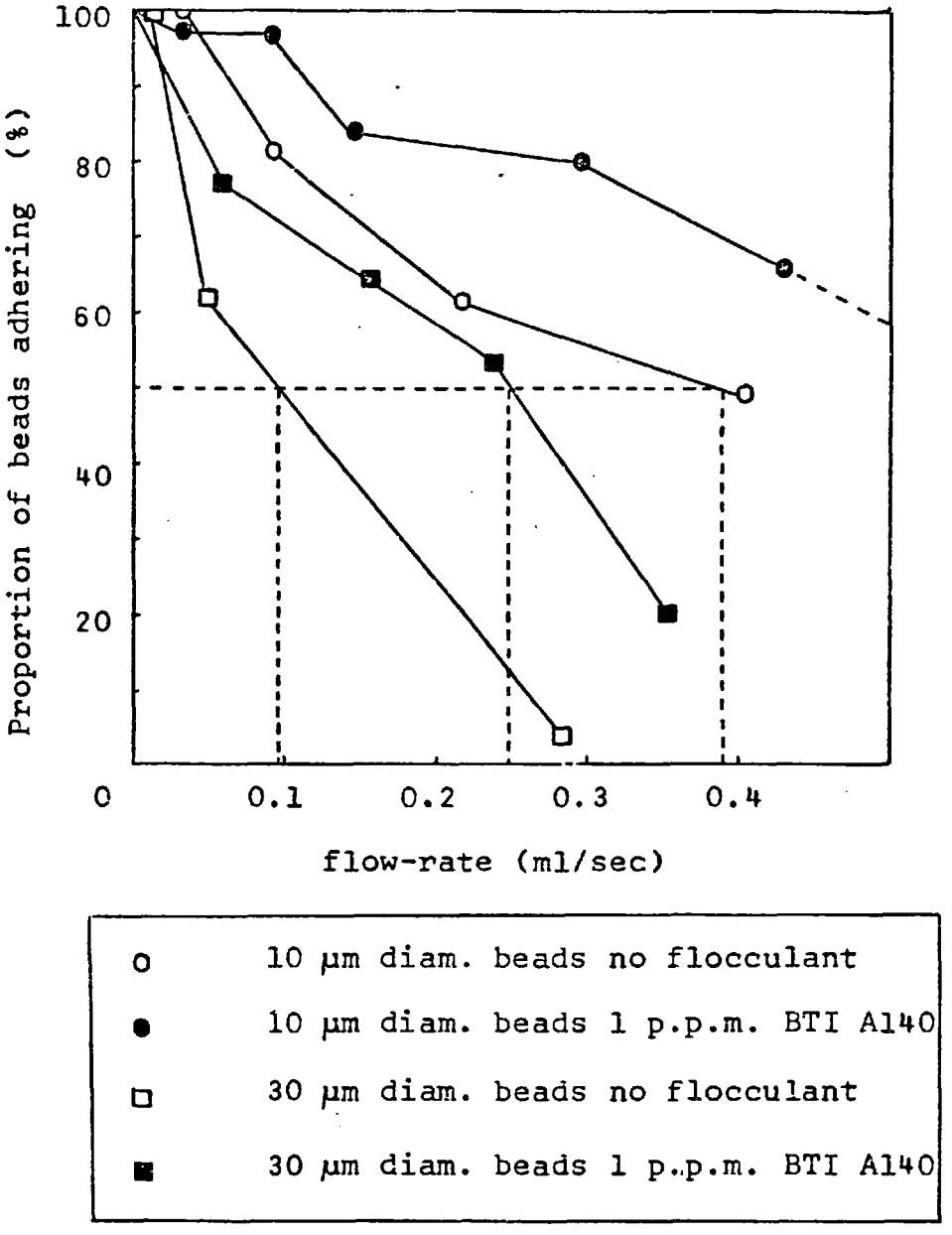
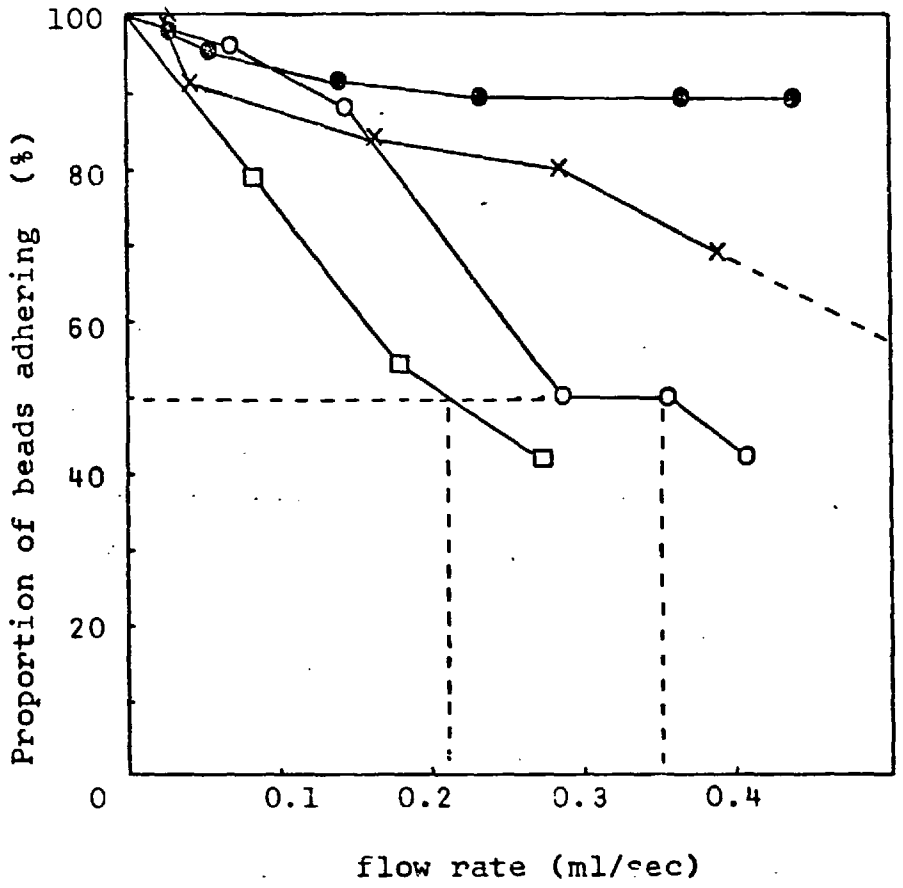



Figure 10 Flow Through Experiments - effect of flow-rate on adhesion with 0.5mM $MgSO_4$ at pH 7




| | |
|---|---|
| o | 10 μm diam. beads no flocculant |
| ● | 10 μm diam. beads 1 p.p.m. BTI A140 |
| □ | 30 μm diam. beads no flocculant |
| × | 30 μm diam. beads 0.5 p.p.m. BTI A140 |

Figure 11 Flow Through Experiments - effect of flow-rate on adhesion with 0.5mM $MgSO_4$ at pH 10

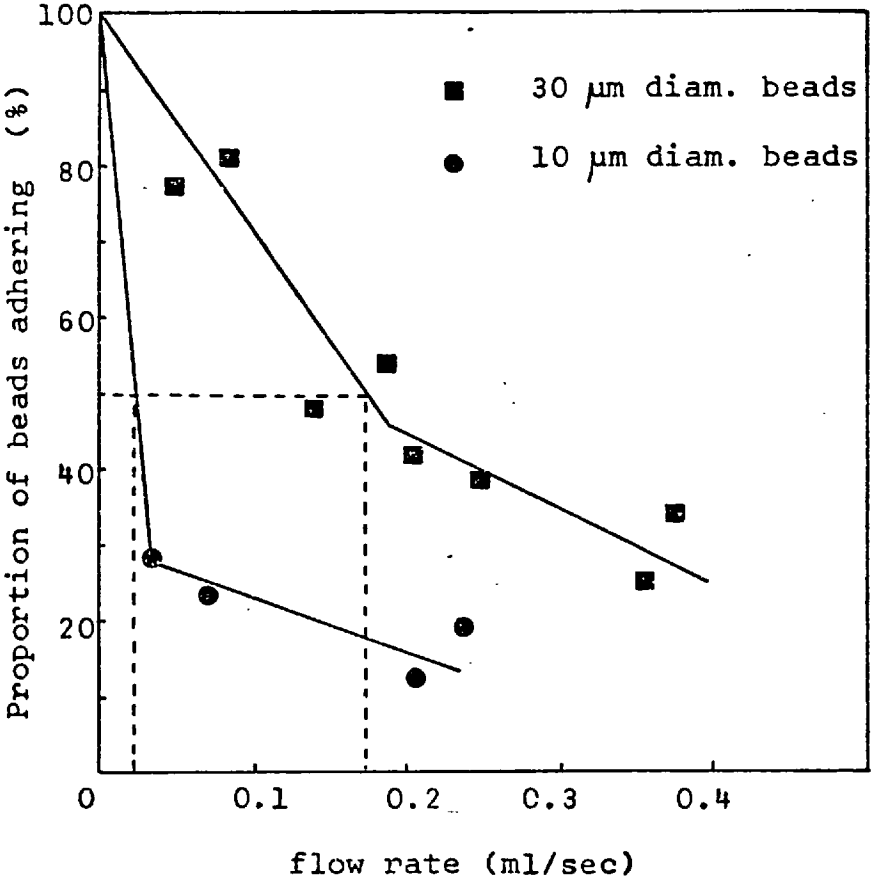



Figure 12 Flow-through Experiments - effect of flow rate on adhesion with 0.5 p.p.m. Magnafloc 292 at pH 7

given in table 7 and are plotted in figures 13 and 14. The increase in adhesion upon increasing the flocculant concentration from 10 p.p.m. to 20 p.p.m. can be seen. The force required to detach 50% of the beads increased correspondingly from 33nN to 84nN. Leaving the disks overnight before spinning also had an effect on adhesion as is shown in figure 14. The force of adhesion increased from 33nN to 45nN.

The second method of deposition used was to settle the beads in an 8mM $MgSO_4$ solution at pH 10 and after 20 minutes to replace it with the flocculating solution of 8mM $MgSO_4$ and flocculant. Deposition could not be carried out in the flocculating medium because the beads formed aggregates before settling onto the disks. The results for the second method of deposition are given in table 8 and plotted in figures 15 and 16. Adhesion with this method of deposition was stronger than for deposition in water alone, e.g. the force of adhesion with 10 p.p.m. flocculant was 60nN compared with 33nN. The increase in adhesion with flocculant concentration can be seen in figure 15. For 5 p.p.m. flocculant the force at which 50% of the beads were detached was 30nN; for 10 p.p.m. the force was 60nN and for 20 p.p.m. it had increased to 140nN. The effect of time on the strength of adhesion was more pronounced with this method of adhesion. Figure 16 shows that when the deposited beads were left overnight before spinning, the force of adhesion for 10 p.p.m. flocculant increased from 60nN to 105nN.

Weaker adhesion than those above could not be measured because of slippage during preparation and centrifuge acceleration. Thus it was not possible to cover the same range of concentrations used in the inversion and flow-through experiments.

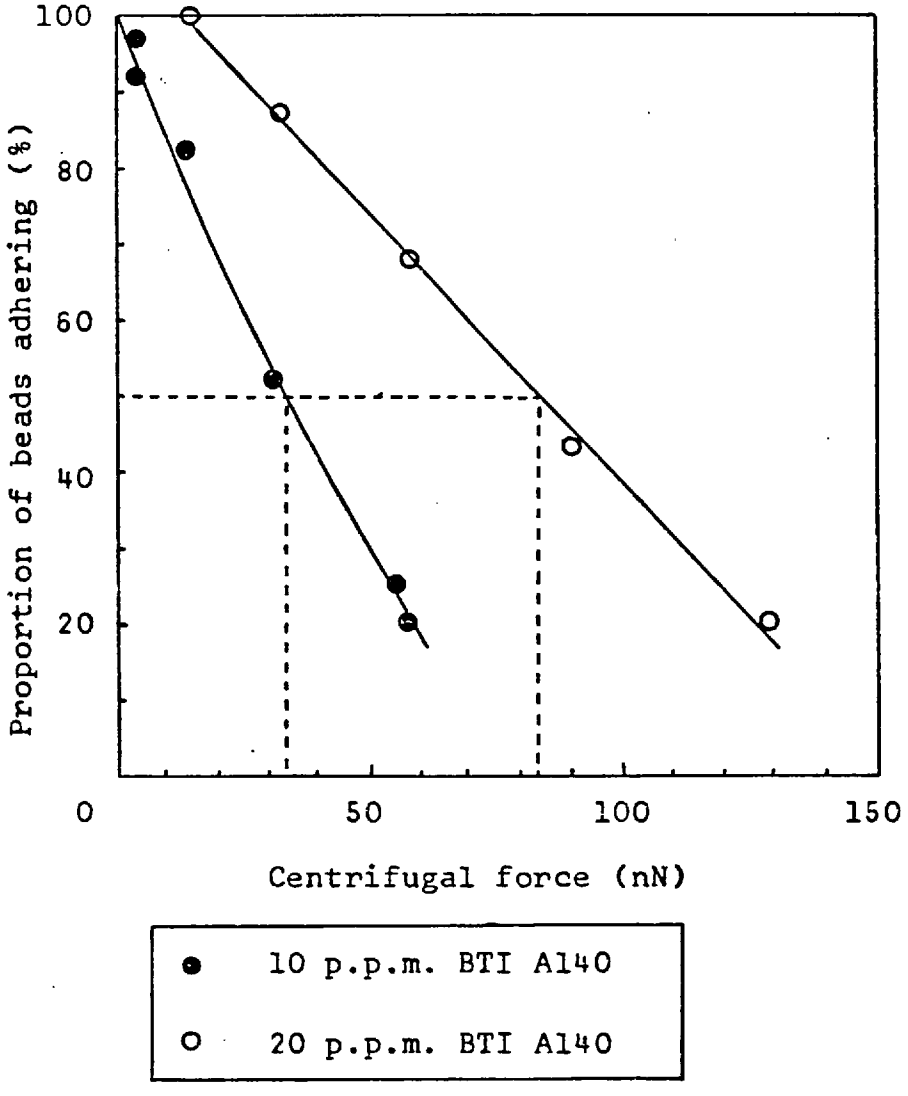



Figure 13 Centrifugal Experiments - water deposition - effect of flocculant concentration on adhesion. Adhesion medium 8mM $MgSO_4$ and BTI A140, pH 10

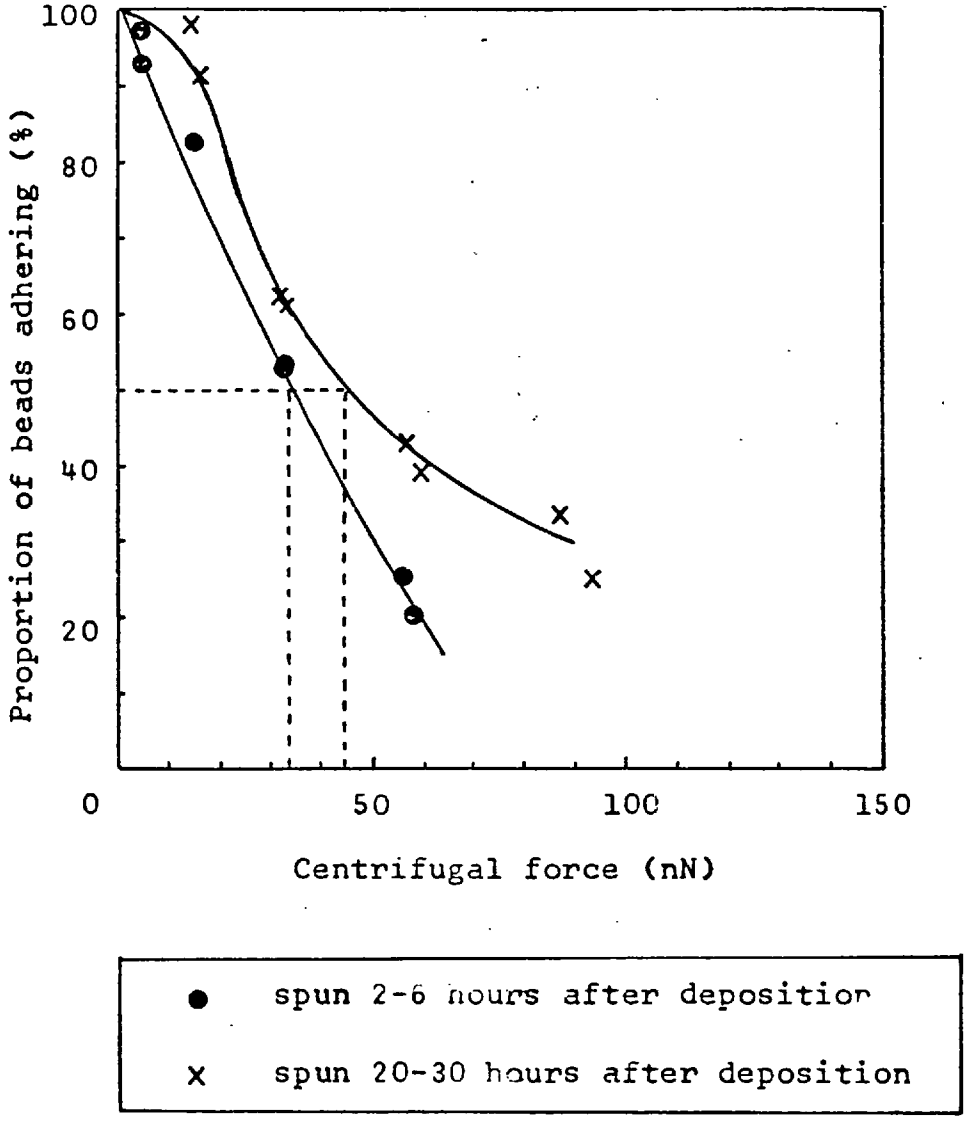



Figure 14 Centrifugal Experiments - water deposition - effect of time on adhesion. Adhesion medium 8mM $MgSO_4$ and 10 p.p.m. BTI A140 pH 10

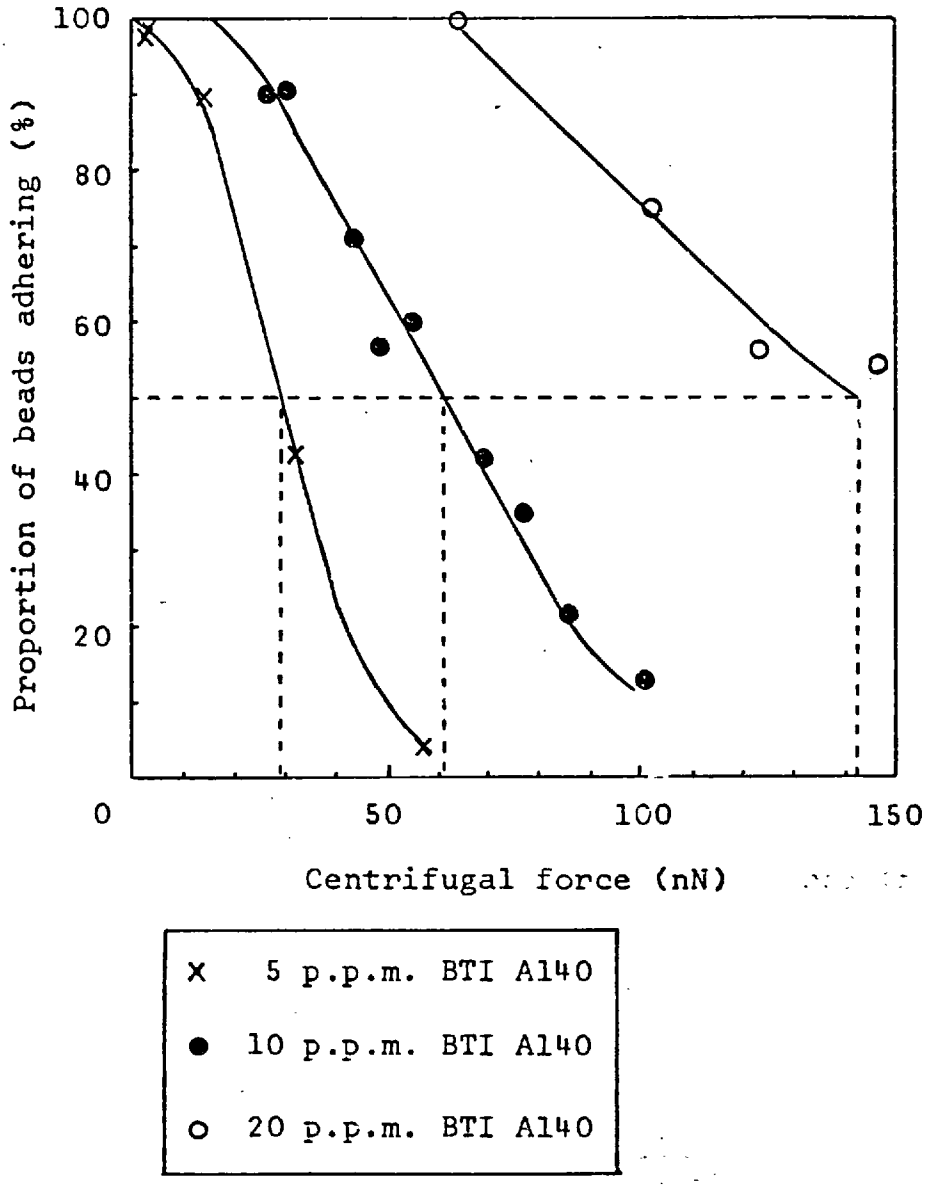



Figure 15 Centrifugal Experiments - $MgSO_4$ deposition - effect of flocculant concentration on adhesion. Adhesion medium 8mM $MgSO_4$ and BTI A140, pH 10

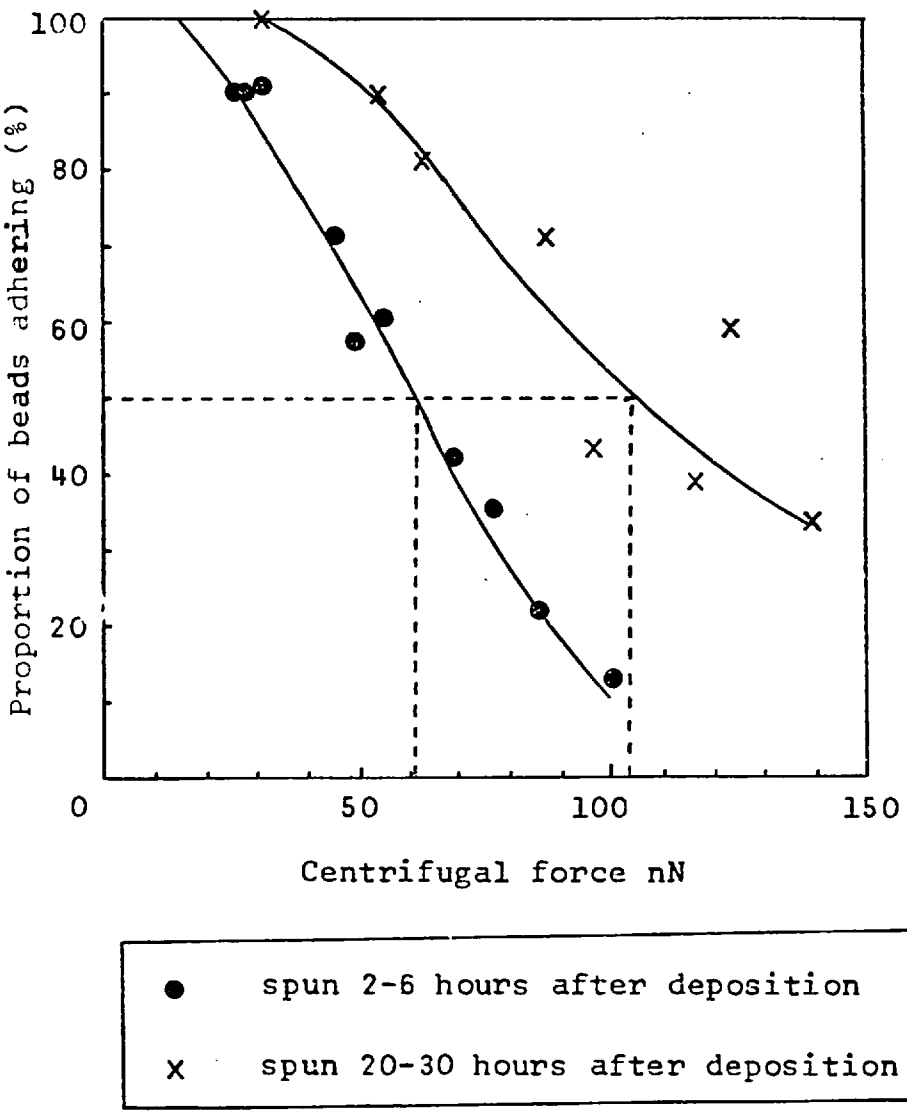



Figure 16 Centrifugal Experiments - $MgSO_4$ deposition - effect of time on adhesion. Adhesion medium 8mM $MgSO_4$ and 10 p.p.m. BTI A140, pH 10

## 4.5. Discussion

The adhesion forces measureable with the inversion and flow-through techniques were very weak. Similar conditions did not show visible coagulation or flocculation in the preliminary beaker tests because the velocity gradients encountered during mixing were too violent and there was little opportunity for particle collision during settling.

The results from the inversion experiments on coagulating systems (figure 8) show that there was little variation in adhesion with pH, except at the lower $MgSO_4$ concentrations where adhesion was slightly stronger at pH 4. The zeta-potential at pH 4 would have been reduced as it approached the point of zero charge. At the higher $MgSO_4$ concentrations, however, the reduction in the double-layer repulsion would have a dominating effect on adhesion. The addition of even very small amounts of anionic flocculant (0.1 p.p.m.) had an effect on adhesion (figure 9). However, for $MgSO_4$ concentrations below 0.1mM no increase was observed, suggesting that the range of double layer repulsion ($1/\kappa$) needs to be reduced to 15nm before flocculation can occur with this particular flocculant.

The results obtained from the flow-through experiments are not true "normal" forces of adhesion because, as explained, the beads were subjected to horizontal hydrodynamic forces, not detachment forces normal to the plane. However, a comparison of results can be made in the case of flocculation with the cationic flocculant. In the inversion tests it was found that 50% adhesion occurred at a flocculant concentration of

0.5 p.p.m. with 10 μm diameter beads, indicating an $F_A$ of 7.7pN. For the same concentration of flocculant and bead size with the flow-through experiments, an $F_c$ of 12pN was found (figure 12). Visser (50) found that results for the force of adhesion of carbon black particles to cellophane substrates in surfactant solutions deduced from a hydrodynamic and centrifugal force were equal although van den Tempel (78) states that the results agreed within a factor of less than 2 as the present values do.

The results for coagulation at pH 7 and 10 (figures 10 and 11) also show that there was little variation in adhesion at 0.5mM $MgSO_4$ concentration with pH but that there is a marked difference in adhesion upon the addition of the anionic flocculant. As the polymer molecule would have a more extended configuration at pH 10 this would lead to improved flocculation.

The increase in the adhesion with bead diameter was x 2.3 at pH 7 and x 5 at pH 10 for the coagulating systems (figures 10 and 11). This indicates a dependence of adhesion on particle size of the power of 0.75 and 1.5 respectively. The increase in the case of anionic flocculation (figure 10) was from 0.28nN to 1.1nN indicating a 1.25 power dependence on particle diameter. The Derjaguin theory for the effect of particle form on the interaction force (18) predicts a first power dependence for sphere/plate interaction. The average of the three cases above is 1.2 showing that Derjaguin's theory is fairly closely followed. However, for cationic flocculation (figure 12) the force at which 50% adhesion occurred increased from 12pN to 760pN as the bead diameter was trebled giving a size dependence of the 3.8th power.

The interaction between the surfaces used here would not be expected to follow Derjaguin's theory exactly because surface irregularities would restrict the effective contact area to a few points. For coagulation and particularly in the case of the adsorbed anionic flocculant, separation of the surfaces may have been sufficiently large for a "smoothing over" of the surface irregularities to occur giving an approximately smooth zone of interaction. However, in the case of the adsorbed cationic flocculant, the molecule would have been strongly attached to the surfaces and with the possibility of charge neutralisation or even alternative patches of positive and negative charge (79), the surfaces may have been much closer. The effect of surface irregularities would be more profound as the separating between the surfaces decreased.

The results obtained in the centrifuge experiments showed an increase in the strength of adhesion with time for both methods of deposition (figures 14 and 16). As very low bead concentrations were used (0.1g of beads in 1200 ml of solution) equilibrium of flocculant adsorption on the surfaces would be reached quickly. Hence an increase in adhesion would not be expected to occur by any great increase in the number of flocculant molecules bridging the gap between the surfaces. However, an increase in the number of points of contact of a flocculant molecule on the surface with time (through molecular rearrangement) could be expected and this would increase the strength of adhesion. Presumably detachment must occur by desorption of the flocculant from the surfaces or by polymer scission or both.

Adhesion was found to be greater if bead deposition occurred in $MgSO_4$ solutions rather than water. Perhaps this result is because deposition in $MgSO_4$ solution would cause a closer approach of the surfaces, giving increased contact area.

An increase in flocculant concentration from 5 p.p.m. to 10 p.p.m. doubled the force of adhesion (figure 15). When the concentration was increased from 10 p.p.m. to 20 p.p.m. a x 2.4 increase in adhesion occurred for deposition in $MgSO_4$ and a x 2.6 increase for deposition in water. Averaging these gives a 1.2 power dependence of the strength of adhesion on flocculant concentration.

## 4.6. Conclusions

These results give a semi-quantitative indication of the strength of attachment in flocculation and in general there is a satisfactory correlation between adhesion strength and floc formation. The other important factor governing the size and strength of flocs is the hydrodynamic conditions to which it is subjected. This aspect is covered in Chapters 5, 6 and 7.

# CHAPTER 5

# HYDRODYNAMICS AND FLOC MODELS

## 5.1. Introduction

As explained in Chapter 1, both the kinetics of particle collisions to form flocs and the maximum size to which flocs will grow are highly dependent on the hydrodynamic conditions of their environment. Thus any investigation of floc formation and break-down should be carried out under controlled shearing conditions. This chapter briefly summarises some types of fluid flow that have been used for studying the behaviour of particles subjected to shearing. In the present study, Couette flow, generated by a rotating concentric cylinder apparatus, was used to investigate the behaviour of flocculating glass suspensions. The equations describing this type of flow and its stability will therefore be discussed.

The motions of particles suspended in Couette flow are described and the forces acting on them are considered. These have been calculated for spheres and spheroidal particles and the behaviour of the other particle shapes can be related to those of ellipses.

This is followed by a review of the models that have been developed of floc (or coagula) growth in laminar flows and of the mathematics of de-agglomeration of aggregates. A summary is given of some models of floc structure and of an analysis that has been made of the stresses within an idealised floc in a uniform shear field.

## 5.2. Simple Flow Fields

To study the motions of particles and analyse the forces exerted on them in a flow field, the flow must be steady, laminar and of a form that is amenable to analysis. Flow fields that have been used are:

i) Couette Flow, the "simple laminar flow" between parallel plates. The flow is created by the uniform motion of one or both plates.

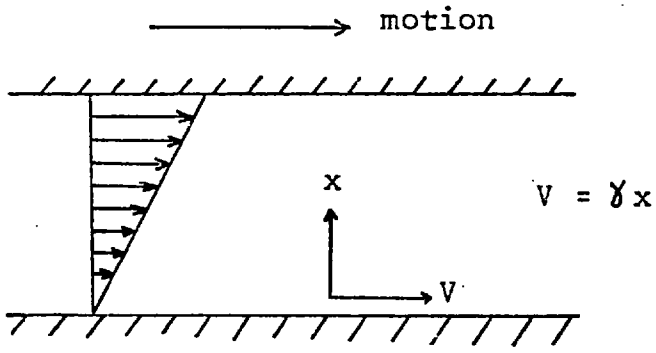



Figure 17. Couette Flow

It has been widely used because the flow is two dimensional, making analysis less complicated and it has the property that the velocity gradient ($\gamma$) is constant (see figure 1). A sphere suspended in Couette flow will rotate with angular velocity $\frac{1}{2}\gamma$. Investigations of Couette flow have been made with parallel-band apparatus (80) but it is more convenient to use the flow in the annulus of concentric rotating cylinders. This is described in section 5.3.

ii) Hyperbolic Flow is also a two dimensional flow with a constant velocity gradient. (figure 2).

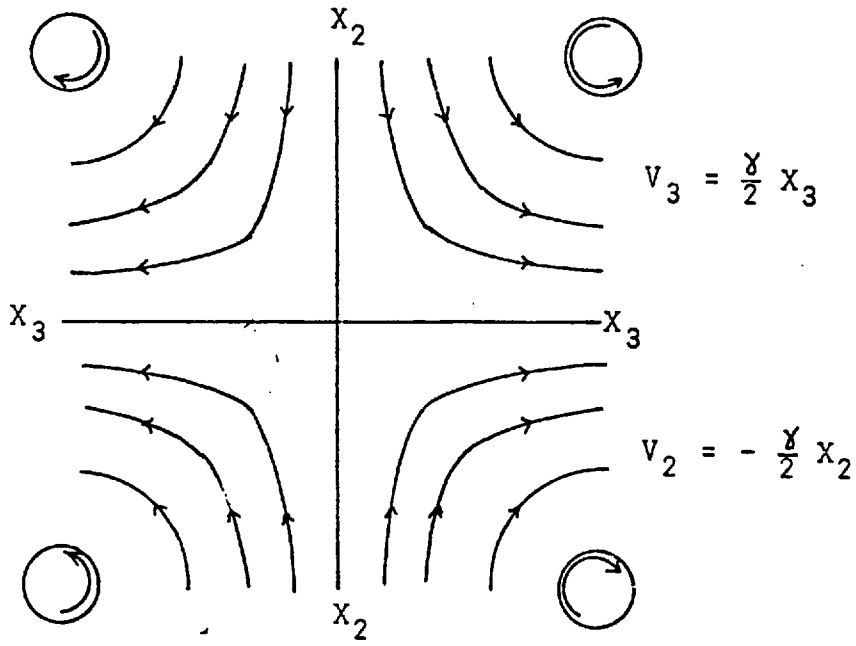



Figure 18. Hyperbolic Flow

A sphere placed at the origin of the flow would not rotate and it can be shown that the forces exerted on the surface of the sphere are identical to those on a sphere at the origin of a Couette flow (81). Hyperbolic flow can be generated by four identical parallel cylinders at the corners a square, rotating in the directions shown in figure 18. An apparatus based on this geometry was used in the classic experiments of Taylor (80).

iii) Poiseuille Flow is the laminar flow between parallel plates (two dimensional) or through a narrow circular pipe.

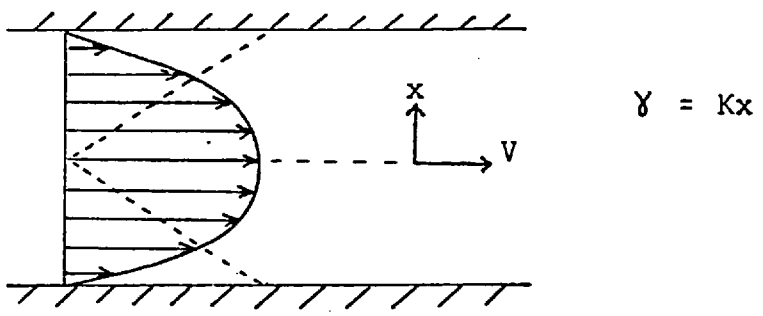



Figure 19. Poiseuille Flow

The velocity profile is parabolic and the velocity gradient varies linearly from zero at the centre to a maximum at the wall. Particles suspended in Poiseuille flow will also rotate with an angular velocity of $\frac{1}{2}\gamma$ providing they are small compared with the radius of the tube. ($b/R < 0.05$).

## 5.3. Fluid Flow Between Rotating Concentric Cylinders

The flow in the annulus between rotating concentric cylinders has been widely used for studying the rheological properties of fluids and suspensions as with the Couette viscometer. Providing the width of the gap is small compared with the radius

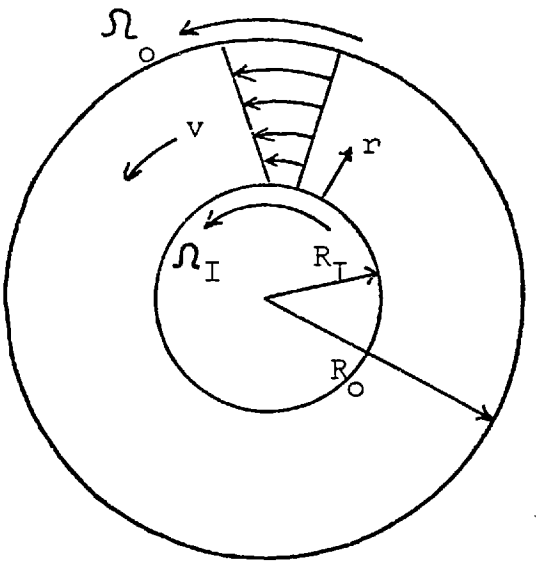



Figure 20. Flow Between Rotating Concentric Cylinders

of the outer cylinder the velocity gradient is nearly constant across the gap; otherwise the gradient can be calculated as follows.

The Navier-Stokes equation for an incompressible fluid with constant viscosity is

$$\rho \frac{D\tilde{v}}{Dt} = -\nabla p + \eta \nabla^2 \tilde{v} + \rho \tilde{g} \quad \ldots\ldots\ldots(5.1)$$

For the arrangement shown in figure 20, equation 5.1. can be solved to give (82)

$$V = \frac{\Omega_o R_o^2 - \Omega_I R_I^2}{R_o^2 - R_I^2} \cdot r - \frac{(\Omega_o - \Omega_I) R_o^2 R_I^2}{R_o^2 - R_I^2} \cdot \frac{1}{r} \quad \ldots(5.2)$$

where $\Omega_o$, $\Omega_I$ are the angular velocities of the outer and inner cylinders

$R_o$, $R_I$ are the radii of the cylinders and r is the radial distance.

For many applications the outer cylinder only rotates and equation 5.2. reduces to

$$V = \frac{\Omega_o R_o^2}{R_o^2 - R_I^2} \left(r - \frac{R_I^2}{r}\right) \quad \ldots\ldots\ldots\ldots\ldots\ldots (5.3)$$

The velocity gradient $\gamma(r)$ is given by (82)

$$\gamma(r) = -2 \frac{(\Omega_o - \Omega_I) R_o^2 R_I^2}{R_o^2 - R_I^2} \left(\frac{1}{r^2}\right) \quad \ldots\ldots\ldots\ldots (5.4)$$

and for the outer cylinder only rotating equation 5.4. becomes

$$\gamma(r) = -\frac{2\Omega_o R_o^2 R_I^2}{R_o^2 - R_I^2} \left(\frac{1}{r^2}\right) \quad \ldots\ldots\ldots\ldots\ldots (5.5)$$

If the gap between the cylinders is small compared with the radius of the outer cylinder ($R_o - R_I \ll R_o$) then an average velocity gradient $\gamma_{av}$ is given by (83)

$$\gamma_{av} = -\frac{2\Omega_o R_I R_o}{R_o^2 - R_I^2} \quad \ldots\ldots\ldots\ldots\ldots (5.6.)$$

The stability of the flow between concentric cylinders has been studied by several workers (84-94). For the system with the inner cylinder rotating, it was found that at Reynolds numbers, below that at which turbulence is found, stratification of the flow occurred. Fluid particles near the inner cylinder experience a higher centrifugal force than those near the outer cylinder and show a tendency to be propelled outwards. Thus toroidal vortices which rotate alternately in opposite directions are formed. This flow is well ordered and turbulence is not found until considerably higher Reynolds numbers. These vortices are called Taylor vortices and a Taylor

number $T_A = \frac{\Omega_I R_I (R_o - R_I)}{\nu} \sqrt{\frac{R_o - R_I}{R_I}}$ has been proposed to characterise the limits for the onset of this type of instability (85) when

$T_A < 41.3$ laminar Couette flow

$41.3 < T_A < 400$ laminar flow with Taylor vortices

$T_A > 400$ turbulent flow.

For the same reasons, the flow when the outer cylinder only is rotated is stabilised by centrifugal forces. A fluid particle opposes being moved inwards because the centrifugal force on it is greater than on particles nearer the inner cylinder. At the same time outward movement is resisted by the higher centrifugal force on the particles nearer the outer cylinder it would have to replace. Thus transition to turbulence takes place at much higher Reynolds numbers than for when the flow is between flat parallel plates.

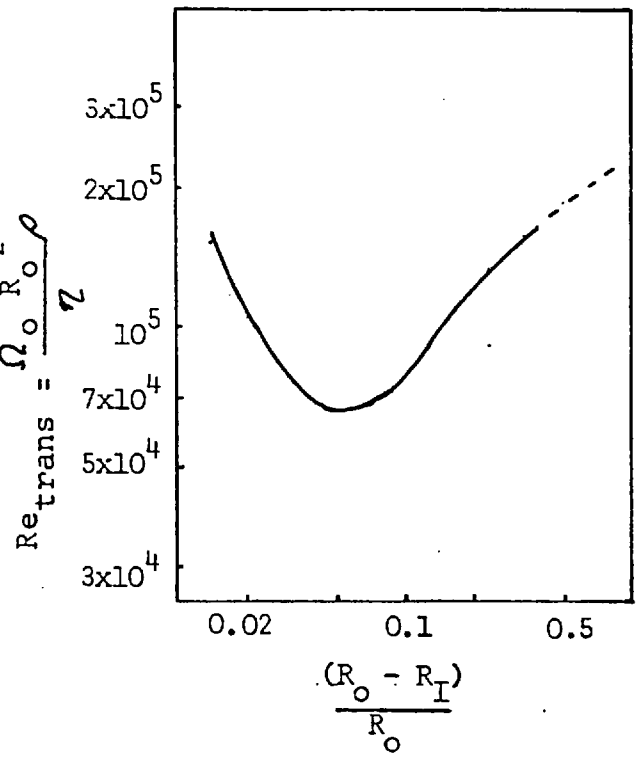



Figure 21 Transition Reynolds Numbers for the Outer Cylinder Rotating (93)

Early workers found that the Reynolds number at which transition to turbulence took place ($Re_{trans}$) was given by the curve in figure 21. However, Schultz-Grunow (94), found that flow was completely stable. Although transition to turbulence did occur during the starting process, flow reverted to laminar when a steady speed was reached. Persistent turbulence was only obtained if an eccentricity was built into the apparatus.

## 5.4. Particle Behaviour in Couette Flow

A comprehensive review of the microbiology of dispersions has been given by Goldsmith and Mason (95). Jeffrey (96) derived equations for the torque acting on an ellipsoid in a uniformly sheared fluid at low Reynolds numbers.

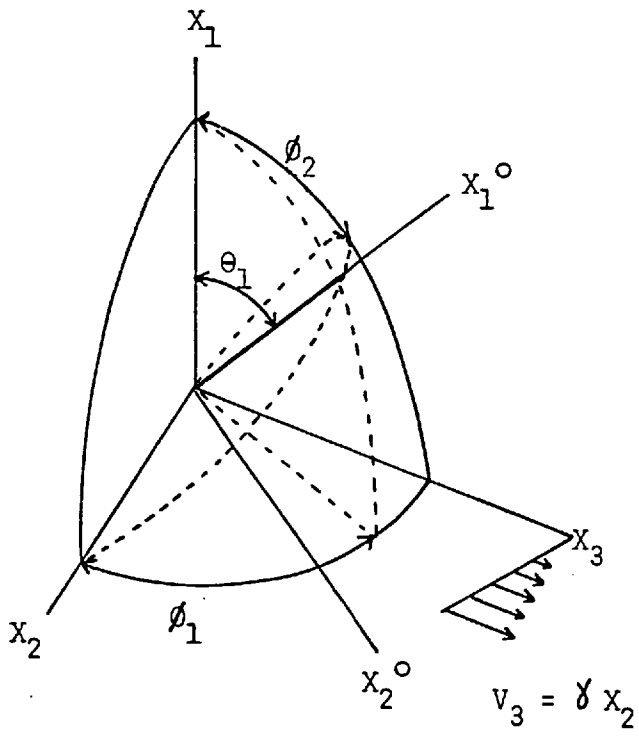



Figure 22 Relative Orientations of an Ellipsoid ($X_1^\circ$, $X_2^\circ$, $X_3^\circ$) with respect to a Flow Field ($X_1$, $X_2$, $X_3$)

For a rigid spheroid with principle axis $b_1$ and secondary axis $b_2$, where $r_p = b_1/b_2$

$$\frac{d\phi_1}{dt} = \frac{\gamma}{r_p^2 + 1} (r_p^2 \cos^2 \phi_1 + \sin^2 \phi_1) \quad \ldots\ldots\ldots(5.7)$$

$$\frac{d\theta_1}{dt} = \frac{\gamma (r_p^2 - 1)}{4 (r_p^2 + 1)} \sin 2\phi_1 \sin 2\theta_1 \quad \ldots\ldots\ldots(5.8)$$

At the same time the spheroid undergoes rotation about its axis of symmetry

$$\omega_1^{\circ} = \tfrac{1}{2} \cos \theta_1 \quad \ldots\ldots\ldots(5.9)$$

For a sphere, $r_p = 1$ and the equations reduce to

$$d\theta_1/dt = 0, \; d\phi_1/dt = \omega_1^{\circ} = \gamma/2$$

These equations have been confirmed by observations of glass and plastic beads (97). Treatment of other shapes of particles, (e.g. rods and discs) at very low Reynolds numbers can be made by calculating an "equivalent ellipsoidal ratio" $r_e$ from the observed period of rotation (97).

The surface of a sphere suspended in Couette flow undergoes alternate periods of compressive and tensile stresses and radial stresses in each of the four quadrants as it rotates as is shown in figure 23.

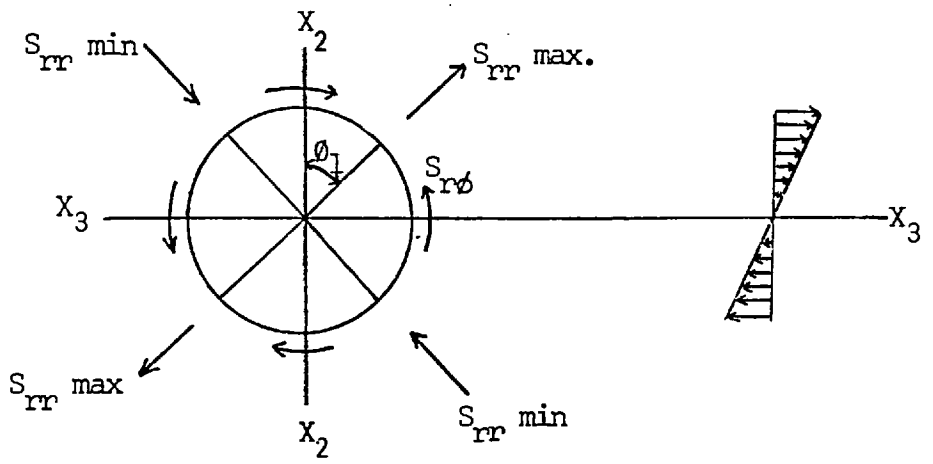



Figure 23 The Stresses Acting in each of the four Quadrants of a Sphere in Couette Flow

The radial stresses are at a maximum when $\phi_1 = \frac{\pi}{4}, -\frac{3\pi}{4}$ (tensile) and a minimum when $\phi_1 = \frac{3\pi}{4}, -\frac{\pi}{4}$ (compressive). At $\phi_1$, = 0, $\pm \frac{\pi}{2}, \pi$ there is no radial stress, but the tangential stress is at a maximum. If the sphere were a fluid drop, these stresses would deform it and set up circulation patterns of the fluid within the drop.

The radial shear stress is given by

$$S_{rr} = \frac{5}{2} \gamma \eta \sin 2\phi_1 \quad \text{.....(5.10)}$$

and the tangential stress by

$$S_{r\phi} = \frac{5}{2} \gamma \eta \cos 2\phi_1 \quad \text{.....(5.11)}$$

Thus the total radial force acting on one quadrant of a sphere diameter b is

$$P_{rr} = \frac{5}{2} \pi b^2 \eta \gamma \quad \text{.....(5.12)}$$

Jeffrey (96) has given the equations for the components of stress acting on the surface of an ellipsoid in the centre of a field with arbitrary components of dilatation and rotation. For the case of a spheroid in Couette flow these reduce to

$$S_{11} = \frac{4\eta J}{b_1 b_2^2}\left\{2j_{11} - b_1 b_2^2\left[j_{11}(\alpha_1 - \alpha_2)\right]\right\}$$

and $S_{12} = S_{21} = \frac{8\eta J}{b_1 b_2^2} \cdot j_{12}$

where J is the perpendicular distance of the tangent plane at the point $(X_1^o, X_2^o, X_3^o)$ from the spheroid centre, given by

$$J = \left[\frac{b_1^4}{X_1^{o\,2}} + \frac{b_2^4}{(X_2^{o\,2} + X_3^{o\,2})}\right]^{\frac{1}{2}}$$

and $j_{ii}$, $j_{12}$ are functions of the spheroid integrals $\alpha_1$, $\alpha_2$ and the components of the rate of shear.

It has been shown (95) that a rotating rigid spheroid is subject to an axial force ($P_1$) given by

$$P_1 = \pi\eta\gamma b_2^2 \sin 2\phi_1 \sin^2\theta_1 \frac{(2r_p^2 - 1)\,U}{2r_p^2 - U(2r_p^2+1)} \quad \ldots\ldots(5.13)$$

where U is a function of the spheroid's size and the spheroidal integral, $U = b_1 b_2^2 \alpha_2$.

This is the axial force acting on half the spheroid surface and it depends on the dimensions of the particle, the product $\gamma\eta$ (fluid flow properties) and on the particle orientation.

When two rigid spheres collide and stick in Couette flow, they may be considered to rotate as a prolate

spheroid with $r_e = 2$, and equation 5.13 becomes

$$P_1 = \pi \eta \gamma b^2 \sin 2\phi_1 \sin^2\theta_1 \frac{3U}{8 - 9U} \quad \text{.....(5.14)}$$

This becomes (95)

$$P_1 = 4.41 \pi \eta \gamma b^2 \sin 2\phi_1 \sin^2\theta_1 \quad \text{.....(5.15)}$$

For $\theta_1 = \frac{\pi}{2}$, the axial force goes through a maximum at $\phi_1 = \frac{\pi}{4}$ of

$$P_1 = 4.41 \pi \eta \gamma b^2 \quad \text{.....(5.16)}$$

This is 1.764 times greater than the instantaneous force on a quadrant of one of the spheres in the same flow.

The equations for particle collisions in laminar flow were first given by von Smoluchowski (98) in 1918. The basic equations are

$$J_{ij} = \frac{4}{3} n_i n_j R_{ij}^3 \frac{du}{dz} \quad \text{.....(5.17)}$$

where $J_{ij}$ is the number of collisions in unit time and volume of i & j size particles
$n_i$&$n_j$ are the concentrations of i and j particles and
$R_{ij}$ is the distance separating the centres of an i & j type particle during a collision.
$\frac{du}{dz}$ is the local velocity gradient.

Thus the equation for the rate of change of the concentration of k type particles is

$$\frac{dn_k}{dt} = \frac{2}{3} \frac{du}{dz} \left[ \sum_{\substack{i=1 \\ j=k-i}}^{k-1} n_i n_j (R_i + R_j)^3 - 2n_k \sum_{i=1}^{\infty} n_i (R_i + R_j)^3 \right] \text{..(5.18)}$$

There are no analytical solutions available for equation 5.18 but it can be solved numercially with the help of a computer.

All the above equations relate to the motions of particles in the creeping flow regime. For higher Reynolds numbers, inertial effects will become significant. Exact solutions of the Navier-Stokes equation are not available in this regime but pertubation methods have been used to solve particular cases. The well recognised lateral migration of particles in Poiseuille flow is an example of the effects of inertia. The unexplained inwards migration of particles in Couette flow has also been reported (83). Also important is the effect that the wall has on the flow in cases where the particle size is comparable to the annular gap and in concentrated suspensions. Karnis et al (99) found that deviations in the particle velocities from the fluid velocity occurred when the volume concentration increased past 2%.

## 5.5. Floc Models

### i) Floc Formation

The Smoluchowski equations for orthokinetic flocculation (98) have been used in a number proposed models of aggregate formation (100-102).

Fair and Gemmell (100) used the simplifying assumptions that all particles were spheres and that when two particles collided they coalesced to become a sphere with the same total volume (as would occur with droplets in an unstable emulsion).

Because of limited computer space, a maximum aggregate size was set at 100 primary units. Four different breakdown modes for the maximum size particle were assumed. Either the aggregate was reassigned to the previous size at which it was stable or it was assumed to break into 2, 3 or 4 equal parts. Initial size distribution and a factor C describing the velocity gradient and concentration were fed in. The variation in average size distributions with relative coagulation time were produced for each breakdown mode. It was found that if the factor C was increased past a certain value, oscillatory growth took place. A Couette apparatus was used to investigate coagula formed on reacting ferric sulphate with sodium bicarbonate and oscillatory growth was indeed observed. The authors suggested that the upper limit to floc growth may be inversely proportional to the velocity gradient.

Harris et al (101) using similar assumptions, developed a mathematical model based on the Smoluchowski equations. Equilibrium size distribution were found for both batch-type flocculation and for a system of coagulation in continuous stirred tank reactors (C.S.T.R's). The variation of size distribution with velocity gradient was plotted and a size distribution function was proposed to describe the shape of the curves. Experiments were carried out using both the standard "jar test" to model a batch run and a modified system to model the C.S.T.R. runs. The Camp formula $\gamma = \sqrt{W/\eta}$ (103), where W is the energy dissipated, was used to describe the fluid flow. Similar size distribution functions were found.

These two models both rely on the assumption that maximum floc size is limited by an arbitrary size, so the size distributions obtained, (with an allowance made for the distortions caused by the break-down modes used) are really possible descriptions of early floc growth before the hydrodynamic limit of floc size has been reached. Ives and Bhole (102), however, incorporated the important principle that maximum aggregate size will depend on the velocity gradient, into their mathematical analysis of aggregation kinetics in the continuous flow through a normal Couette apparatus and in a "tapered" apparatus. They found that, when a normal apparatus was used, a narrower size distribution was predicted than for the tapered apparatus, but that the tapered flocculator should be more efficient at removing the smaller particles. This prediction was qualitatively supported by experiments.

ii) De-agglomeration Model

The reverse situation was investigated by Patterson and Kamal (104), who developed a statistical model of aggregate break-down under shearing. Differential equations were developed to describe the rates of change of particle concentration assuming that only break-down occurred, that no particular mode of break-down was favoured and that the strength distribution function was independent of particle size. Glass beads stuck together by polystyrene were sheared and the shear dependence of the aggregate break-down rate was determined and was then used in the mathematical model to obtain theoretical size distributions.

It is likely, in practice, that the strength distribution function will depend on aggregate size and that re-aggregation of the smaller sizes will occur. Large aggregates formed by the collision of two or more smaller aggregates may have a different strength distribution from that of similar size aggregates formed by individual primary particles. This complication could also effect the way in which break-down occurs and some particular modes (i.e. into two equal parts), are likely to be favoured.

iii) Floc Structure

Computer simulation models of aggregate structure have been made by several authors (105-107, 109, 111). An aggregate growth pattern is postulated and a computer used to build-up the aggregate according to the pattern. The shape of the simulated aggregate is then analysed and compared with that of real systems.

A basic model of aggregate structure was first proposed by Vold (105) and later corrected by Sutherland (106). Vold proposed that aggregate build-up was caused by single particle addition to the growing aggregate. The particles were assumed to be spheres of uniform size, and an aggregate growth was generated by fixing the co-ordinates of one particle and generating random numbers to specify the initial position and trajectory of a second particle. If the second particle's trajectory caused it to collide it was assumed to stick. The cluster was then rotated randomly and the process repeated until all

available particles had been used. This model predicts an aggregate of approximately spherical shape and of uniform porosity.

In practice, (except at the very initial stages) aggregate growth is not likely to occur by the collision of single particles alone with an aggregate. Small clusters will be formed by this process but then they will collide with each other (and with single particles too) to build-up aggregates. Sutherland (107) therefore extended the model by taking into account the collision rates predicted by Smoluchowski's theory of perikinetic aggregation (108). This approach was further extended by Sutherland and Goodarz-Nia (109) to take into account the different sizes of the colliding species. Each collision was calculated by randomly rotating the colliding clusters and moving one along a randomly chosen linear trajectory until collision occurred. Sutherland and Goodarz-Nia also tested a model in which aggregate growth was assumed to progress by single spheres colliding with single spheres to produce doublets. Doublets collided with doublets only to produce quadruplets etc. This scheme leads to "maximum cluster addition" (which is taken to mean greatest removal of smaller aggregate sizes) and the growth of chain-like aggregates.

The aggregate structures generated by computer were compared with each other and with Medalia's carbon black data (110) by studying their morphological properties. Following Medalia's proposal (110), the aggregates were represented

by dynamically equivalent ellipsoids and the projected areas, anisometry, bulkiness, radius of gyration etc., compared. It was found that the computer models produced more open structures than the carbon black aggregates which were actually more closely described by Vold's single particle model.

Goodarz-Nia and Sutherland (111) extended their model further by allowing for polydisperse systems and variations in particle shape. They found that varying the initial size distribution by a standard deviation of up to 30% did not alter the floc shapes. However, if a significant proportion of small sizes were used, aggregate densities decreased, in contrast with close packing theory. Aggregate shapes were not affected by the primary particle shapes.

iv) Model of Floc Strength Under Shear

Tomi and Bagster (112) analysed the stresses on an aggregate suspended in simple shear flow. They considered a floc to be a network of spheres joined together by relatively long, perfectly elastic links. Various structural shapes of the floc were considered, near spherical and chain-like. The stresses within the floc were analysed by considering it to be instantaneously placed at rest in a simple laminar flow, so that the force on each spherical particle would be given by the Stokes formula :

$$F = 6\pi\eta b V_a$$

A structural frame analysis was used to calculate

the stresses within each link and find the one of greatest stress for a particular orientation of the floc. It was found that the maximum diameter of a floc was related to the velocity gradient by

$$d_{max} \propto 1/\gamma^{0.5}$$

This result is to be compared with the findings of Fair and Gemmell (100), and Ritchie (113) who conclude that for coagula

$$d_{max} \propto 1/\gamma$$

and Michaels and Bolger (114) whose results seem to show

$$d_{max} \propto 1/\gamma^{0.3}$$

There are many assumptions in this analysis. The particles are assumed to be small compared with the lengths of the links - which is unrealistic. Tomi and Bagster state that a greater dependence on the velocity gradient would be expected for more compact flocs. Also, the floc was considered to be placed instantaneously at rest in the shear field. A particle thus placed, would undergo some deformation and rotation to minimise stresses, but, most importantly, a floc would never be at rest. It would be carried by the flow streamlines and the Stokes force would therefore be considerably less.

## 5.6. Conclusions

There is a lack of quantitative results on the formation of aggregates. There are some results for coagula but

none for systems undergoing flocculation. Tomi and Bagster (112) have made an analysis of the stresses within a floc in a shear field but to solve it, some incorrect assumptions have to be made. No doubt more elaborate theories will be developed but experimental results on well recognised materials under controlled conditions are needed.

Hence, a rotating concentric cylinder apparatus was constructed and a study made of the flocculated glass suspensions, the adhesion of which was described in the first part of this thesis. While the apparatus was being constructed, standard "jar tests" were carried out to determine suitable shearing conditions and broad patterns of floc behaviour under shear.

# CHAPTER 6

## EXPERIMENTAL - Floc Properties

### 6.1. Materials

The materials used in the experiments on floc behaviour in shear were the same as those used in the earlier adhesion experiments. (Details are given in Chapter 3).

### 6.2. "Jar Tests"

A two-speed multiple-stirrer constructed in the Department was used to carry out standard "jar tests" simultaneously on up to 6 flocculating suspensions of glass particles. The apparatus could be adapted to take a number of different sized beakers and a range of paddle shapes and sizes were available. For the present tests, 600ml polypropylene beakers were used (to avoid difficulties with flocculating beads sticking to the beaker surface in the "dead zone" directly under the paddle). The paddles used had four vertical rectangular blades with dimensions 28 x 19mm. The outer edges of the paddles were 30mm from the centre of the shaft. Two speed settings were available; 97 rpm and 193 rpm. The belts driving the paddles were of non-slip design so that the speeds in all the beakers were identical.

A mean velocity gradient in stirred tanks can be estimated by the Camp equation (103)

$$\gamma = (W/\eta)^{\frac{1}{2}}$$

where W is the power dissipated in stirring the suspension per unit volume.

The power transmitted to the suspension can be measured directly by using a torquemeter or calculated from the drag force equation (115)

$$P = C_d A_p \rho (V_p - V)^3 / 2$$

where P is the power, $C_d$ the drag coefficient, $A_p$ the area of the blade normal to the direction of motion, $V_p$ the mean paddle velocity and V the mean suspension velocity.

Bhole (115) noted that in previous publications, $C_d$ had been assumed to be between 0.8 and 2.0, but he found when calibrating a similar system that $C_d$ decreased from 1.81 to 0.94 as the velocity gradient increased from 10 $sec^{-1}$ to 50 $sec^{-1}$. Bhole also found by experiment that the ratio of maximum fluid velocity to maximum blade velocity was 0.52 for velocity gradients between 10 and 50 $sec^{-1}$.

If a value of 0.9 is assumed for $C_d$ (as higher velocity gradients are expected here) and 0.52 for $V/V_p$, then for a paddle speed of 193 rpm and the paddle geometry described,

$$P \approx 3 \times 10^{-3} \text{ J/sec}$$

Thus for a suspension volume of 400ml and water velocity 1 cP ($1 \times 10^{-3}$ kg/m-sec),

$$\underline{\gamma = 86 \text{ sec}^{-1}}$$

Each experiment was carried out by placing 400ml of distilled water at the required pH into the beakers; the necessary quantities of beads and $MgSO_4$ were then added and the stirrers set at the higher speed.

After 2 minutes, the required amount of 0.01% w/v flocculant solution was simultaneously added to all beakers and high-speed stirring was continued for a further 15 seconds before switching to the lower speed. The stirring was stopped after 1 minute and the size of the flocs formed was noted visually and recorded. (It was found that 1 minute of low-speed stirring was necessary to reach maximum floc size, but any further low-speed stirring had no effect on the size of the flocs). The stirrers were then switched to the higher speed for 15 seconds after which the floc size was again noted. This was continued for increasingly larger durations of stirring until complete floc break-down had occurred. These tests gave a semi-quantitative measure of floc strength under various conditions.

## 6.3. The Rotating Concentric Cylinder Apparatus

The laminar shear apparatus was designed to provide a well characterised shear field in which to study the behaviour of flocculating glass particles. From the "jar tests", it was known that floc diameters of the order of 1 mm could be expected and that because of the more stable flow conditions, velocity gradients of $> 100\ sec^{-1}$ would be needed. To avoid wall effects, the ratio of floc diameter to annular thickness should be small, $(b/R_o - R_I) \leq 0.1$, but a wide annular gap would result in a considerable variation in the velocity gradient across the gap. A compromise was made with an annular gap of 1cm. It was possible to obtain precision-bore glass tubing with an internal diameter of 14.0cm and this was used as the outer cylinder. Hence, the ratio of annular gap to outer cylinder radius $(R_o - R_I/R_o)$ was 0.143 which is within the range of values used by Taylor (85) for his "narrow gap" experiments. The angular velocity necessary to create

an average velocity gradient of 200 $sec^{-1}$ using van Duuren's formula (83).

$\gamma_{av} = 2\Omega_o R_o R_I/(R_o^2 - R_I^2)$ is 31 rad./sec, which gives the required outer cylinder speed of 295 rpm.

As mentioned, precision-bore glass was used as the outer cylinder. A length of 14cm internal diameter glass was cut into 20cm lengths and the piece with the least variation in internal diameter was chosen for the apparatus. Its internal diameter was 14.05 $\pm$ 0.01 cm. The inner cylinder was made from an acrylic resin, with carbon black mixed in it to give opacity, cast onto a stainless steel rod and machined to 12.00 $\pm$ 0.005 cm diameter. A diagram of the apparatus (constructed in the Department's workshop) is shown in figure 24. The carbon black in the inner cylinder gave a matt black background to photograph against. One of the end-plates was made of "Perspex" and its surfaces polished. A flash of light could be beamed through this end-plate down the annulus to illuminate the flocs for photography. The other end-plate was made from brass. It had a pulley attached to it which was driven by a timing belt. In this brass end-plate there was also a small vent hole which was used to remove any trapped air bubbles. The outer cylinder was sealed against the end-plates by rubber O-rings and held together by three long bolts. The end-plates were sealed onto the stainless steel shaft by rubber O-rings and a "Teflon" sleeve. Holes 2mm in diameter were drilled through each end of the stainless steel shaft, leading to 8 holes evenly spaced around the perimeter of the inner cylinder so that a solution or suspension could be introduced evenly into the annular gap at each end. The whole apparatus was mounted on

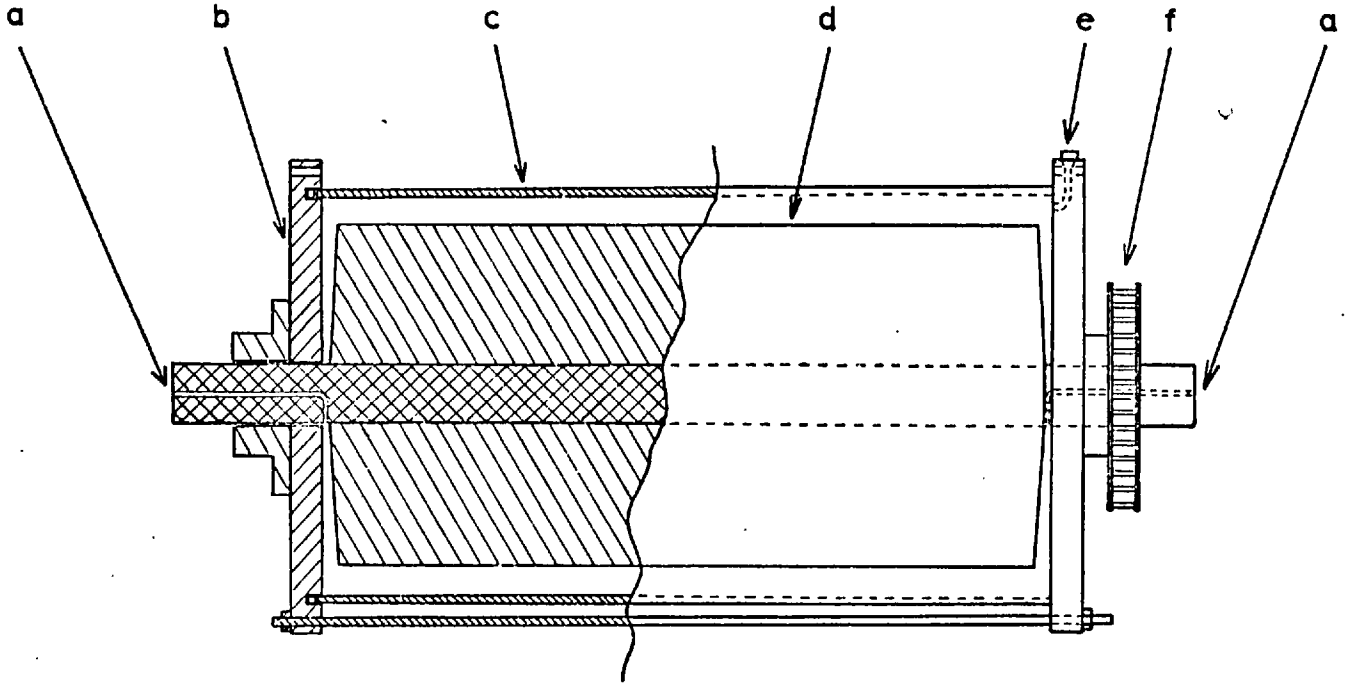



Figure 24 Diagram of horizontal concentric rotating cylinder apparatus.

a. 2 mm dia. holes to permit flow of liquid during operation.
b. end plate - polished Perspex.
c. outer cylinder - glass 14 cm i.d.
d. inner cylinder - cast acrylic 12 cm o.d.
e. vent to remove trapped air bubbles
f. belt drive from variable speed motor

an aluminium plate which could be tilted through $60^{o}$ to assist in the removal of trapped air bubbles.

The outer cylinder was driven by a 0.25 h.p. shunt-wound motor whose speed could be continuously varied between 60 and 360 rpm. Also attached to the motor drive shaft was a disk with eight holes drilled evenly around it. A light was positioned to shine through these holes onto a photocell, the pulses from which were integrated and a D.C. voltage reading proportional to the speed of the apparatus was produced. The meter was calibrated using a tachometer to measure the outer cylinder's speed.

If a concentric cylinder apparatus were "infinitely" long and the cylinders perfectly circular, the flow in the annulus would be perfectly laminar and two-dimensional. However, because of inevitable limitations in the construction of an apparatus, and particularly because rather short lengths have to be used resulting in noticeable end-effects, secondary flows are present. It was important to carry out flow tests to study the actual nature of the flow patterns. This information was obtained by injecting small quantities of latex suspensions into the annulus near an end-plate. Annular rings were formed showing that the flow was laminar. The inherent end-effects caused a slow circulation along the outside wall towards the centre of the apparatus and back along the inside cylinder as described by van Duuran (83). This resulted in the latex dispersion, after approximately 3 minutes, migrating to the centre and forming a sharp edge as shown in figure 25. There was no mixing between each half of the apparatus. This behaviour was noted at all speeds up to 300 rpm; above this speed rapid dispersion

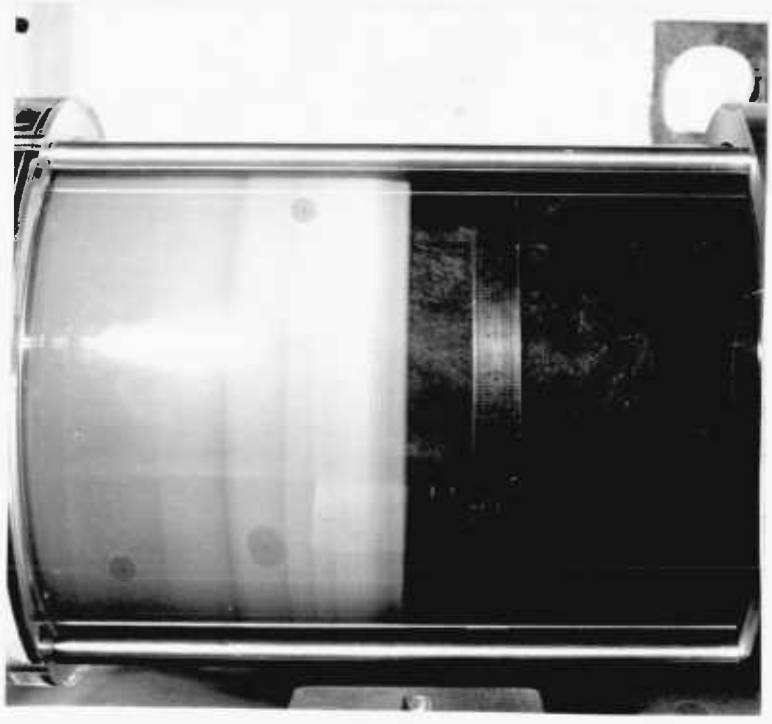
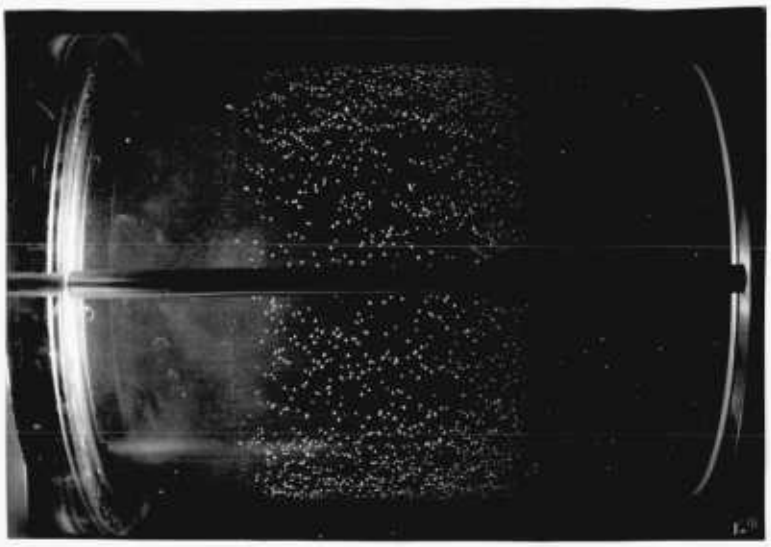


Figure 25 Dye tests. Formation of annular rings and their migration to the centre of the apparatus

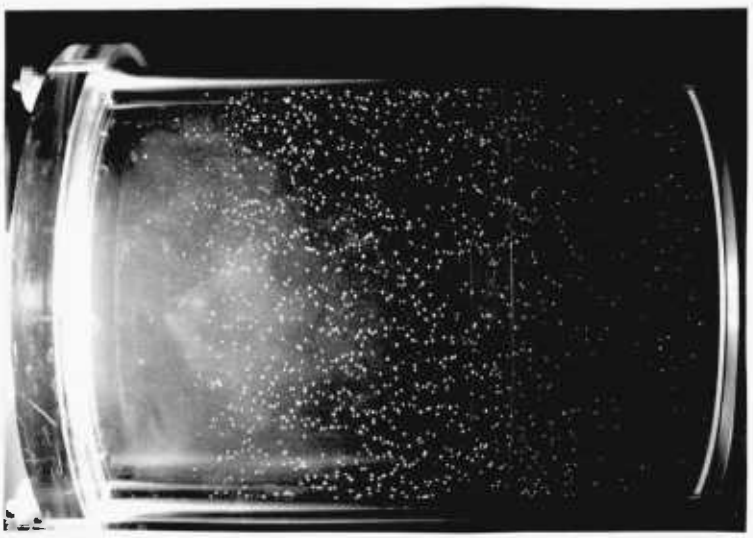
of the latex was caused by the onset of turbulence. The critical speed of 300 rpm corresponds to a Reynolds number of $1.54 \times 10^5$ which is slightly higher than the figure of $0.9 \times 10^5$ predicted by the earlier workers for this annular gap. (see figure 21), but well below those found by Shultz-Grunow (94). However, dye tracer tests have shown that the flow is stable up to this level.

To determine the extent of the secondary flows on particle trajectories, ion exchange beads (with a comparable density and size to those of the expected flocs) were introduced into the annulus and the position they adopted at various speeds of rotation of the outer cylinder were noted. At low speeds where end-effects were more pronounced, the beads travelled in a band approximately 10cm wide at the middle (see figure 26a). As the speed was increased, the beads became evenly distributed over the whole length of the apparatus (figure 26b). The beads were obviously slowly carried by the secondary circulation until they reached a stagnant zone near the middle of the apparatus where the slight centrifuging effect on them was sufficient to prevent them moving closer to the inner cylinder and continuing the circulation. The width of the stagnation zone was smallest at low speeds but covered the whole apparatus at higher speeds (above 200 rpm) where the flow was stabilized by the higher centrifugal forces.

From these observations, it was decided to restrict observations of flocs to the central 10cm zone where the effects of secondary flows would be small compared with that of the primary velocity gradient caused by



a) Rotation at 80 rpm



b) Rotation at 200 rpm

Figure 26 Photographs showing distribution of beads caused by secondary flows

rotation of the outer cylinder.

A photograph of the apparatus with its ancillary equipment is given in figure 27.

The experimental procedure used was as follows. The apparatus was filled from the primary header tank with distilled water which had been adjusted to pH 10 and contained the required quantity of $MgSO_4$. The filling was carried out very slowly to prevent excessive entrapment of air bubbles. The apparatus was then run for bursts of a minute, stopped and any air bubbles removed. This procedure was continued until all the air bubbles had been removed. The primary header tank was then refilled with the flocculating medium and this solution was rapidly run into the apparatus while it was running at 200 rpm. Then 1600ml of flocculating solution was run through the apparatus (i.e. twice the volume of the space in the annular gap). The speed was reset to 300 rpm and the beads, which had already been suspended in a $MgSO_4$ solution in a cylinder attached to the outlet side of the apparatus (not shown in figure 27), were rapidly drawn into the annulus by the suction created by a peristaltic pump. After 1 minute of high-speed rotation, the outer cylinder was abruptly stopped, creating severe turbulence which thoroughly dispersed the beads throughout the annular length. The outer cylinder was reset at a chosen low speed and the growth of flocs observed.

The method described above for the introduction of the beads was the only method found which gave consistent

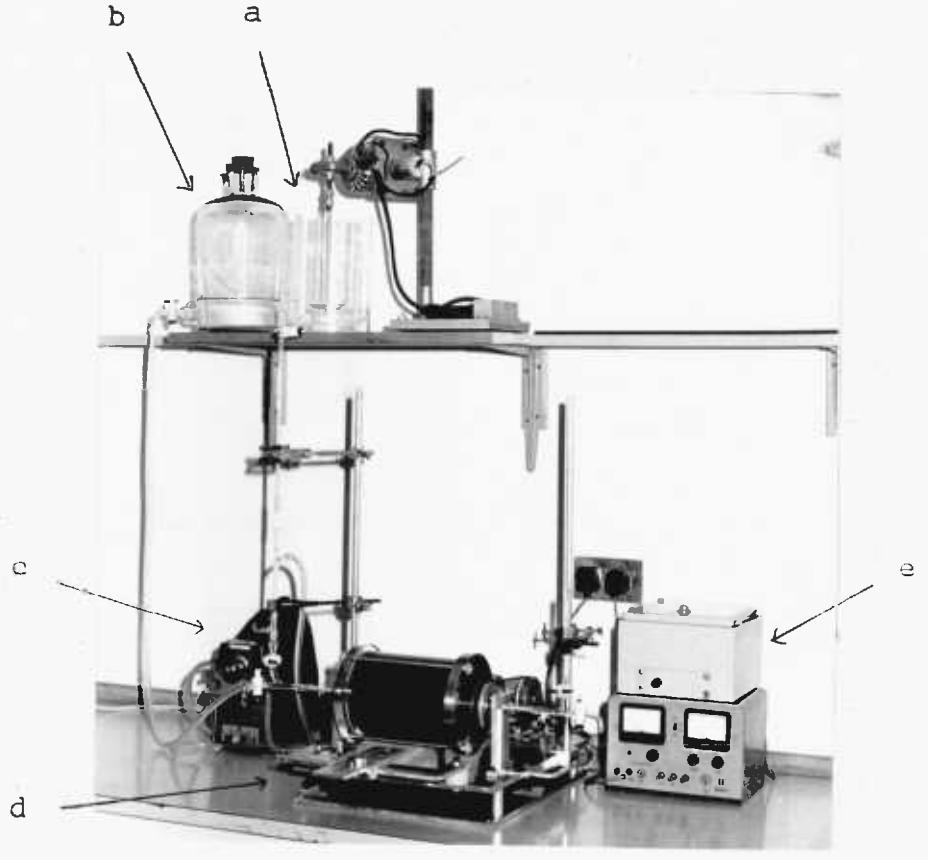



Figure 27 Photograph of rotating cylinder apparatus and ancillary equipment

a) primary header tank
b) secondary header tank
c) peristaltic pump
d) rotating cylinder apparatus
e) speed controller and indicator

results. Ideally, the flocculant should have been metered into the bead suspension as it entered the apparatus; but it was found impossible to prevent the beads flocculating while entering and a varying proportion of them sticking to the entry tubes. Another method considered was to suspend the beads in the annulus and add the flocculant in one quick dose. However, a concentrated flocculant solution would have been needed to prevent excessive displacement loss of the beads and thorough mixing of the flocculant throughout the annulus could not be achieved sufficiently quickly to prevent "over-dosing" of some beads and under-dosing of others. Hence, the reverse procedure of adding the beads to the already mixed flocculant solution was adopted.

The growth of flocs was recorded by photography. A high speed flash gun (Sunpak Auto Zoom 4000) capable of giving a flash of 1/50,000 second duration was used to illuminate the flocs, which were photographed through the wall of the outer cylinder.

It was calculated that flocs near the outer wall would have maximum speeds of 200 cm/sec and to "stop" them, movement during photographing must be less than 1/10th of their size. For a 1mm diameter floc, a movement of 0.1mm would take 1/20,000 seconds. A Pentax SLR camera with an f1.8 55mm focal length lens, mounted on a tripod 45cm from the outer cylinder was used to photograph the flocs. This gave a reduction of the image to 0.15 full size, but analysis of the film was carried out by

projecting the negatives onto a screen with a grid pattern printed on it. This gave an overall magnification of X2.5 full size. This was checked for each film by the spacings on a scale attached to the outer cylinder. The floc sizes could be determined to the nearest 0.5mm (magnified size) i.e. 0.2mm actual size. By taking photographs in this way, rather than by direct magnification of the image by close-up photography, the depth of focus was sufficient to give sharp images of all the flocs in the annular gap. Blurring only occurred at the top and bottom of the photograph because of curvature of the cylinders, but these areas were not included in the counting. The zone to be analysed was marked out on the grid and the projected floc sizes (maximum dimension) were read off into a tape recorder which was later played back to give the size distributions.

It took up to five minutes to reach an equilibrium (steady state) size distribution of floc growth; then the speed of rotation of the outer cylinder was increased in steps and the size distributions for each shear rate determined as before.

Using the previously mentioned equation for the tensile force acting on a doublet in Couette flow

$$P_1 = 4.41 \pi \eta \gamma b^2,$$

the range of forces on two adhering 1mm flocs as the speed was varied from 80 - 300 rpm was 0.75-2.81 $\mu$N, a factor of 10 greater than the forces required for single bead detachment in the centrifugal adhesion experiments.

The results obtained in this series of experiments are reported in Chapter 7.

# CHAPTER 7

## RESULTS AND DISCUSSION - Floc Properties

### 7.1. Jar Tests : Results

The jar test experiments were used to determine semi-quantitatively, the effect of the parameters ($MgSO_4$) and flocculant concentration, pH and bead size on the strength of flocculated glass beads. For the hydrodynamic conditions created in the size of beaker used, with the paddles described and at the two in-built speeds, it was found that $MgSO_4$ concentrations in the range 8 - 16 mM and flocculant concentrations of 5 - 30 p.p.m. were required.

The results for experiments carried out with a mixed size range of beads (5 - 40 μm diameter) are shown in figures 28-34. It can be seen from figure 28 that at 8mM $MgSO_4$ concentration, larger flocs were produced as the flocculant concentration was increased and that they persisted longer. Similarly, from figure 29 for which a constant flocculant concentration of 15 p.p.m. was used, the floc size and break-down resistance increased with increasing $MgSO_4$ concentration. The increase in floc size and resistance to break-down with pH at two $MgSO_4$ concentrations is shown in figure 30. At the high $MgSO_4$ concentration of 16 mM, a reversal in the resistance to break-down was found with flocculant concentration, as is shown in figure 31. This phenomenon was only observed with bead mixtures containing an appreciable proportion of smaller sizes beads (over 30% in the size range 5 - 15 μm). Increasing the bead concentration reduced the average floc size, as is shown in figure 32. However, the very small flocs produced at the higher bead concentration persisted longer (up to 30 minutes)

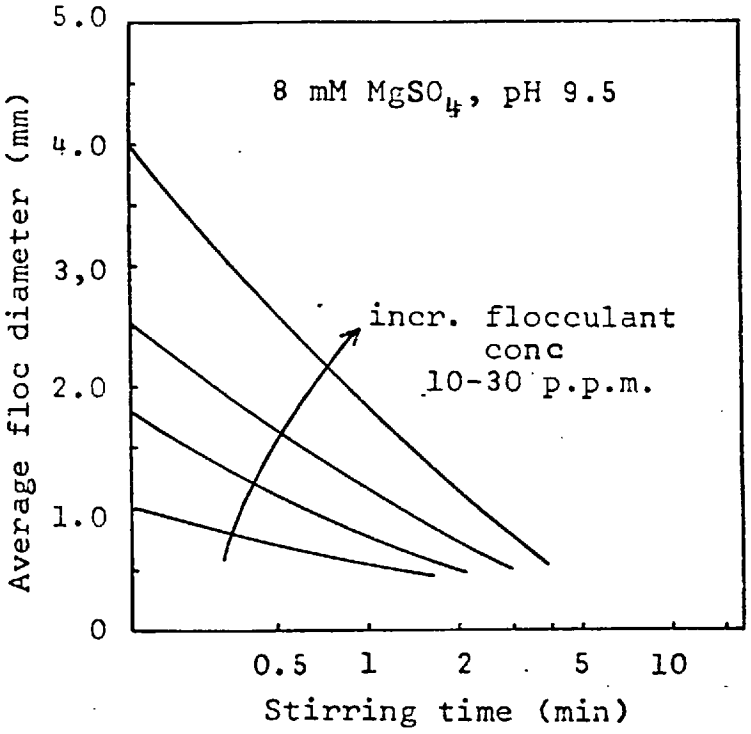



Figure 28 Jar tests - effect of flocculant concentration on floc size

0.25% w/v mixed size beads

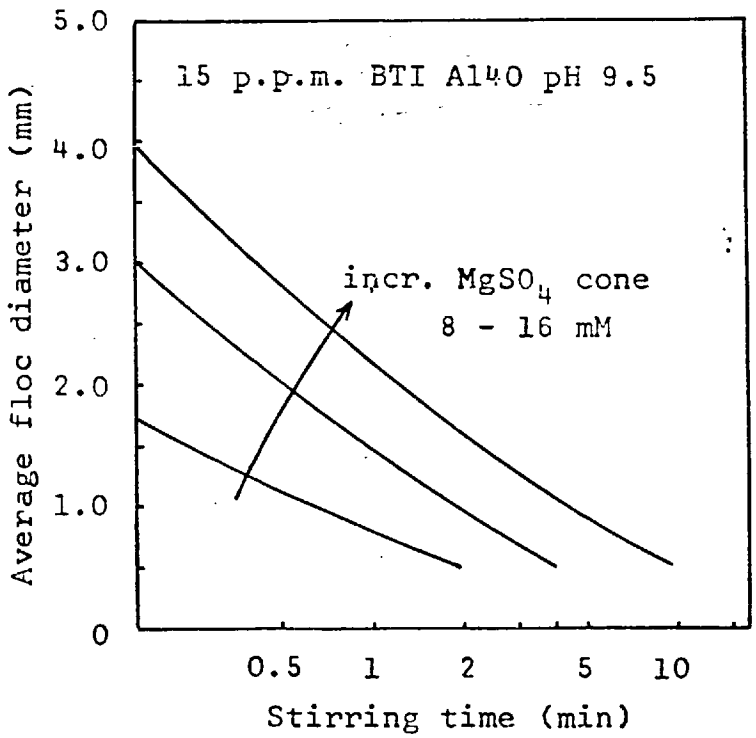



Figure 29 Jar tests - effect of $MgSO_4$ concentration on floc size

0.25% w/v mixed size beads

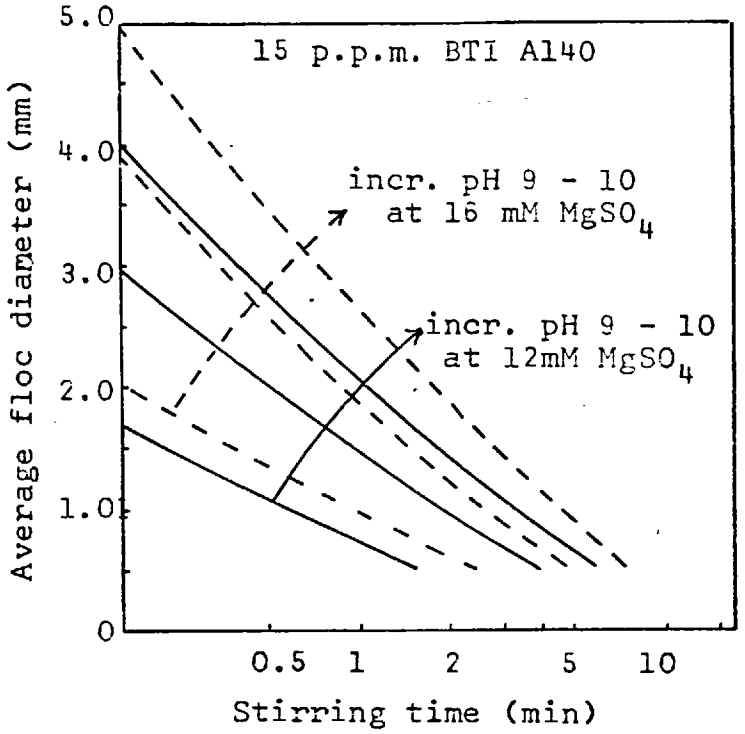



Figure 30 Jar tests - effect of pH on floc size
0.25% mixed size beads

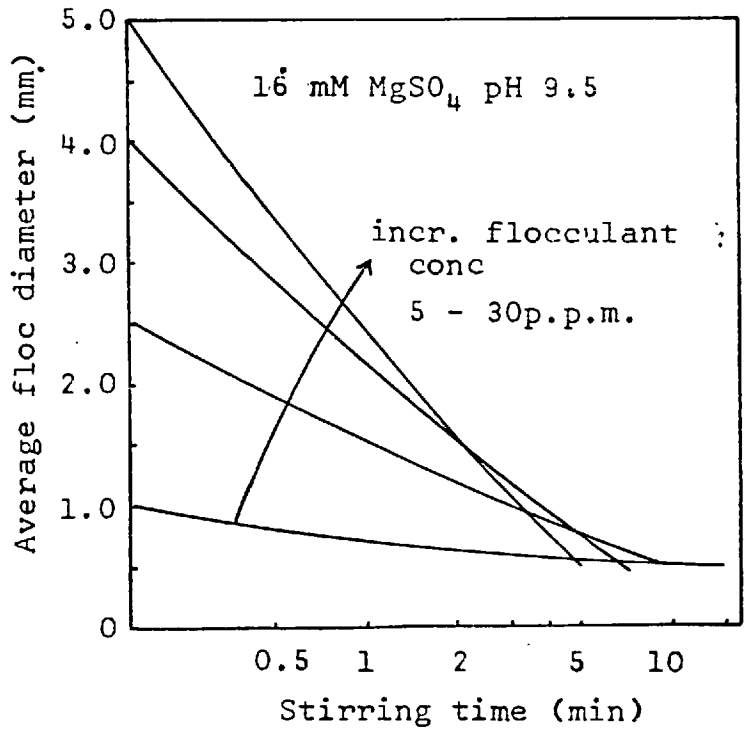



Figure 31 Jar tests - effect of flocculant concentration on floc size at a high $MgSO_4$ concentration (mixed and small bead sizes only)

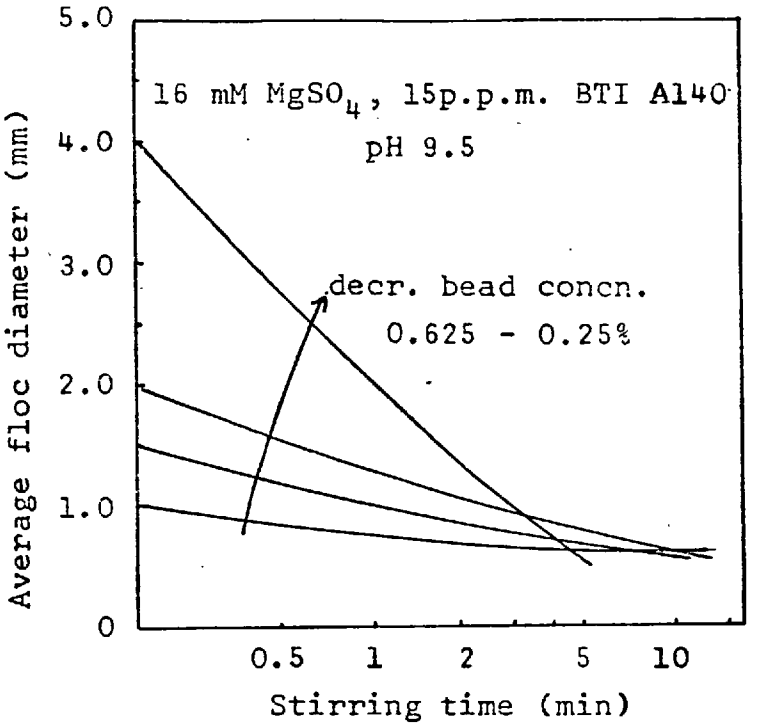



Figure 32 Jar tests - effect of bead concentration on floc size (mixed size beads)

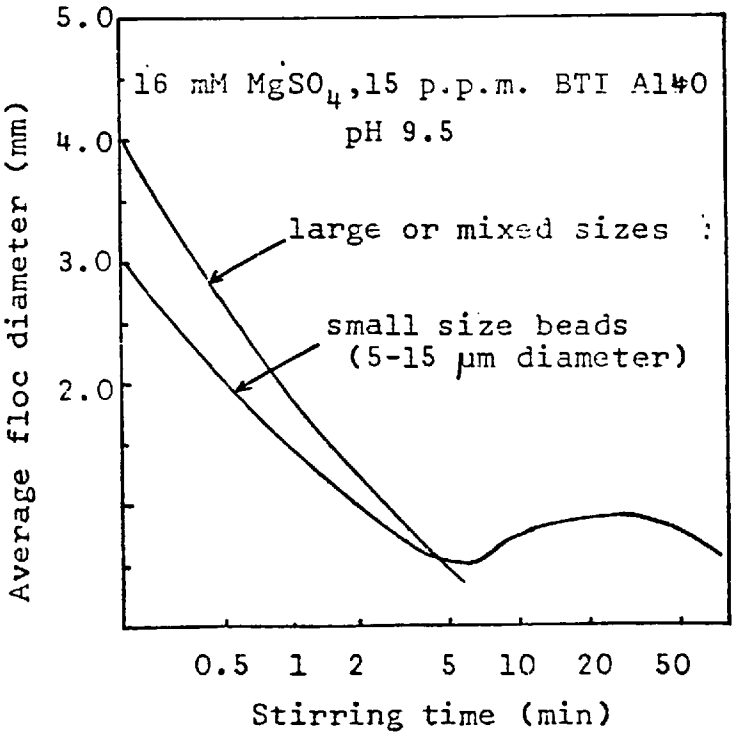



Figure 33 Jar tests - effect of bead size on floc size 0.25% bead concentration

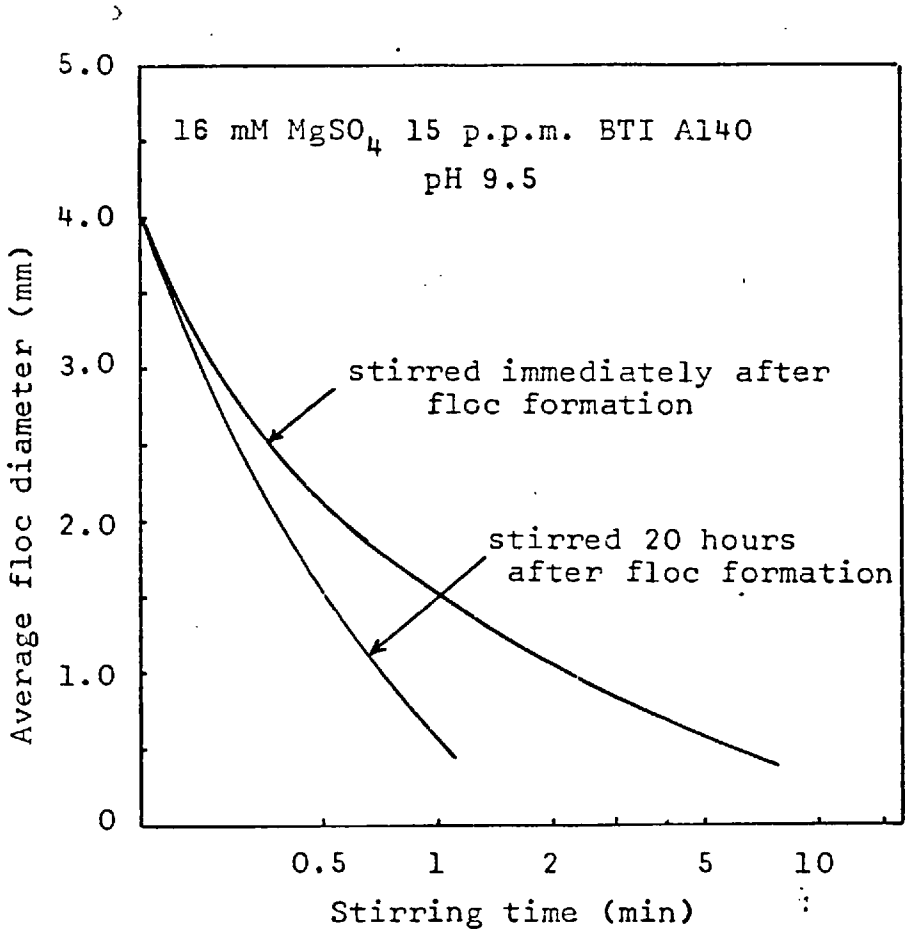



Figure 34 Jar tests - effect of delayed stirring on floc size

0.25% mixed size beads

before complete break-down.

At lower $MgSO_4$ concentrations, no visible difference in the size of flocs formed or their break-down resistance was observed with changing bead size over the range 5 - 40 μm. However, at 16 mM $MgSO_4$ concentration, there was a slight difference in the size of flocs formed (see figure 33). The small sized beads (5 - 15 μm) formed more compact flocs, which persisted longer and eventually re-agglomerated to form aggregates of flocs. These persisted for up to 1 hour before breaking down.

The effect of leaving the flocs overnight after their formation, before determining their behaviour at high speed stirring is shown in figure 34. Contrary to the finding in the adhesion measurements (where adhesion increased with time), it can be seen that flocs left overnight before shearing broke down considerably faster, indicating that they were weaker.

## 7.2. Rotating Concentric Cylinder Apparatus : Results

A range of $MgSO_4$ and flocculant concentrations were found at which floc formation could be observed for an outer cylinder speed of 80 rpm (average $\bar{\gamma}$= 54 $sec^{-1}$). Initially, a mixed size range of beads was used, 5 - 40 μm diameter, and the results for 0.125% w/v suspensions (1g in the annular volume of 800ml) are given in table 9 and figures 35-40.

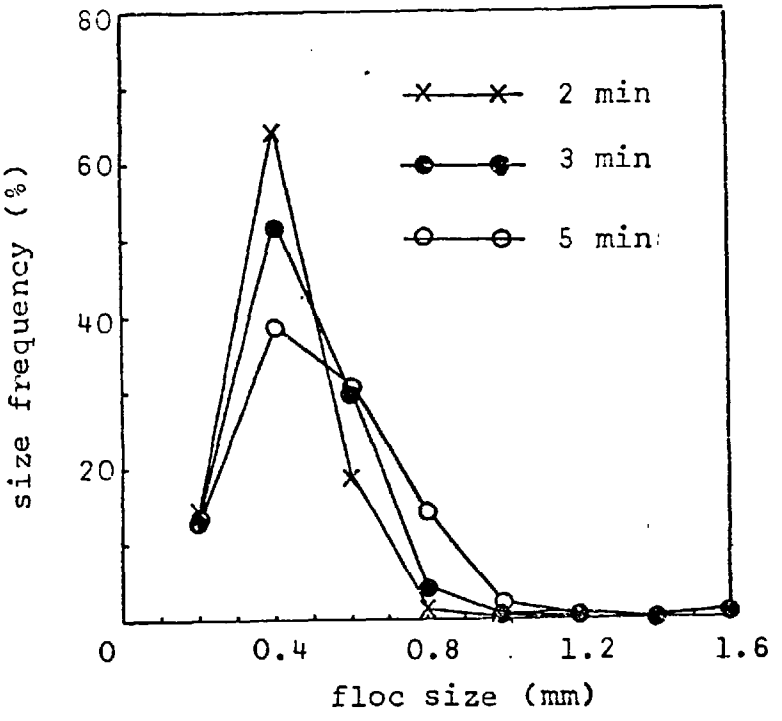



Figure 35a

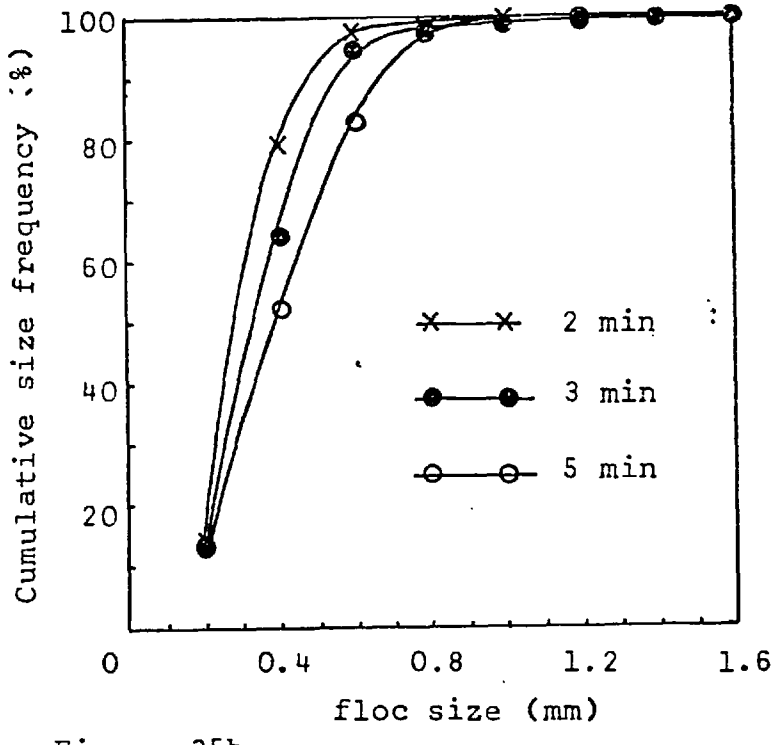



Figure 35b
Rotating cylinder experiments - floc formation at 80 rpm - variation of size distribution with time

0.125% w/v suspension of 5-40 μm beads, 4mM $MgSO_4$ 2.5 p.p.m. BTI A140 at pH 10

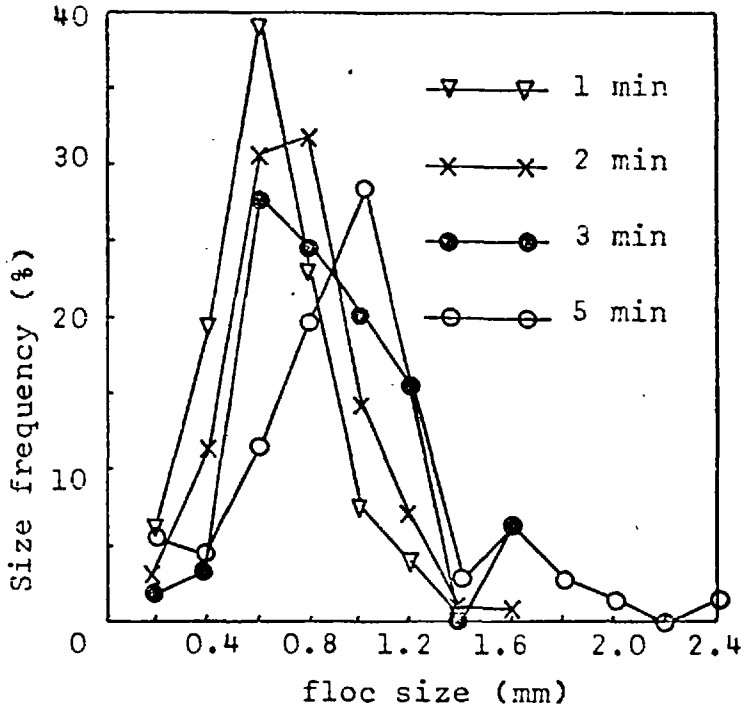



Figure 36a

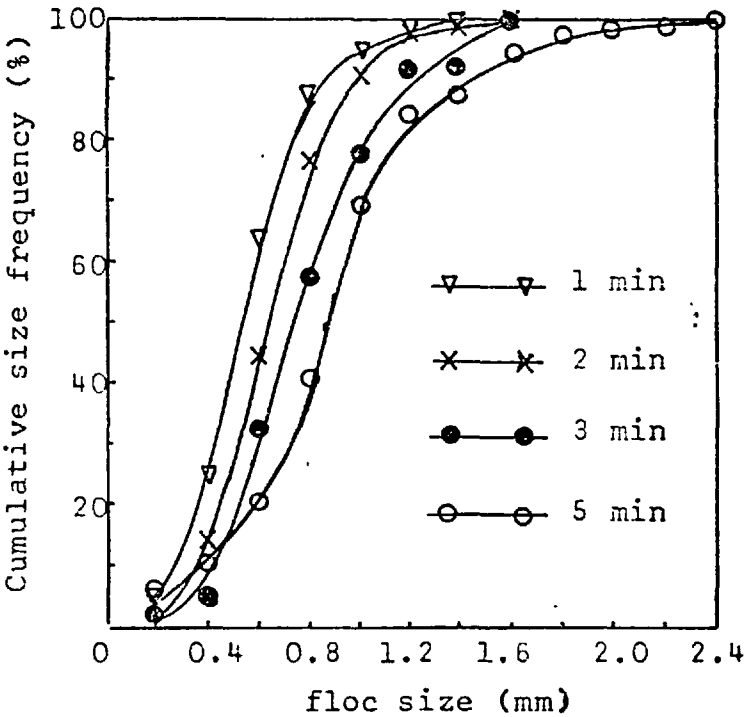



Figure 36b

Rotating cylinder experiments - floc formation at 80 rpm - variation of size distribution with time

0.125% w/v suspension of 5-40 μm beads, 4mM $MgSO_4$ 5 p.p.m. BTI A140 at pH 10

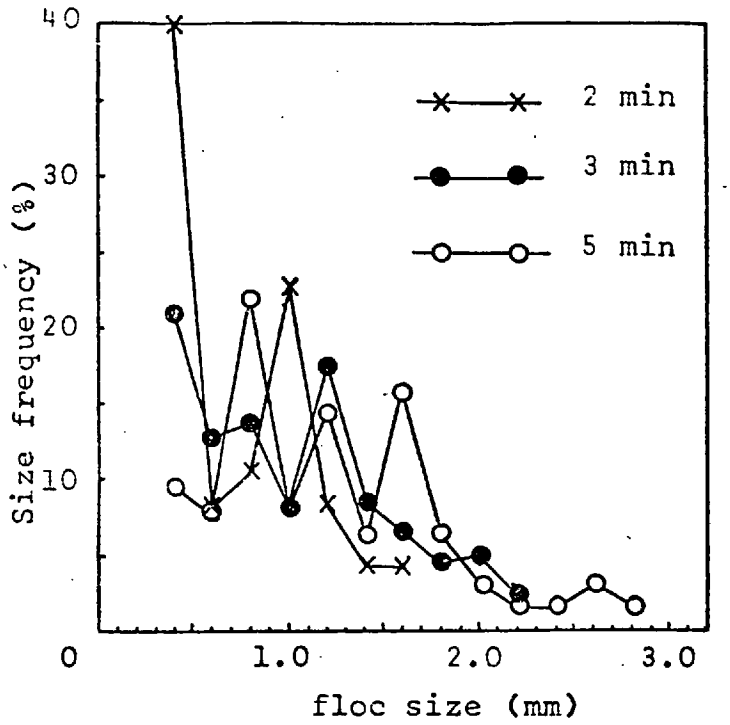



Figure 37a

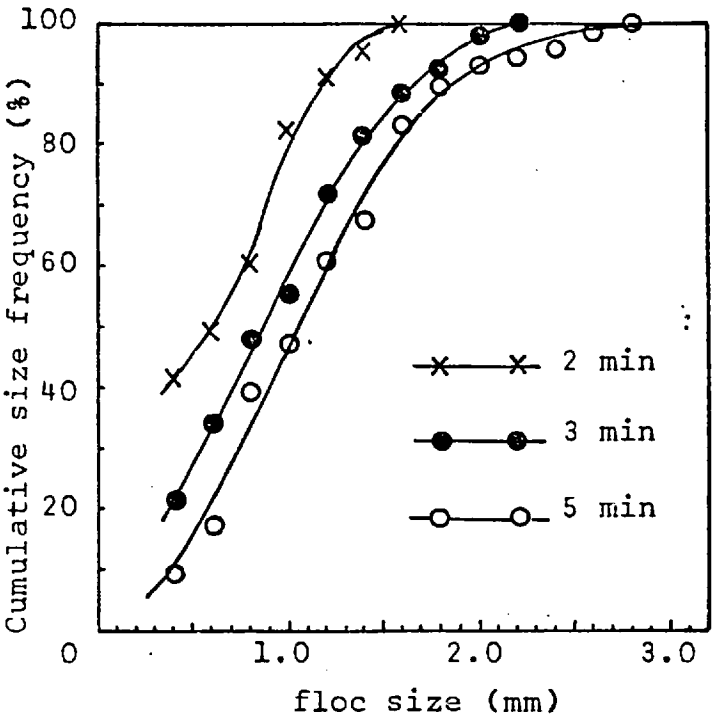



Figure 37b

Rotating cylinder experiments - floc formation at 80 rpm - variation of size distribution with time

0.125% w/v suspension of 5-40 μm beads, 6mM $MgSO_4$ 5 p.p.m. BTI A140

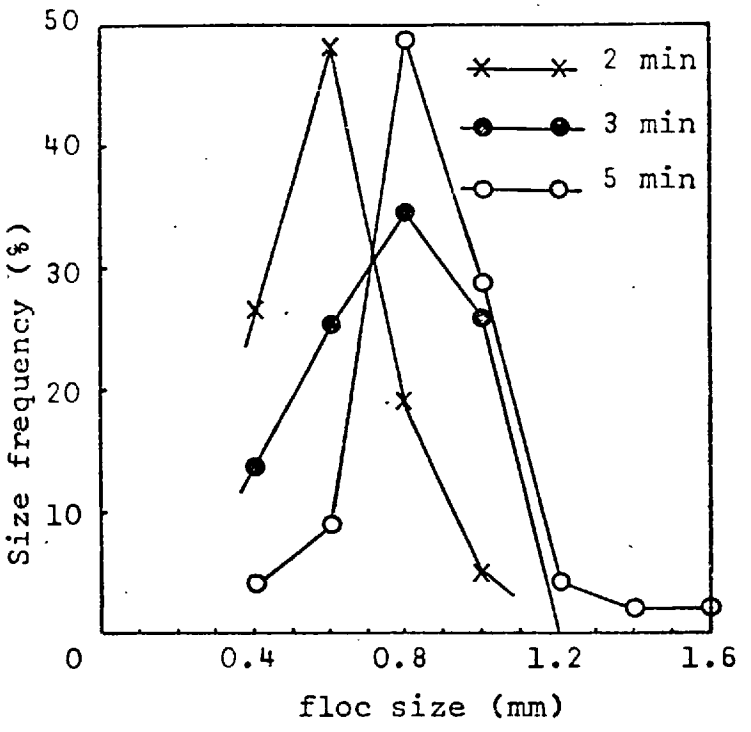



Figure 38a

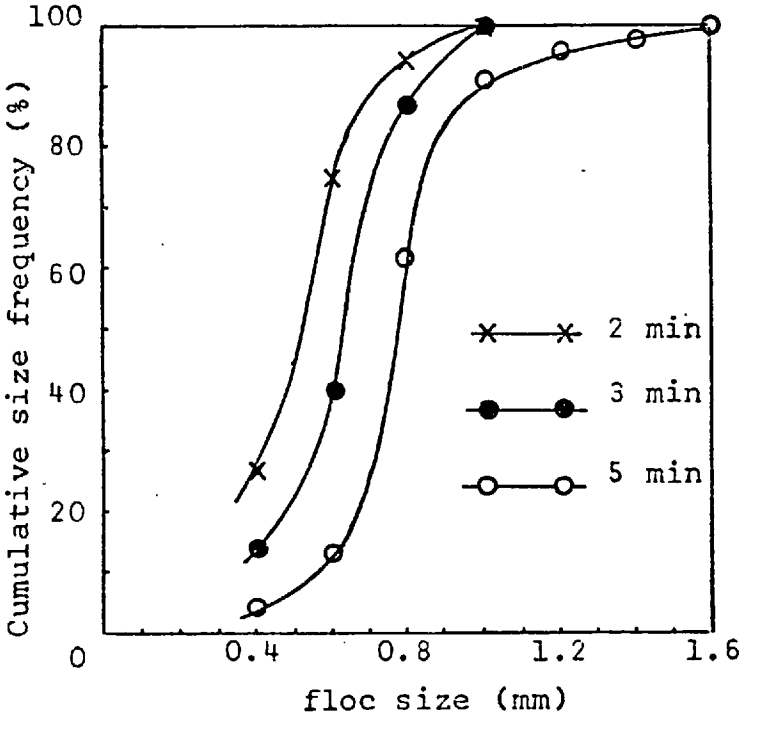



Figure 38b

Rotating cylinder experiments - floc formation at 80 rpm - variation of size distribution with time

0.125% w/v suspension of 5-40 μm beads, 8mM $MgSO_4$ 2.5 p.p.m. BTI A140 at pH 10

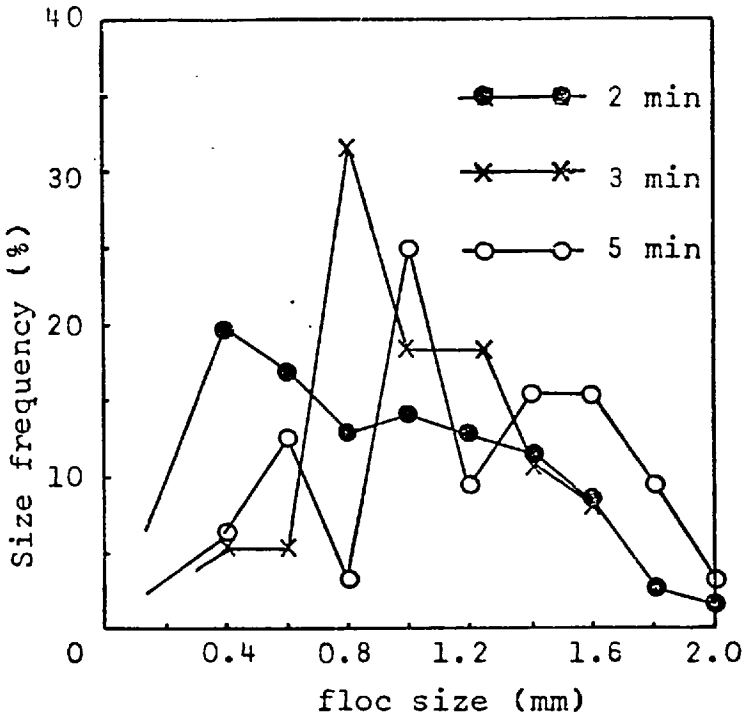



Figure 39a

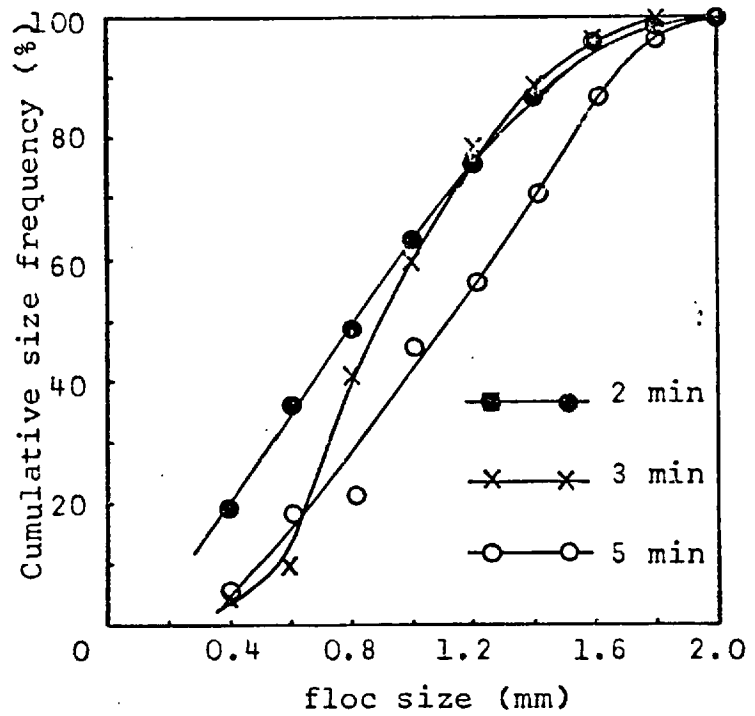



Figure 39b

Rotating cylinder experiments - floc formation at 80 rpm - variation of size distribution with time

0.125% w/v suspension of 5-40 μm beads, 8mM $MgSO_4$ 5 p.p.m. BTI A140 at pH 10

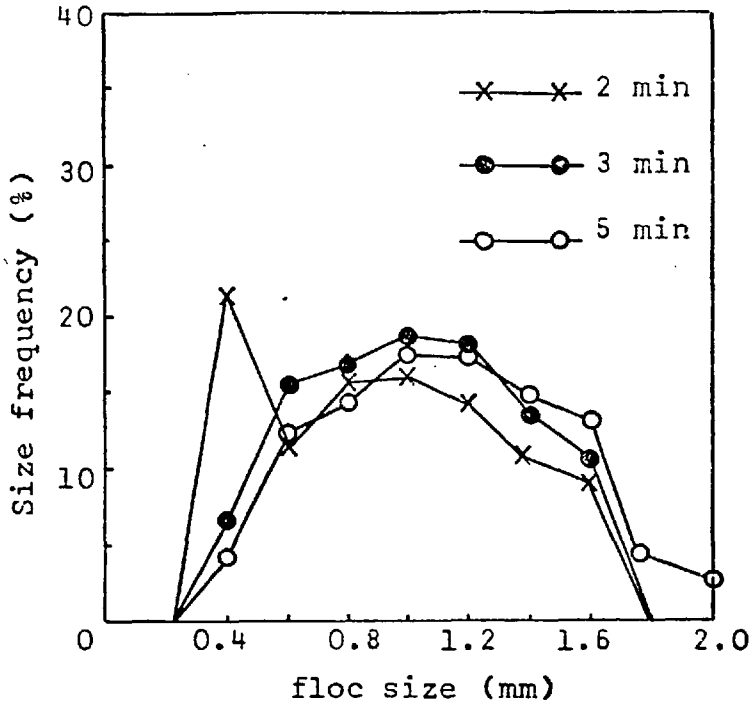



Figure 40a

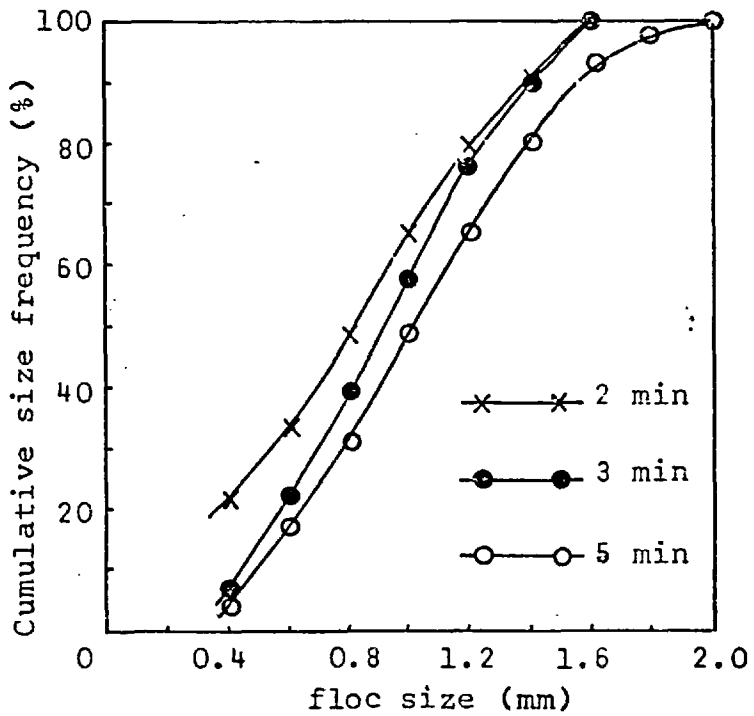



Figure 40b

Rotating cylinder experiments - floc formation at 80 rpm - variation of size distribution with time

0.125% w/v suspension of 5-40 μm beads, 16mM $MgSO_4$ 2.5 p.p.m. BTI A140 at pH 10

When flocculant concentrations less than 2.5 p.p.m. were used, no observable flocculation occurred with 4 mM $MgSO_4$; when 8 mM or 16 mM $MgSO_4$ concentrations were used, flocculation did occur but the flocs were too small to be measured. When flocculant concentrations of 10 p.p.m. or higher were used, flocculation was strong and rapid. However, the flocs formed were large (sometimes as big as 5mm) and consequently there were too few to obtain reproducible size distributions from the photographs. These large flocs could not be broken by increasing the speed of rotation up to 360 p.p.m. but only by suddenly stopping the outer cylinder from rotating at maximum speed, thus creating severe turbulence in the annulus.

The results shown in figures 35-40 all show that larger flocs and wider size distributions were obtained, as might be expected, when the time of flocculation was increased. Some experiments were continued for 10 or 15 minutes at 80 rpm but there was no change in the size distributions beyond those obtained at 5 minutes. However, beyond 15 minutes, degradation of the flocs began to occur, as shown by the appearance of a fine haze indicating that attrition of the flocs was occurring.

The average sizes of flocs obtained after 5 minutes for 0.125% suspensions are given in table 1.

TABLE 1

Variation of Average Equilibrium Floc Sizes with $MgSO_4$ and Flocculant Concentration 0.125% w/v Suspension of 5 - 40 μm beads. Rotation at 80 rpm

| $MgSO_4$ concn. (mM) | Flocculant concn. (p.p.m) | Average floc size (mm) |
|---|---|---|
| 4 | 2.5 | 0.51 |
| 4 | 5.0 | 0.99 |
| 6 | 5.0 | 1.22 |
| 8 | 2.5 | 0.87 |
| 8 | 5.0 | 1.19 |
| 16 | 2.5 | 1.13 |

The results obtained when the above suspensions were subjected to greater shear rates by increasing the speed of rotation are given in table 10 and figures 41-43. These results only cover the 6 mM and 8 mM $MgSO_4$ concentration suspensions. When the 4 mM suspensions were subjected to an increased shearing, the flocs grouped together to form loose aggregates of flocs and individual floc sizes could not be determined. The flocs (and aggregates) however, did break-down at still higher speeds. The results for the 16 mM $MgSO_4$ and 2.5 p.p.m. flocculant has not been tabulated because no floc break-down occurred with them.

All the flocs formed in the above suspensions could be completely broken-down by suddenly stopping rotation at high speed. If rotation was then immediately resumed (before the beads had settled out) the flocs could be re-formed, although there was always some background "haze", showing that

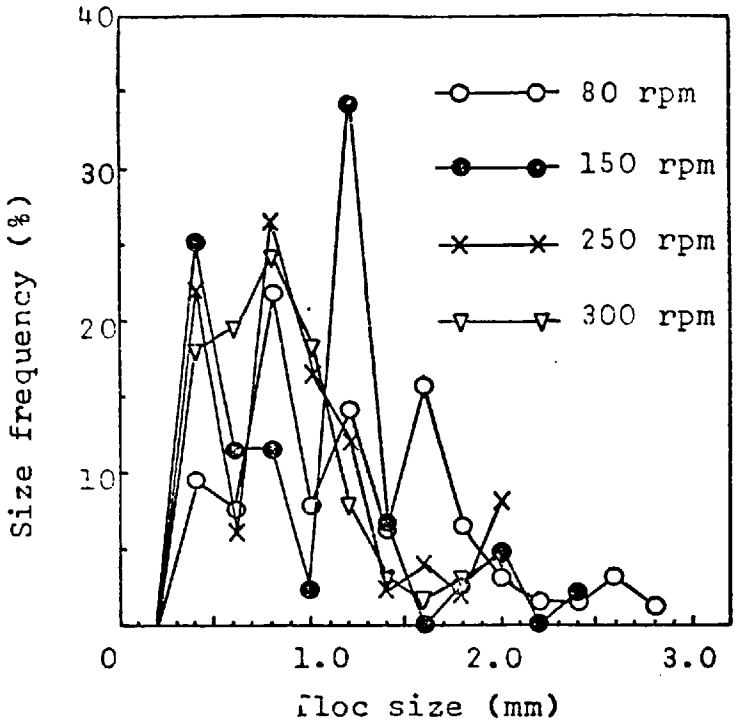



Figure 41a

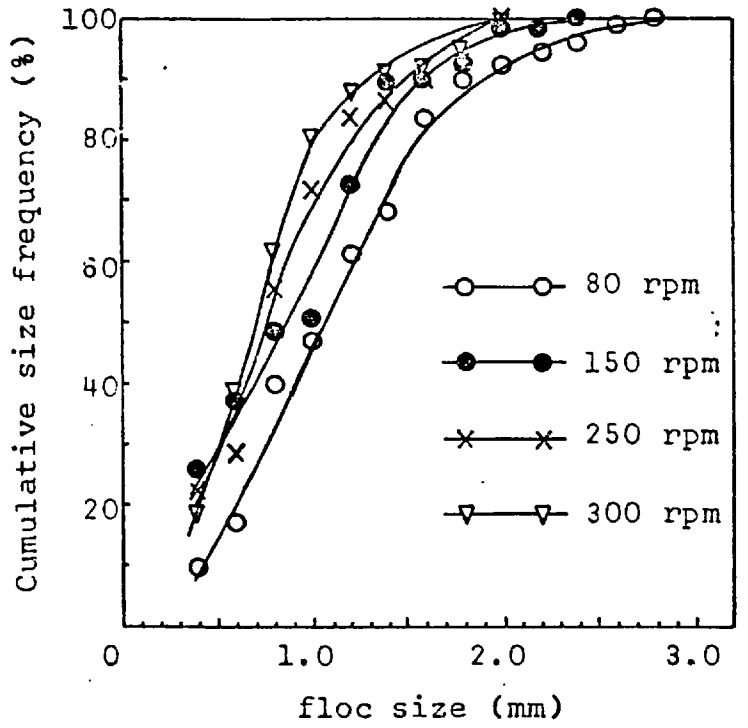



Figure 41b

Rotating cylinder experiments - floc break-down - variation of size distribution with speed of rotation

0.125% w/v suspension of 5-10 μm beads, 6mM $MgSO_4$, 5 p.p.m. BTI A140 at pH 10

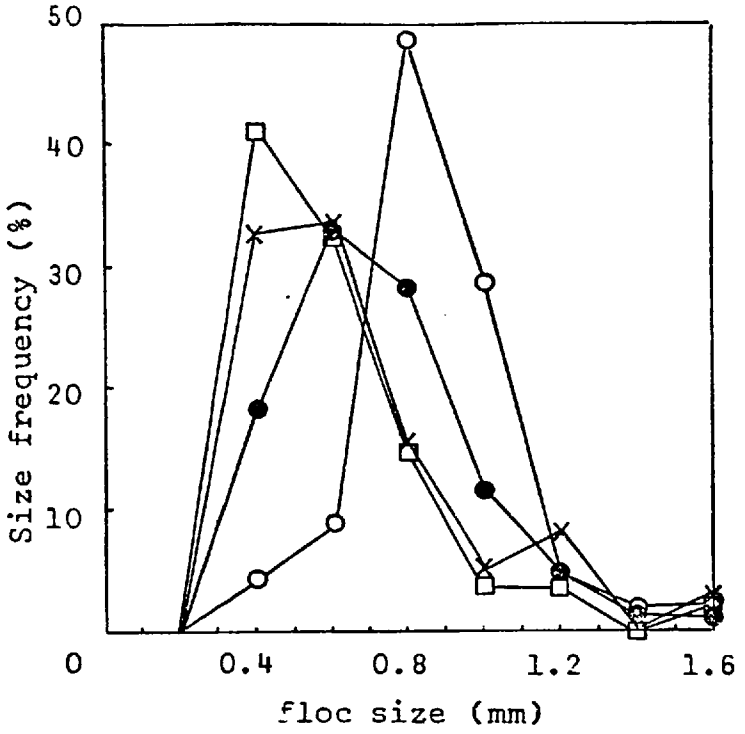



Figure 42a

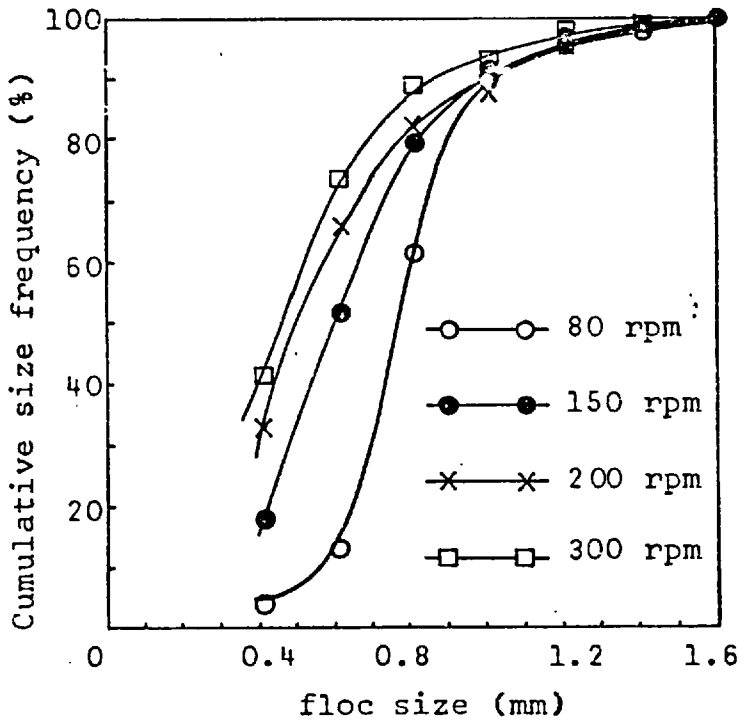



Figure 42b

Rotating cylinder experiments - floc break-down - variation of size distribution with speed of rotation

0.125% w/v suspension of 5-40 μm beads, 8mM $MgSO_4$, 2.5 p.p.m. BTI A140 at pH 10

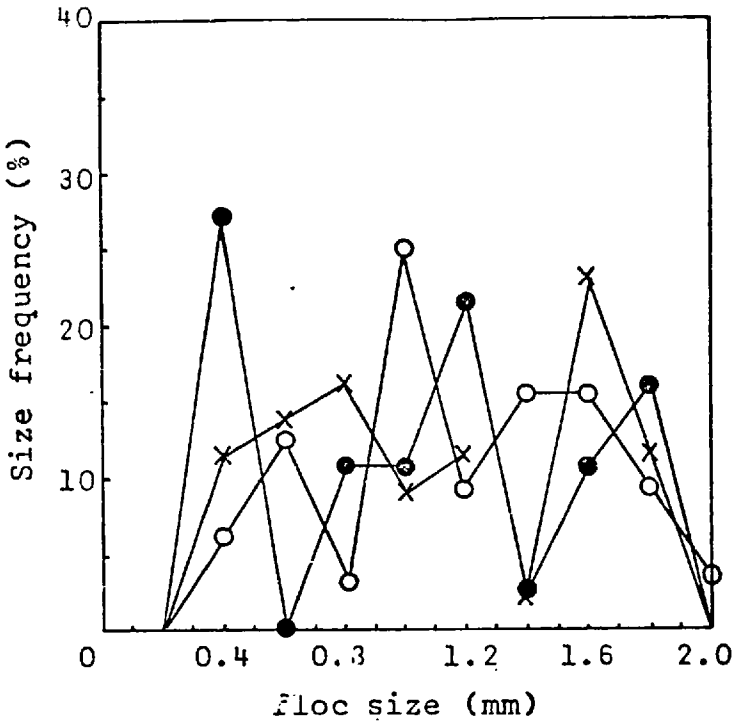



Figure 43a

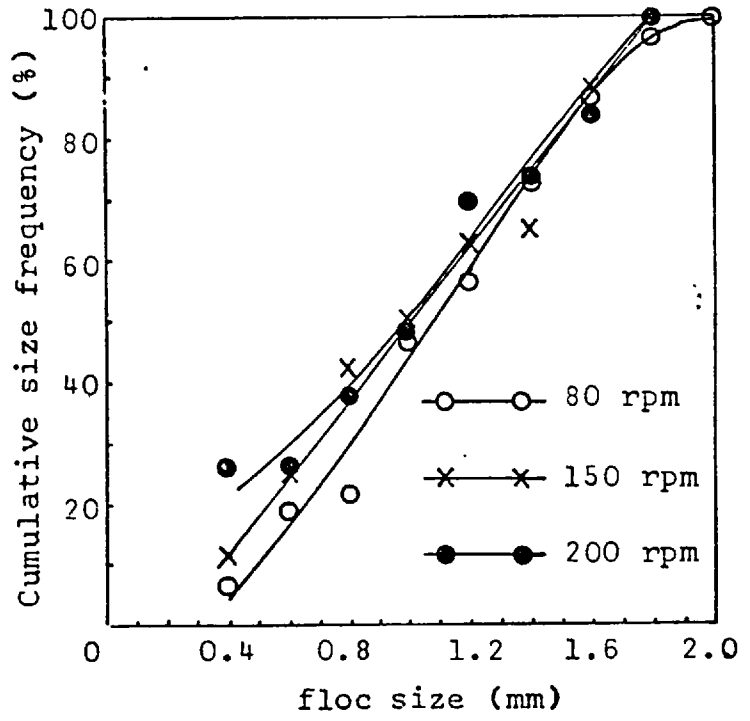



Figure 43b

Rotating cylinder experiments - floc break-down - variation of size distribution with speed of rotation

0.125% w/v suspension of 5-50 μm beads, 8mM $MgSO_4$, 5 p.p.m. BTI A140 at pH 10

some beads had been prevented from re-flocculating. Also, the flocs formed were weaker, breaking-down more easily when the speed was increased. Successive break-down and subsequent re-formation could be obtained a number of times, particularly at the lower flocculant concentrations.

The reduction in average floc size as the speed was increased in the case of 6 mM $MgSO_4$ and 5 p.p.m. flocculant and 8 mM $MgSO_4$ and 2.5 p.p.m. flocculant can be seen in figures 41 and 42. However, figure 43 shows that for at 8 mM $MgSO_4$ and 5 p.p.m. flocculant, little change in the floc size distribution occurred.

An attempt to determine the effect of bead concentration on floc size and strength was not successful, because at higher bead concentrations than 0.125% w/v, the clustering of aggregates previously mentioned occurred. The same trends of variation in size distribution with $MgSO_4$ and flocculant concentration were observed, but for smaller average floc sizes, but definitive results could not be obtained. When a lower bead concentration was used, only small sized flocs were produced that were generally too small to be measured or at higher chemical concentrations, the large numbers of relatively small flocs also formed clusters. The only case in which clustering did not occur was for a 0.0625% suspension (0.5g in 800ml) with 8 mM $MgSO_4$ and 5 p.p.m. BTI A140, the results for which are given in table 11 and figure 44. It can be seen that there was a high proportion of small sizes compared with the similar case for a 0.125% w/v suspension. The average floc size was only 0.57mm, compared with 1.03mm. The size distribution did not alter appreciably when the speed of rotation was increased.

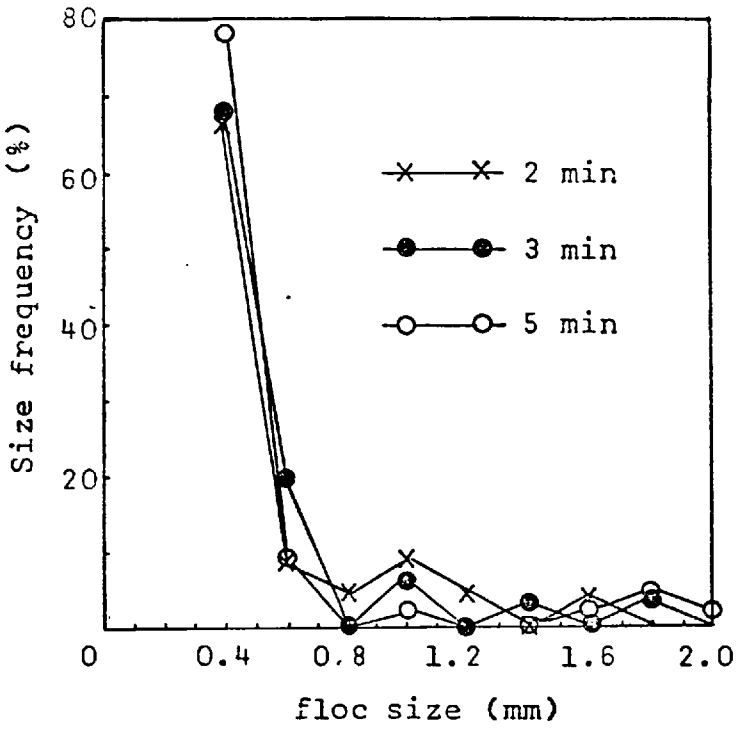



Figure 44a

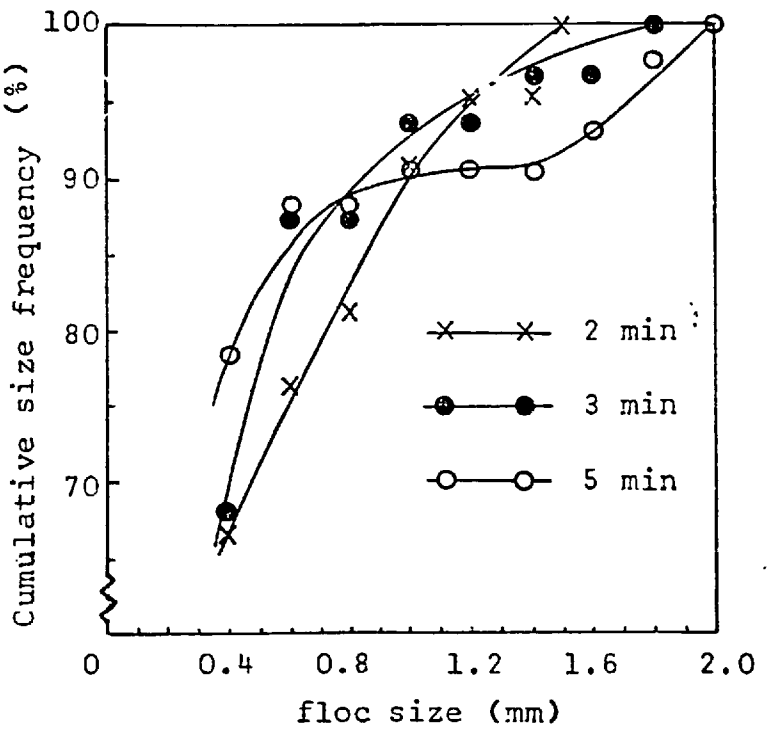



Figure 44b

Rotating cylinder experiments - floc formation at 80 rpm - variation of size distribution with time

0.0625% w/v suspension of 5-40 μm beads, 8mM $MgSO_4$, 5 p.p.m. BTI A140 at pH 10

The effect of bead size on floc properties was determined for a 0.125% suspension at 8 mM $MgSO_4$ and 5 p.p.m. flocculant concentration. When small sized beads were used (10 - 16 μm diameter range with an average size of 13 μm) flocculation was improved. A floc size distribution with an average (number average, $\Sigma nx/n$) size of 1.60mm resulted, compared with 1.18mm for the wider size range (5 - 40 μm). On increased shearing, the average floc size was reduced to 1.42mm at 150 rpm (100 $sec^{-1}$) and 1.60mm at 200 rpm (135 $sec^{-1}$). The results are given in table 12 and figure 45. However, when large sized beads were used (32 - 45 μm diameter range, average 35 μm), poor flocculation resulted as is shown in table 13 and figure 46. Most of the flocs were confined to the 0.4 - 0.6mm range and the proportion of these sizes increased with the speed of rotation.

Some experiments were also carried out with crushed glass powder to determine whether having angular particles instead of spherical beads had any noticeable effect on floc behaviour. In the first experiments flocculation appeared to be improved by using the crushed glass; but when the particle size distributions were more closely matched by reducing the proportion of very small sizes of crushed glass or spherical beads identical results were obtained. These results are given in table 14 and figure 47.

## 7.3. Discussion

The jar tests have confirmed that floc strength, as indicated by the size of flocs formed and their resistance to break-down by shearing, increases with increasing $MgSO_4$ and flocculant concentrations and increasing pH. (The conditions employed were such

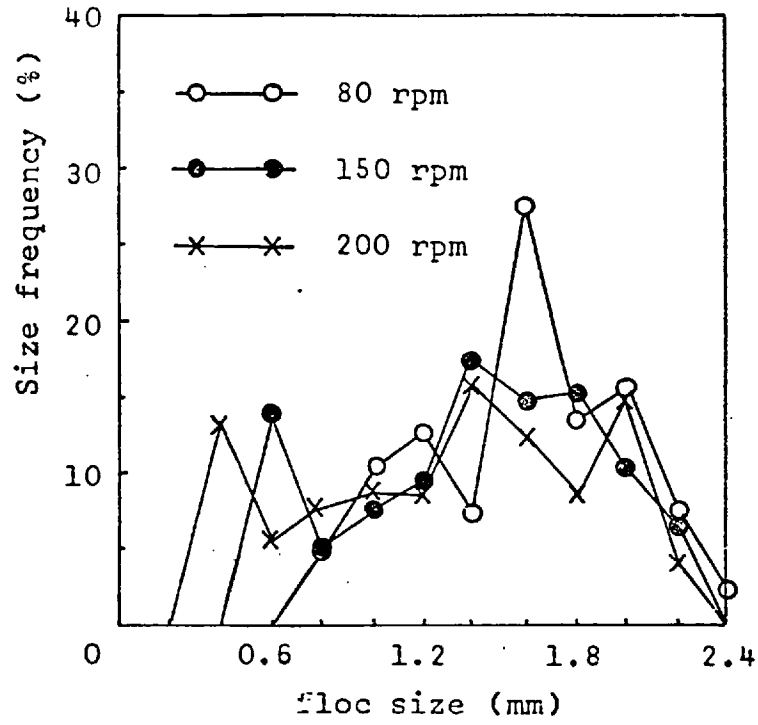



Figure 48a

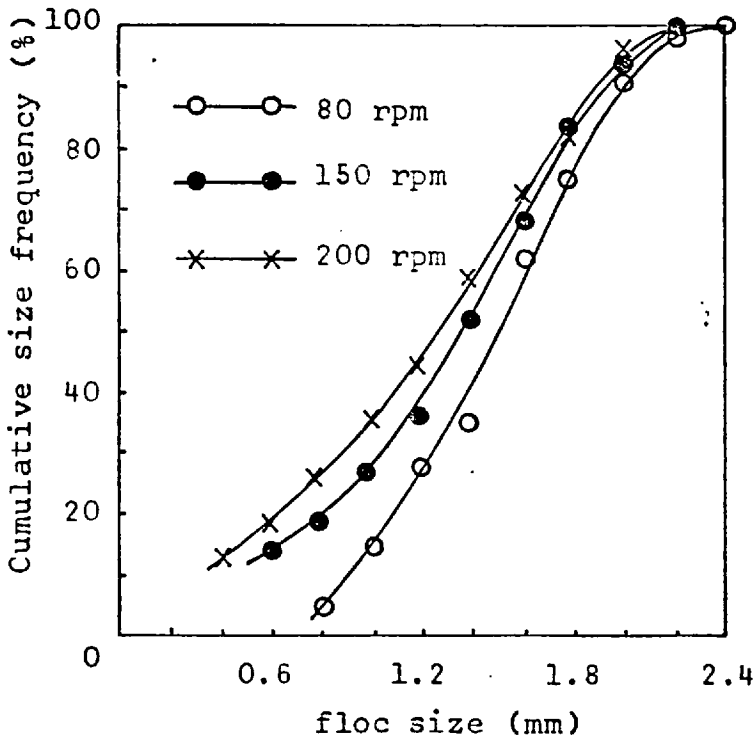



Figure 45b

Rotating cylinder experiments - floc break-down - variation of size distribution with speed of rotation

0.125% w/v suspension of 10-16 μm beads, 8mM $MgSO_4$, 5 p.p.m. BTI A140 at pH 10

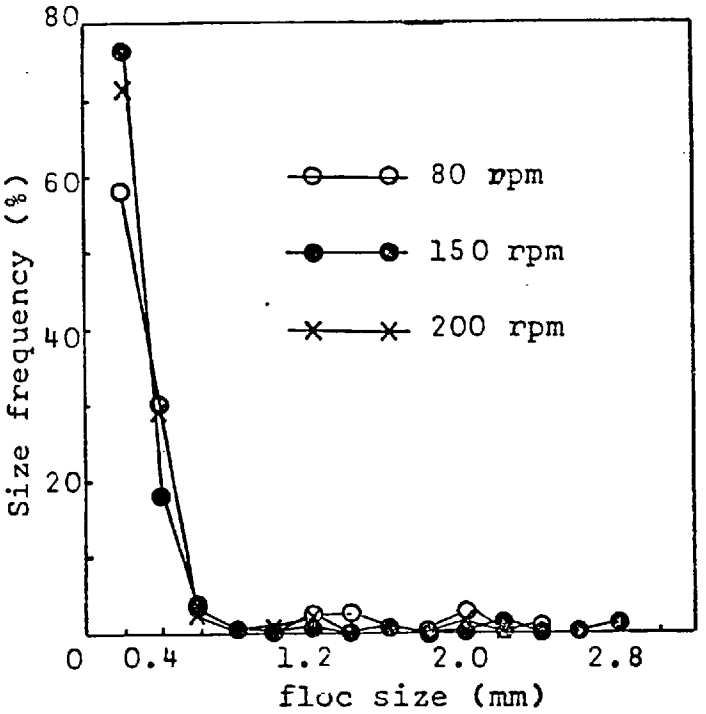



Figure 46a

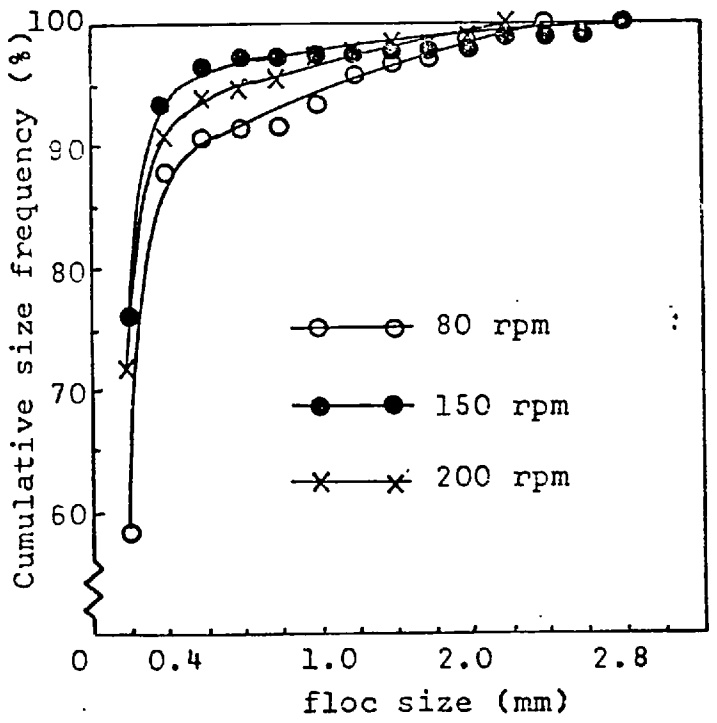



Figure 46b

Rotating cylinder experiments - floc break-down - variation of size distribution with speed of rotation

0.125% w/v suspension of 32-45 μm beads, 8mM $MgSO_4$ 5 p.p.m. BTI A140 at pH 10

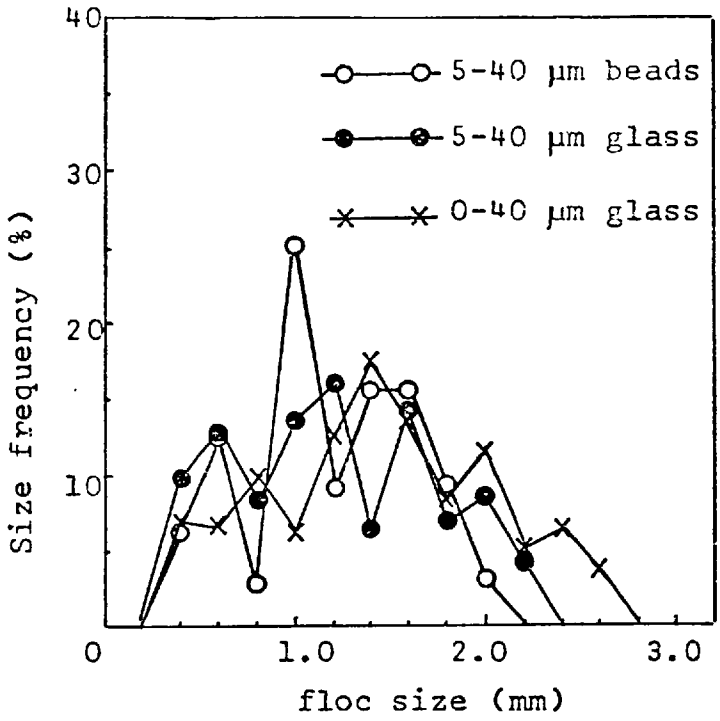



Figure 47a

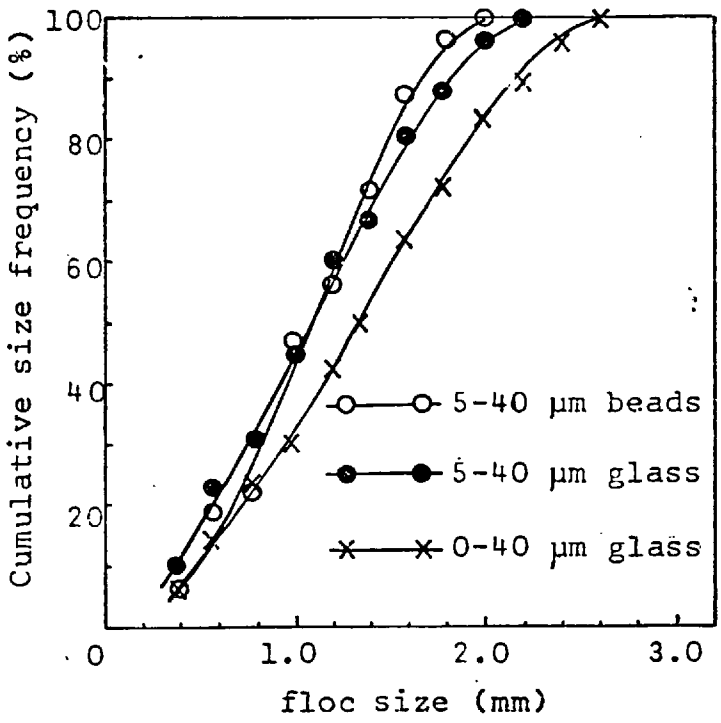



Figure 47b

Rotating cylinder experiments - size distributions after 5 minutes rotation at 80 rpm - variation of size distribution with particle-type

0.125% w/v suspensions, 8mM $MgSO_4$, 5 p.p.m. BTI A140 at pH 10

that no precipitation of $Mg(OH)_2$ occurred and that precipitation of the flocculant by $MgSO_4$ could only be observed in solutions where there were no beads present and the solutions had been left standing for a long time). Parallel results were previously found in the adhesion measurements, confirming that the strength of the inter-particle bonds governs the strength of the floc. However, contrary to the adhesion measurements, the strength of the flocs was found to decrease markedly when already formed flocs were left for 20 hours before commencing break-down by high speed stirring. This effect can be explained by recognising that although it may become more difficult to break the inter-particle bond with time, once a bond has been broken by polymer scission or detachment of the flocculant molecule from the surface, re-arrangement of the polymer molecules on the surface and the reduction in average polymer length will make re-flocculation more difficult. A floc subjected to shearing will have stresses set up throughout the aggregate. These will progressively break the weakest links within the floc but re-formation of the bonds may be possible as the floc rotates and the stress field alters. However, if because of a shortening of the polymer chain and fewer adsorption sites being available, re-flocculation is reduced, the floc break-down will occur more readily. Thus the essential difference between the two types of experiment lies in the fact that one is static adhesion while the other is a dynamic make-and-break situation.

The increase in the strength of adhesion with $MgSO_4$ and flocculant concentration was also demonstrated by the increase in the average floc size in the rotating cylinder apparatus (figure 48). The mean increase in floc size upon doubling the flocculant concentration from 2.5 - 5.0 p.p.m. was x 1.9 for 4 mM $MgSO_4$ and x 1.4 for the 8 mM $MgSO_4$ results. This is not as great

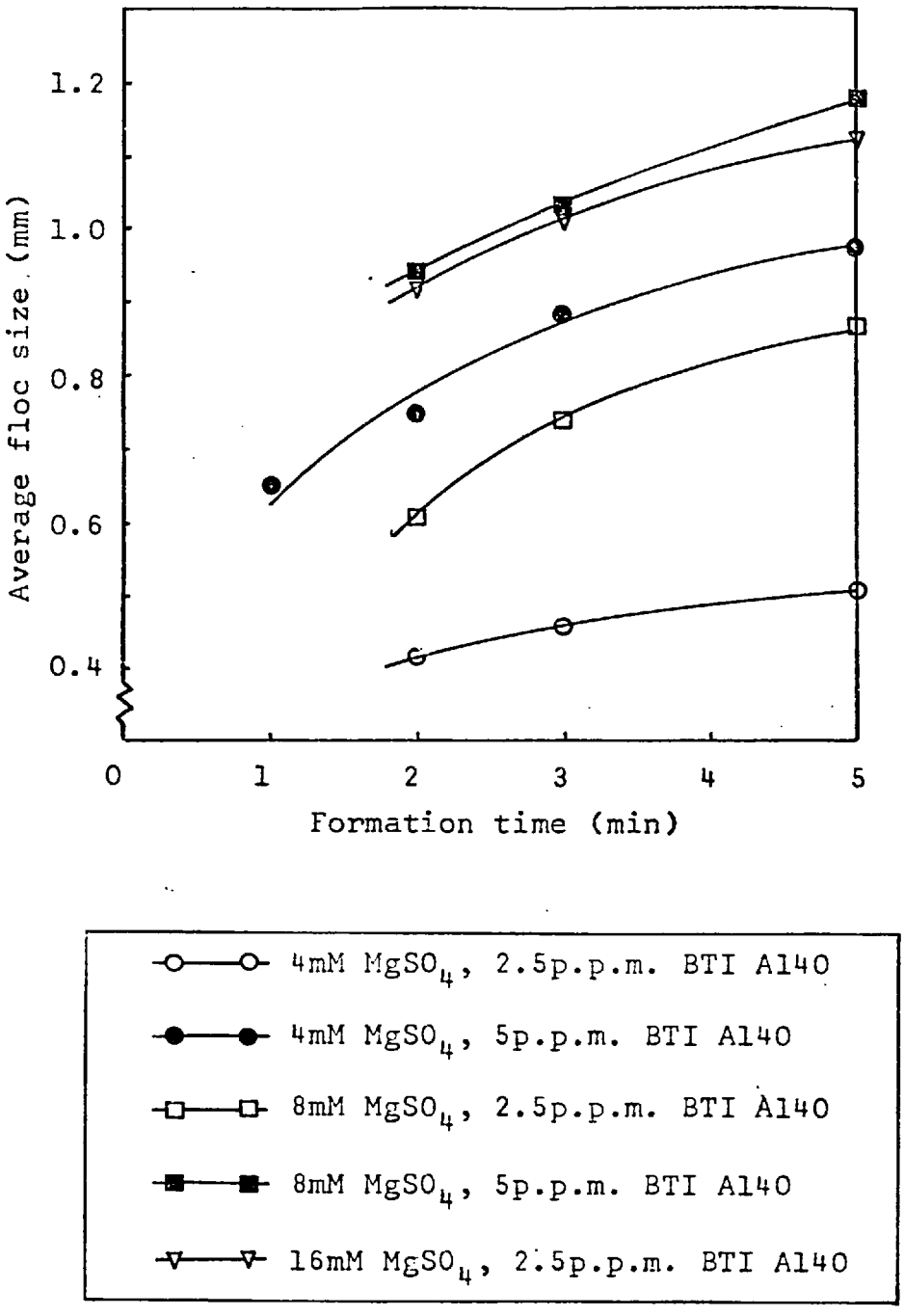



Figure 48

Rotating cylinder experiments - effect of $MgSO_4$ and flocculant concentration on average floc size

0.125% w/v suspensions, rotation at 80 rpm

as the x 2.5 result for the strength of adhesion measured by the centrifugal method for 8 mM $MgSO_4$. However, as the floc size is not only controlled by the strength of adhesion but also by the shearing conditions, there will be a limit to the formation of larger floc sizes with increased adhesion and a simple x 2.5 result would not be expected here.

Figures 41 - 43 show that floc size did, indeed, decrease as the speed of rotation was increased, in agreement with the jar test results. These data have been replotted on logarithmic scales against the shear rate (figure 49). The slopes of the lines are - 0.12, - 0.25 and - 0.23 giving an average floc size

$$d_{av} \propto \gamma^{-0.2}$$

where $d_{av}$ is the average floc diameter. This result differs from Tomi and Bagster's prediction of $d_{max} \propto \gamma^{-0.5}$ (112); however, there are many restrictive assumptions in their model. Also, the relationship found from these results is for an average floc size not for a maximum floc size.

A comparison of figures 37 and 44 shows that considerably poorer flocculation was obtained at the lower bead concentration of 0.0625%, there being a high proportion of small sizes present. Slower flocculation would be expected from kinetic considerations because the collision frequency would be reduced. In the present dynamic process of flocculation a particle's availability for flocculation becomes reduced with time as the potential sites for adsorption decrease; hence if the collision process is slower, poorer flocculation will result.

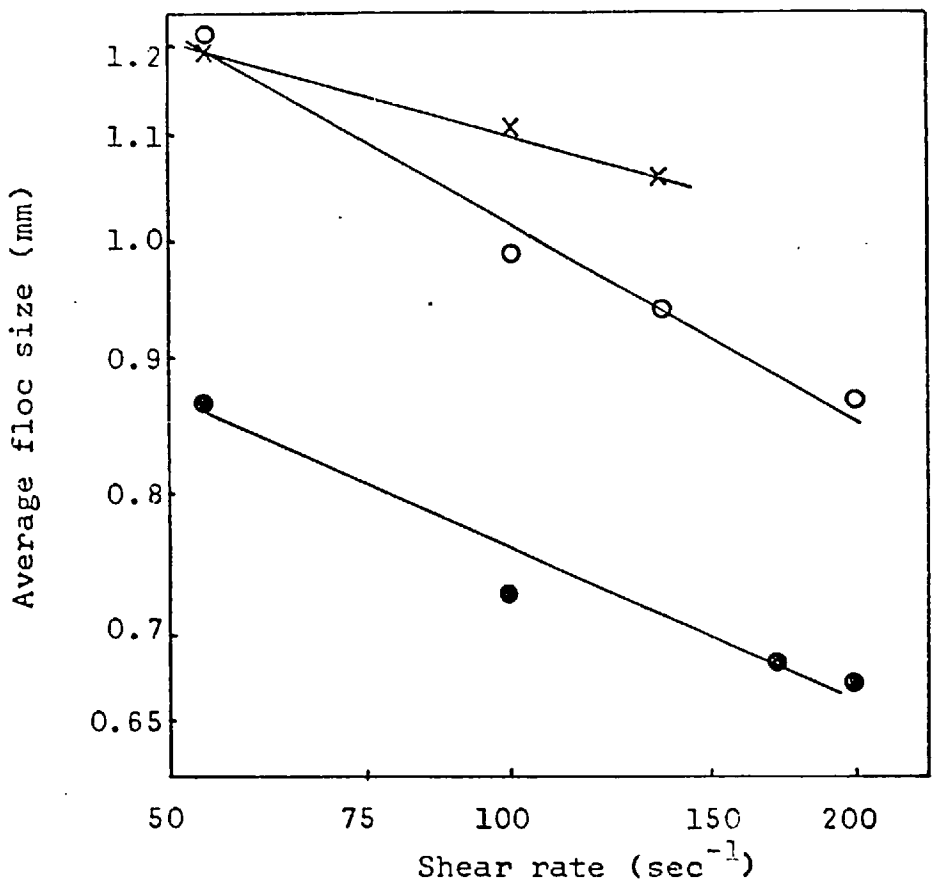



Figure 49

Rotating cylinder experiments - variation of average floc size with shear-rate (log scales)

0.125% w/v suspensions

The bead size also has a pronounced effect on flocculation, as can be seen by comparing figures 37, 45 and 46. These results have been replotted as average floc diameters (figure 50). The results for the small beads (13 μm diameter) show a - 0.23 power dependence on shear rate, in agreement with the results for the wider size range beads. A calculation was not made for the larger beads because of the errors inherent in counting the large numbers of small flocs in this case. Suspensions containing an appreciable proportion of small sized beads would be expected to give improved flocculation results for two reasons. Firstly, there will be a greater number of particles in suspension and for the reasons described above, this will result in more rapid flocculation and, hence, stronger flocculation. Secondly, the stresses acting on a floc in a shear field will cause some rearrangement of the structure to reduce the stresses (i.e. to tend towards approximately spherical shape - and this was what was observed, flocs were compact and nearly spherical). If there are a significant number of small particles present these will be able to give a denser packing, resulting in an increase in the number of links for any given plane of observation through the floc. Hence flocs will be stronger. This was also demonstrated in the case of the crushed glass particles (figure 47) when there was a high proportion of small sizes particles. When the size distributions of the beads and crushed glass were similar, there was little difference, as predicted by Goodarz-Nia and Sutherland's model of aggregate structure (111).

The results obtained in these experiments are probably not exactly the same as those that would be found in the more usual case where "colloidal" particles are flocculated, because the perikinetic stage of aggregate formation is not present. Floc formation usually first proceeds by the aggregation of the sub-micron

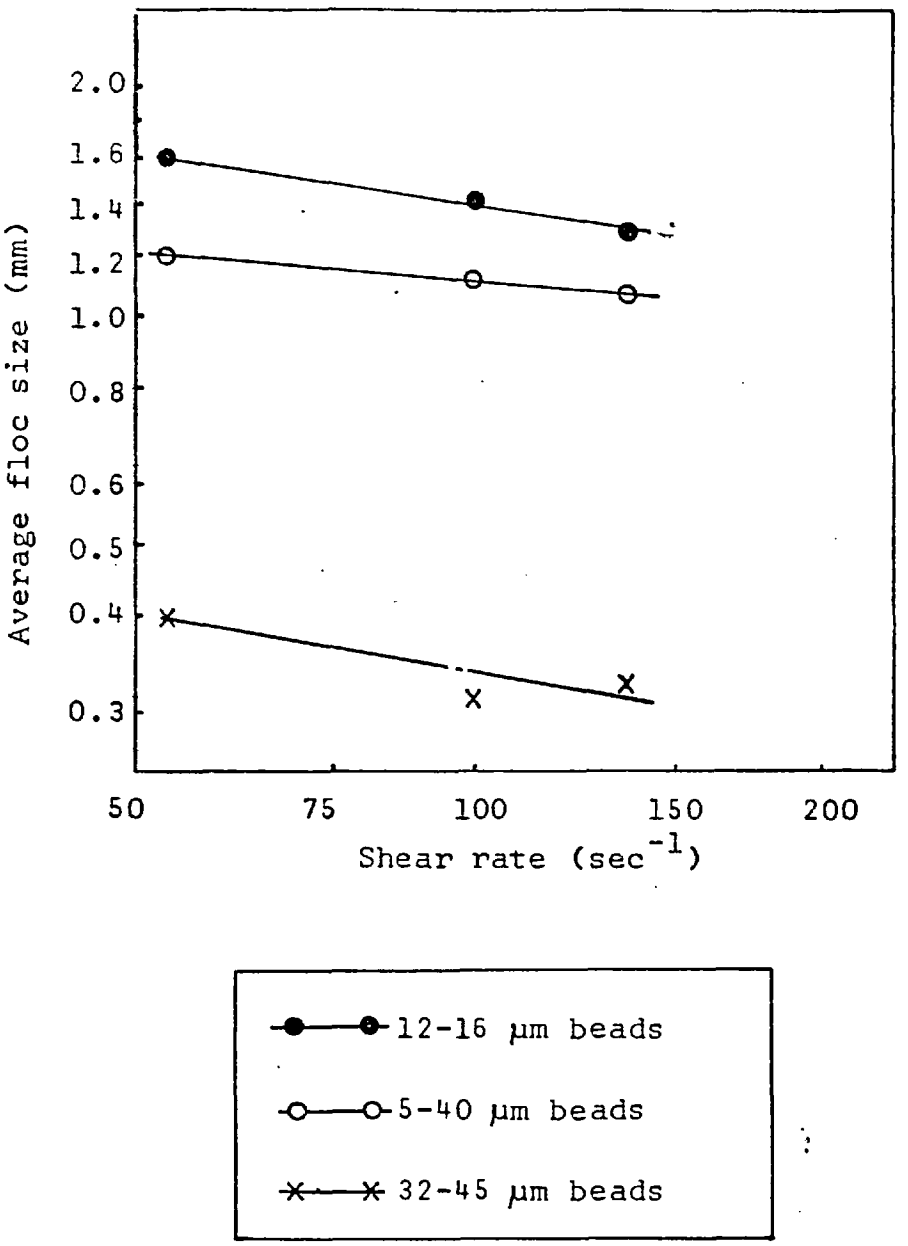



Figure 50

Rotating cylinder results - effect of bead size on average floc size

8mM $MgSO_4$, 5p.p.m. BTI A140, 0.125% w/v suspensions

sized particles by collision through Brownian motion until the aggregates are about 1 - 10 μm in size when the rate of shear also becomes important and orthokinetic flocculation continues until the flocs reach a limiting size and are broken down. These experiments do however, model orthokinetic flocculation and floc break-down in moderate shear which (presumably) does not release the - 1 μm particles (even if they were originally present). Only at excessive shear rates will the smaller flocs be ruptured releasing primary particles.

Also, the amount of flocculant added is usually (in practice) kept as low as possible, practically all is adsorbed, but the quantity is less than would be needed for "½ coverage". Hence, particles remain adhesive for some time, and reflocculation can be obtained after gentle de-aggregation (though rarely with complete restoration of floc strength). In these experiments only a fraction of the flocculant available would have been adsorbed on the surface (see Appendix IV), but as it was approaching a maximum (as indicated by the slope of the line in this region of figure 55 ) there would have been little further adsorption with time.

The range of strengths of flocculation measurable with the rotating cylinder apparatus was limited at one extreme by flocculation being too strong and there being too few flocs to give statistically significant results, while at the other extreme, in cases of weak flocculation, an improvement in flocculation could not be made by increasing the concentration of beads used because "clustering" (the formation of loose aggregates of beads) occurred. This phenomenon was undoubtedly a hydrodynamic effect. The increased number of particle collisions in such systems result in

fluctuations of particle trajectories and enhance the formation of wakes behind particles. Even in laminar flows, small particles can be entrained in the wakes behind larger ones.

The forces acting on a 2mm floc modelled as two 1.0mm spheres in contact can be calculated from equation (5.16)

$$P_1 = 4.41 \pi \eta \gamma b^2$$

The axial force acting on a floc at 45° to the flow streamlines at various shear rates is

| $\gamma$ ($sec^{-1}$) | 50 | 100 | 150 | 200 |
|---|---|---|---|---|
| $P_1$ ($\mu N$) | 0.69 | 1.39 | 2.08 | 2.77 |

These forces are a factor of 10 greater than the forces required to produce detachment in the centrifugal adhesion experiments. The cleavage plane of a floc, however, would contain many inter-particle links which would not all rupture simultaneously. Rupture would occur progressively across the plane and a force large enough to break all the links simultaneously would not be required.

Although the average velocity gradients used in the jar tests were less than those used in the rotating cylinder apparatus, flocs of potentially greater strength (higher $MgSO_4$ and flocculant concentrations) could be broken down. This was because the flow conditions in the jar tests were far from laminar.

A floc would be forced across many streamlines of flow and thus be subject to greater forces. The forces acting on a floc when it becomes caught in turbulent eddies or when its velocity is markedly different from that of the fluid immediately surrounding it are considerably greater. Although experiments using equipment such as the rotating cylinder apparatus to produce a uniform laminar flow field are obviously useful in studying the fundamental properties of flocs, they cannot be applied directly to the design of flocculation equipment until the dynamic flow conditions of flocculating suspensions in the equipment is known.

# CHAPTER 8

## SUMMARY OF CONCLUSIONS FROM THIS RESEARCH

1. Negatively charged glass particles in water can be flocculated by cationic polyacrylamide flocculants, and also by certain anionic flocculants if the double-layer repulsion has been reduced. Experiments with $MgSO_4$ and BTI A140 at pH 10 showed that a minimum $MgSO_4$ concentration of 0.1mM (corresponding to $1/\kappa$ of 15nm) was necessary before an increase in adhesion with flocculant addition was detected.

2. By using techniques with which very small adhesion forces could be measured, (12 - 200 pN) it was found that interactions between glass beads and silica plates could be detected at $MgSO_4$ or flocculant concentrations (0.025 mM and 0.1 p.p.m) far below those at which coagulation or flocculation could be visually observed in beaker tests.

3. The strength of adhesion for coagulation with $MgSO_4$ was not affected by pH over the range 4 - 10 for $MgSO_4$ concentrations of 0.1 mM or greater. However, at lower concentrations the adhesion was stronger at pH 4 corresponding to the lower surface potential. Flocculation with BTI A140 was considerably improved as the pH was increased to 10, corresponding to the increased bridging length of the polymer chain.

4. Visual observations that flocculation improves with increasing $MgSO_4$ and flocculant concentrations have been shown to correlate with a corresponding increase in the measured forces of adhesion. The force of adhesion for

flocculation with $MgSO_4$ and BTI A140 was found to increase on average by a factor of 2.5 when the flocculant concentration was doubled.

5. The dependence of the force of adhesion for electrolytic coagulation or anionic flocculation on particle size was found to agree approximately with Derjaguin's theory of particle interaction - (i.e. first power of radius of curvature). However, for cationic flocculation where the surfaces are presumably closer and hence the effect of surface irregularities more important, a greater dependence on particle size was found.

6. Although the strength of the inter-particle bonding increased with time (because of rearrangement of the polymer on the surface) aged flocs were more easily broken down, showing that the reduction in a particle's availability for re-forming a broken bond with time is an important factor in floc strength. There is a fundamental difference between "coagula" and flocs.

7. The increase in the strength of the particle-particle bond observed with an increase of $MgSO_4$ and flocculant concentration was paralleled by an increase in average floc size under controlled conditions of formation, although the dependence of floc size on flocculant concentration was not as marked as that of the inter-particular bond. The average floc size increased only by a factor of 1.9 for 4 mM $MgSO_4$ and by a factor of 1.4 for 8 mM $MgSO_4$ when the flocculant concentration was doubled. Doubling the $MgSO_4$ concentration resulted in a 1.5 times increase in average floc size for 2.5 p.p.m. flocculant and a 1.2 times increase for 5 p.p.m. flocculant concentration.

8. Observations of floc formation at different suspension concentrations were limited by the formation of clusters at particle concentrations greater than 0.125% w/v. At lower particle concentrations floc formation was considerably reduced, as indicated by the high proportion of small flocs.

9. Particle shape was found to have no detectable influence on the behaviour of flocs; crushed glass gave similar results to those obtained with spherical beads, providing the size distributions were alike. The effect of particle size was more pronounced, floc size was found to decrease as the particle size was increased.

10. A limited range of floc strengths was obtained for which break-down of the flocs could be observed as the shear rate was increased over the values obtainable with the rotating cylinder apparatus (50 - 200 $sec^{-1}$). The average floc size was found to be inversely proportional to the 0.2 power of the shear rate. This is a lower dependence on shear rate than the value of 0.5 predicted by Tomi and Bagster's model of floc strength (112) and the reported values for coagula.

Considerations for Future Work

Other factors of floc behaviour that were not part of this investigation are the elasticity of flocs and the mode of their fragmentation when subjected to brief periods of high shearing. Because of the coiled nature of flocculant molecules in solution it is expected that some types of flocs should have considerable elasticity. The stress-strain characteristics could only be satisfactorily determined by observing the deformations of flocs under controlled shearing, such as with the four-roller apparatus described

in Chapter 5. The mode of fragmentation of flocs to ascertain whether break-down is into a few moderate size pieces or if small fragments are broken off could be investigated by injecting single pre-formed flocs into a short shearing zone, followed by a divergent diluting flow to keep the fragments apart. It is not, however, easy to position single flocs in shear fields and perhaps it is necessary to develop sophisticated optical high-speed photomicroscopy (as used by S.G. Mason and co-workers (116)) to study the behaviour of single small flocs.

It would also be useful to compare the size distributions of flocs formed in a practical stirred tank with those obtained in the rotating cylinder apparatus, perhaps testing whether the Camp formula for average velocity gradient does give a useful representation of effective shear rate or not.

# CHAPTER 9

## FULL LIST OF REFERENCES


1. V.K. LaMer, J. Coll. Sci., 19, 291-293, 1964. Introduction to Coagulation Symposium

2. B.C. Edwards, J. Appl. Chem., 19, 141-149, 1969. Role of polymeric flocculants in sediment removal in condenser cooling systems

3. M. Yusa and A.M. Gaudin, Ceram. Bull., 43, 402-406, 1964. Formation of pellet-like flocs of kaolinite by polymer chains

4. J.V. O'Gorman and J.A. Kitchener, Int. J. Min. Proc., 1, 33-49, 1974. The flocculation and dewatering of Kimberlite clay slimes

5. M. Freundlich and E. Loening, Kolloidchem. Beihefte, 16, 1-26, 1922. Das Verhalten des Carey Lea'schen Silbersoles gegen Elektrolyte und hydrophile Kolloide

6. R.A. Rhuehrwein and D.W. Ward, Soil Sci., 73, 485-492, 1952. Mechanism of clay aggregation by polyelectolytes

7. A.S. Michaels, Ind. Eng. Chem., 46, 1485-1490, 1954. Aggregation of suspensions by polyelectrolytes

8. W.F. Linke and R.B. Booth, Trans. Am. Inst. Min. Metall. Eng., 217, 364-371, 1960. Physical chemical aspects of flocculation by polymers

9. J.A. Kitchener, Brit. Polym. J., 4, 217-229, 1972. Principles of action of polymeric flocculants

10. C.J. Fleer and J. Lyklema, Proc. V Intern. Congr. Surf. Act. Subst., (Barcelona), 2, 247-256, 1968. Stability of AgI sols in the presence of small amounts of polyvinyl alcohol

11. J. Rubio and J.A. Kitchener, Trans. Inst. Min. Met. C, to be published

12. N. Sarkar and A.S. Teot, J. Coll. Interf. Sci., 43, 370-381, 1973. Coagulation of negatively-charged colloids by anionic polyelectrolytes and metal ions

13. V.K. LaMer and R.H. Smellie, J.Coll. Sci., 11, 710-719, 1956. Starches as agents for improving flocculation, subsidence and filtration of phosphate slimes

14. O. Griot and J.A. Kitchener, Trans. Far. Soc., 61, 1026-1031, 1965. Role of surface silanol groups in the flocculation of silica suspensions by polyacrylamide. Part I

15. J. Rubio and J.A. Kitchener, J. Coll. Interf. Sci., 57, 132-142, 1976. The mechanism of adsorption of polyethylene oxide flocculant on silica

16. K.J. Ives and A.G. Bhole, Water Res., 9, 1085-1092, 1975. Study of flowthrough Couette flocculators - I. Design for uniform and tapered flocculation

17. B.V. Derjaguin, Kolloid Z., 69, 155-164, 1934. Theorie des Anhaftens kleine Teilchen

18. H. Krupp, Adv. Coll. Interf. Sci., 1, 111-239, 1967. Particle adhesion - theory and experiment

19. J.A. Kitchener, J. Soc. Cosmet. Chem., 24, 709-725, 1973. Surface forces in the deposition of small particles

20. H.C. Hamaker, Physica, 4, 1058-1072, 1937. The London-van der Waals attraction between spherical particles

21. E.M. Lifshitz, Sov. Phys. JETP, 2, 73-83, 1956. Theory of molecular attractive forces between solids

22. B.V. Derjaguin, Disc. Far. Soc., 18, 85-98, 1954. A theory of heterocoagulation, interaction and adhesion of dissimilar particles in solutions of electrolytes

23. G. Bohme, H. Krupp, H. Rabenhorst and G. Stanstede. Trans. Inst. Chem. Engrs., 40, 252-259, 1962. Adhesion measurements involving small particles

24. J. Visser, Rept. Progr. Appl. Chem., 53, 714-729, 1968. Adhesion of colloidal particles

25. B.B. Morgan, Brit. Coal Utilis. Res. Assoc. Monthly Bull., 25, 125-137, 1961. The adhesion and cohesion of fine particles

26. D. Beischer, Koll. Z., 89, 214-219, 1939. Festigkeitsuntersuchungen und Aerosolsedimenten Gerichete Koagulation in Aerosolen, III

27. H. Rumpf, Pharm. Ind., 34, 270-281, 1972. Adhesion and solidity of agglomerates. Comparison between a model calculation and experiment. (In German)

28. H.S. Eisner, G. Fogg and T.W. Taylor, Proc. III Intern. Congr. Surf. Act. (Cologne), 2, 378-382, 1960. Cohesion of particles and the effect of atmospheric moisture

29. R.L. Brown and J.C. Richards, Trans. Inst. Chem. Engrs., 38, 243-256, 1960. Profile of flow of granules through apertures

30. A.H.M. Andreasen, N. Hofman-Bang and N.H. Rasmussen. Kolloidzschr. 86, 70-77, 1939. Über das Stäubungsvermogen der Stoffe

31. J.G. Dowes, S.M.R.E. Res. Rep. No's 36 and 49, 1952. Dispersion of dust deposits by blasts of air. I and II

32. M.M. Benarie, Brit. J. Appl. Phys., 12, 514-518, 1961. Rheology of granular material II - a method for the determination of the inter-granular cohesion

33. E. Cremer, Th. Krans and F. Conrad. Angew. Chem., 64, 10-11, 1952. Die Haftfähigkeit von Pulvern und ihre Anwendung zur Bestimmung von Korngrössen

34. W. Batel, Chem. Ing. Tech., 31, 343-345, 1959. Über die Haftfähigkeit trockener feinkörniger Stoffe

35. A.von Buzagh, Koll. Z., 47, 370-372, 1929. Über eine Methode zur Untersuchung von Koagulations- und Peptisationserscheinungen

36. A.von Buzagh, Koll. Z., 51, 105-112 and 230-239, 1930. Über die Haftfähigkeit mikroskopischer Teilchen an Wänden von gleicher Beschaffenheit I und II

37. A.von Buzagh, Koll. Z., 76, 2-9, 1936. Über die Beziehungen zwischen der Haftfähigkeit der Teilchen mikroskopischer Grosse und den Aktivitätskoeffizienten der Elektrolyte

38. A.von Buzagh, J. Phys. Chem., 43, 1003-1014, 1939. The structure of the adsorption layer and the adhesion of microscopic particles

39. A.von Buzagh, Proc. III Intern. Congr. Surf. Act. (Cologne) 2, 383-390, 1960. Über den Zusammenhang zwischen der Adhäsion und der Stabilität disperser Systeme

40. R.C. Palmer and E.K. Rideal, J. Chem. Soc., (1939), 573-577, Adhesion in detergence.

41. G.I. Fuks, W.M. Klitshnikov and E.W. Ziganova, Dokl. Akad. Nauk. SSR., 65, 307-310, 1949. On the adhesion of microscopic particles to solid surfaces in liquids (In Russian)

42. V. Franknoy-Körös and J. Szabo, Proc. IV Intern. Congr. Surf. Act. (Brussels) 2, 457-465, 1964. Die Haftfähigkeit von Pulvern in apolaren-polaren Mischungen

43. D.W. Jordan, Brit. J. Appl. Phys., 5, S194-197, 1954. The adhesion of dust particles

44. T. Gillespie, J. Coll. Sci., 10, 266-280, 1955. On the adhesion of drops and particles on impact at solid surfaces.

45. R.I. Larsen, Am. Ind. Hyg. Assoc. J., 19, 265-270, 1958. The adhesion and removal of particles attached to air filter surfaces.

46. M. Corn and L. Silverman, Am. Ind. Hyg. Assoc. J., 22, 337-347, 1961. Removal of solid particles from a solid surface by a turbulent air stream.

47. A.D. Zimon, Colloid J. U.S.S.R. (Eng. Transl.) 27, 155-158, The necessity of accounting for the adhesion forces in determining the initial rate of entrapment of particles by a flow. Some aspects of the adhesion of powder particles to liquids.

48. E.J. Clayfield and E.C. Lumb, Disc. Far. Soc., 42, 285-293, 1966. Detachment of adhered colloidal particles by non-aqueous surfactant solutions

49. E.J. Clayfield and A.L Smith, Envir. Sci. Techn., 4, 413-416, 1970. Adhesion and detachment of solid colloidal particles in aqueous inorganic surfactant media

50. J. Visser, J. Coll. Interf. Sci., 34, 26-31, 1970. Measurement of van der Waals forces between sub-micron carbon black particles and a cellophane substrate

51. J. Visser, J. Coll. Interf. Sci., 55, 664-677, 1976. The adhesion of colloidal polystyrene particles to cellophane as a function of pH and ionic strength

52. B.V. Derjaguin and A.D. Zimon, Colloid J. U.S.S.R. (Eng. Transl.) 23, 454-460, 1961. Adhesion of powder particles to plane surfaces

53. A.D. Zimon, Colloid J. U.S.S.R. (Eng. Transl.), 29, 660-662, 1967. Estimation of particle adhesion

54. W. Stone, Phil. Mag., 9, 610-620, 1930. Some phenomena of the contact of solids

55. P.G. Howe, D.P. Benton and I.E. Puddington, Can. J. Chem., 33, 1375-1383, 1955. London-van der Waals attractive forces between glass surfaces

56. J.S. McFarlane and D. Tabor, Proc. Roy. Soc., A202, 224-243, 1950. Adhesion of solids and the effects of surface films

57. R.S. Bradley, Phil. Mag., 13, 858-862, 1932. The cohesive force between solid surfaces and the surface energy of solids

58. J.S. McFarlane and D. Tabor, Proc. Roy. Soc., A202, 244-253, 1950. The relation between friction and adhesion

59. G.A. Tomlinson, Phil. Mag., 6, 695-712, 1928. Molecular collision

60. G.A. Tomlinson, Phil. Mag., 10, 541-544, 1930. Further experiments on the cohesion of quartz fibres

61. B.V. Derjaguin, A.S. Titijevskaia, I.I. Abricossova and A.D. Malkina, Disc. Far. Soc., 18, 24-41, 1954. Investigations of the forces of interaction of surfaces in different media and their application to the problem of colloid stability

62. F. Van Voorst Vader and H. Dekker, Proc. VI Intern. Congr. Surf. Act. (Zurich), 2, 735-744, 1972. Measurement of adhesion by means of the crossed filament method

63. F. Van Voorst Vader and H. Dekker, J. Adhesion, 7, 73-89, 1974. The influence of surfactants on the adhesion between solids

64. J.W. Beams, J.B. Breazeale and W.L. Bart, Phys. Rev., 100, 1657-1661, 1955. Mechanical strength of thin films of metal

65. T. Gillespie and E.K. Rideal, J. Coll. Sci., 10, 281-298, 1955. On the adhesion of drops and particles on impact at solid surfaces II

66. M.C. Kordecki and C. Orr, Arch. Envir. Health, 1, 13-21, 1960. Adhesion of solid particles to solid surfaces

67. A.D. Zimon and B.V. Derjaguin, Colloid J. U.S.S.R. (Eng. Transl.), 25, 135-139, 1963. Adhesion of particles to a plane surface. Adhesion in an aqueous medium.

68. B.V. Derjaguin, Y.P. Toporov and I.N. Aleinikova, Colloid J. U.S.S.R. (Eng. Transl.), 26, 335-336, 1964. Evaluation of the strength of adhesion of spherical dielectric particles to metal surfaces

69. G. Bohme, W. Kling, H. Krupp, H. Lange and G. Stanstede, Z. Angew. Phys., 16, 486-490, 1964. Haftung kleiner Teilchen an Feststoffen. Teil I. - Messungen der Haftkraft in gasförmigen Medien

70. G. Bohme, Z. Egey and H. Krupp, Proc. IV Intern. Congr. Surf. Act. (Brussels), 2, 419-428, 1964. Ultrazentrifugen zur Messung der Haftung kleiner Feststoffteilchen an festen Körpern

71. G. Bohme, H. Krupp, G. Stanstede, G. Walter, W. Kling and H. Lange, Proc. IV Intern. Congr. Surf. Act. (Brussels) 2, 439-446, 1964. Über das Haften fester Teilchen an Feststoffen bei immergierten Systemen

72. G. Bohme, W. Kling, H. Krupp, H. Lange, G. Stanstede and G. Walter, Proc. IV Intern. Congr. Surf. Act. (Brussels), 2, 429-437, 1964. Measurement of adhesion of small particles

73. G. Bohme, W. Kling, H. Krupp, H. Lange, G. Stanstede and G. Walter, Z. Angew. Phys., 19, 265-270, 1965. Haftung kleiner Teilchen an Feststoffen. Teil III - Immergierte Systeme

74. H. Krupp, G. Walter, W. Kling and H. Lange, J. Coll. Interf. Sci., 28, 170-172, 1968. Adhesion of small gold particles to solid substrate immersed in water and in aqueous solutions of surfactants and of alkaline salts

75. R.M. Pashley, Private communication

76. A.J. Goldman, R.G. Cox and H. Brenner, Chem. Eng. Sci., 22, 653-660, 1967. Derivation of formulae for force on a sphere near a wall in Couette flow

77. M.E. O'Neill, Chem. Eng. Sci., 23, 1293-1298. 1968. A sphere in contact with a plane wall in slow linear shear flow

78. M. van den Tempel, Adv. Coll. Interf. Sci., 3, 137-159, 1972. Interaction forces between condensed bodies in close contact

79. J. Gregory, J. Coll. Interf. Sci., 42, 448-456, 1973. Rates of flocculation of latex particles by cationic polymers

80. G.I. Taylor, Proc. Roy. Soc., A146, 501-523, 1934. The formation of emulsions in definable fields of flow

81. W. Bartok and S.G. Mason, J. Coll. Sci., 13, 293-307, 1958. Particle motions in sheared suspensions. VII. Internal circulations in fluid droplets

82. R.B. Bird, W.E. Stewart and E.N. Lightfood, "Transport Phenomena", 1962, John Wiley and Sons Inc., N.Y. p 94.

83. F.A. Van Duuren, A.S.C.E., 94, SA4, 671-682, 1968. Defined velocity gradient model flocculator

84. M.M. Couette, Annales chem (Phys) 21, 433-510, 1890. Etudes sur le frottement des liquides

85. G.I. Taylor, Phil. Trans., A223, 289-293, 1923. Stability of a viscous liquid contained between two rotating cylinders

86. G.I. Taylor, Proc. Roy. Soc., A157, 546-576, 1936. Fluid friction between rotating cylinders

87. F. Wendt, Ing. Arch., 4, 577-595, 1933. Turbulente Strömungen zwischen zwei rotierenden konaxialen Zylindern

88. A. Mallock, Phil. Trans., A187, 41-56, 1986. Experiments on fluid viscosity

89. S. Chandresakar, Mathematika, 1, 5-13, 1954. The stability of viscous flow between rotating cylinders

90. R.J. Donelly, Proc. Roy. Soc., A246, 312-325, 1958. Experiments on the stability of viscous flow between rotating cylinders. I. Torque measurements

91. R.J. Donelly and D. Fultz, Proc. Roy. Soc., A258, 101-123, 1960. Experiments on the stability of viscous flow between rotating cylinders. II. Visual observations

92. H. Schlicting, Nachr. Ges. Wiss., Götingen, Math. Physik. Kl., 160-198, 1932. Über die Entstehung der Turbulenz in einem rotierenden Zylinder

93. H. Schlicting, "Boundary-Layer Theory", 6th edition, 1968. McGraw-Hill, N.Y. p 480.

94. F. Schultz-Grunow, ZAMM, 39, 101-110, 1959. Zur Stabilität der Couette-Strömung

95. H.L. Goldsmith and S.G. Mason, in "Rheology, Theory and Applications", IV edit. F.R. Eirich, 1967. Academic Press, N.Y. pp 85-250, The microrheology of dispersions

96. G.B. Jeffrey, Proc. Roy. Soc., A102, 161-179, 1923. The motion of ellipsoidal particles immersed in a viscous fluid

97. W. Bartok and S.G. Mason, J. Coll. Sci., 12, 243-262, 1957. Particle motions in sheared fluids. V. Rigid rods and collisions of doublets of spheres

98. M. von Smoluchowski, Z. Physik. Chem., 92, 129-168, 1918. Versuch einer Mathematischen Theorie der Koagulationskinetik Kolloide Losungen

99. A. Karnis, H.L. Goldsmith and S.G. Mason, Can. J. Chem. Eng., 44, 181-193, 1966. The flow of suspensions through tubes. V Inertial effects

100. G.M. Fair and R.S. Gemmell, J. Coll. Sci., 19, 360-372, 1964. A mathematical model of coagulation

101. H.S. Harris, W.J. Kaufman and R.B. Krone, ASCE, 92, SA6, 95-111, 1966. Orthokinetic flocculation in water purification

102. K.J. Ives and A.G. Bhole, ASCE, 99, EEI, 17-34, 1973. Theory of flocculation for continuous flow

103. T.K. Camp, Trans A.S.C.E., 120, 1-16, 1955. Flocculation and Flocculation Basins

104. I. Patterson and M.R. Kamal, Can. J. Chem. Eng., 52, 306-315, 1974. Shear de-agglomeration of solid aggregates suspended in a viscous liquid

105. M.J. Vold, J. Coll. Sci., 18, 684-695, 1963. Computer simulation of floc formation in a colloidal suspension

106. D.N. Sutherland, J. Coll. Interf. Sci., 22, 300-302, 1966. Comments on Vold's Simulation of floc formation

107. D.N. Sutherland, J. Coll. Interf. Sci., 25, 373-380, 1967. A theoretical model of floc structure

108. M. von Smoluchowski, Physik. Z. 17, 557-571, 1916. Drei Vortäge über Diffusion, Brownsche Molekularbewegung und Koagulation von Kolloidteilchen

109. D.N. Sutherland and I. Goodarz-Nia, Chem. Eng. Sci., 26, 2071-2085, 1971. Floc simulation: the effect of collision sequence

110. A.I. Medalia, J. Coll. Interf. Sci., 24, 393-404, 1967. Morphology of aggregates

111. I. Goodarz-Nia and D.N. Sutherland, Chem. Eng. Sci., 30, 407-412, 1975. Floc simulation: effects of particle size and shape

112. D. Tomi and D.F. Bagster, Chem. Eng. Sci., 30, 269-278, 1975. Model of floc strength under hydrodynamic forces

113. A.R. Ritchie, Ph.D. Thesis, Univ. of Lond., 1955. Certain aspects of flocculation as applied to sewage purification

114. A.S. Michaels and J.C. Bolger, Ind. Eng. Chem. Fund., 1, 153-162, 1962. The plastic flow behaviour of flocculated kaolin suspensions

115. A.G. Bhole, Ph.D. Thesis, Univ. of Lond., 1970. Hydrodynamics of flocculation in water treatment

116. E.B. Vadas, H.L. Goldsmith and S.G. Mason, J. Coll. Interf. Sci., 43, 632-648, 1973. The microrheology of colloidal dispersions

117. R.W. Slater, Ph.D. Thesis, Univ. of Lond., 1967. A study of the flocculation of mineral suspensions by polymers

# APPENDIX I

## The Forces Acting on a Bead in the Inversion Experiments

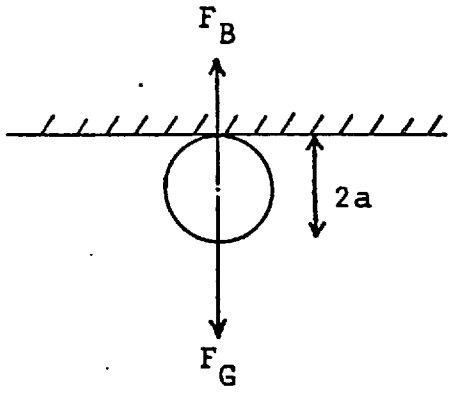



Figure 51 The Forces Acting on a Bead in the Inversion Experiments

The maximum gravitational force will act on a bead of radius a when the cell has been completely inverted and the situation will be as shown in figure 51.

The net force acting on the sphere will be given by

$$F = \frac{4}{3} \pi a^3 (\rho_p - \rho_f)$$

where $\rho_p$ is the density of the particle and $\rho_f$ the density of the fluid.

Using $g = 9.8\ m/sec^2$, $\rho_p = 2.5 \times 10^3 kg/m^3$ (glass) and $\rho_f = 1.0 \times 10^3 kg/m^3$ (water), then for a 10 $\mu$m diameter bead, the net force will be F = 7.7pN, and for a 30 $\mu$m diameter bead F = 208pN.

# APPENDIX II

## The Hydrodynamic Force Acting on a Bead in the Flow-Through Experiments

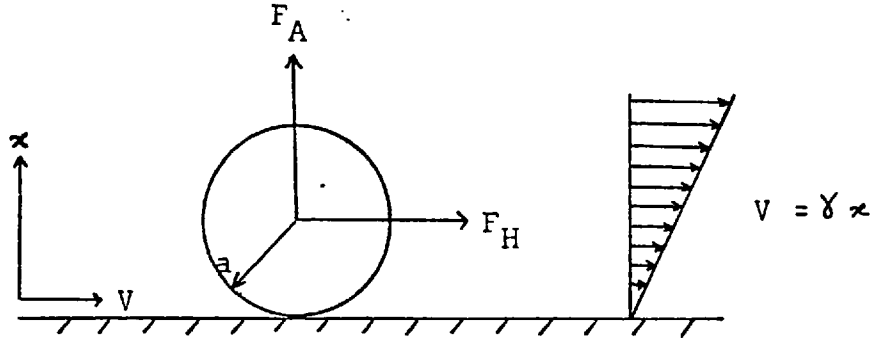



Figure 52 The Hydrodynamic Force Acting on a Sphere at rest on the Surface in Couette Flow.

According to Goldman et al (76) and O'Neill (77), the hydrodynamic force $F_H$ acting on a sphere of radius a at rest on the surface in Couette flow is given by

$$F_H = 1.7 \times 6\pi\eta\, a\, V_a \quad \text{.....(A2-1)}$$

i.e. it is 1.7 times the Stokes force that would act on the sphere if it were still at rest, in an infinite fluid.

As the width of the cell wall was 10mm and the distance between walls only 1mm, the flow through the cell can be considered equivalent to the flow between parallel plates and this would have a parabolic profile as shown in figure 53.

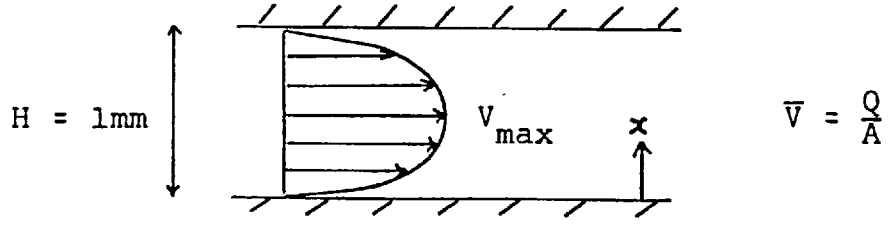



Figure 53 The Velocity Profile in the Flow between Parallel Plates

If Q is the flowrate through the cell, the average velocity $\bar{V}$, will be Q/A when A is the cross-sectional area of the cell. Using $Re = H\bar{V}\rho_f/\eta$, for a cell of cross sectional 10mm x 1mm and a maximum flow-rate of 0.5ml/sec, the maximum Reynolds number was 50.

For flow between parallel plates the maximum velocity Vmax is given by

$$Vmax = \frac{3}{2}\bar{V}$$
$$= \frac{3}{2} \cdot \frac{Q}{A} \qquad \text{.....(A2-2)}$$

The velocity profile shown in figure 53 is described by

$$V = \frac{4}{H} Vmax\, x\left(1 - \frac{x}{H}\right)$$

substituting equation A2-2

$$V = \frac{4}{H} \cdot \frac{3}{2} \cdot \frac{Q}{A} \cdot x\left(1 - \frac{x}{H}\right)$$

For $H = 1 \times 10^{-3}$m

and $A = 1 \times 10^{-5}$m$^2$ (10mm x 1mm)

$$V = 6 \times 10^8\, Q\, x\, (1 - x \times 10^3) \text{.....(A2-3)}$$

As the bead sizes were very small compared with the spacing of the walls of the cell, the velocity equation (A2-3) reduces to

$$V = 6 \times 10^8\, Q\, x \text{.....(A2-4)}$$

which is linear in x. Thus the flow near the wall is approximately Couette flow and equation (A2-1) can be used to calculate the force acting on a bead on the surface of the cell.

For a sphere of diameter b

$$F_H = 1.7 \times 6\pi\eta \frac{b}{2} \times 6 \times 10^8\, Q \frac{b}{2}$$

Taking $\eta = 10^{-3}$kg/m-sec (1.0cP, for water)

$$F_H = 4.81 \times 10^6 \times Q\, b^2 \text{ Newtons}$$

For a 10 μm diameter bead and a minimum and maximum flow of 0.01 and 0.5ml/sec respectively

$$F_{H\ min} = 4.8\text{pN and } F_{H\ max} = 240\text{pN}$$

For a 30 μm diameter bead the minimum and maximum forces are

$$F_{H\ min} = 43.2\text{pN and } F_{H\ max} = 2.16\text{nN}$$

The moment acting on the point of contact is given by $F_H \times a$ and for a 10 μm diameter bead varies from $0.024 - 1.2 \times 10^{-12}$N-m, and for a 30 μm diameter bead varies from $0.648 - 32.4 \times 10^{-12}$N-m.

# APPENDIX III

## The Force Acting on a Bead being Detached by the Centrifugal Method

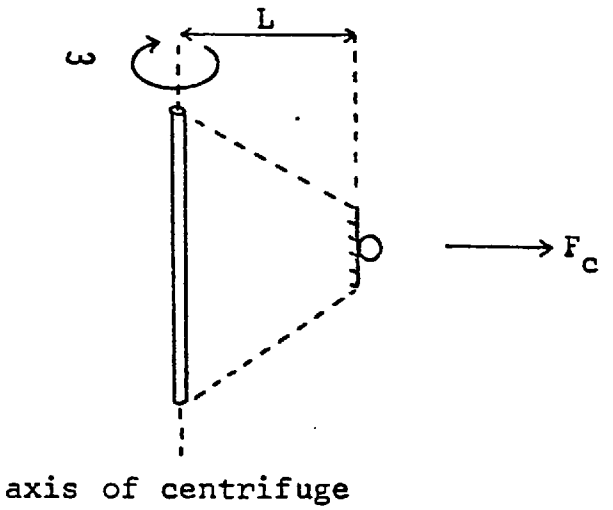



Figure 54 The Force Acting on a Bead in the Centrifuge Experiments

The centrifugal force $F_c$ acting on a particle as shown in figure is

$$F_c = m L \omega^2$$

where $\omega$ is the angular velocity given by

$$\omega = \frac{n}{60} \times 2\pi$$

and n is the number of revolutions per minute.

As $m = \frac{4}{3}\pi\left(\frac{b}{2}\right)^3 (\rho_p - \rho_f)$

and for L = 0.205m

$\rho_p = 2.5 \times 10^3 kg/m^3$ and $\rho_1 = 1 \times 10^3 kg/m^3$

$$F_c = \frac{4}{3}\pi\frac{b^3}{8} \times 1.5 \times 10^3 \times 0.205 \left(\frac{n}{60} \times 2\pi\right)^2$$

$$= \underline{1.764\ b^3\ n^2\ \text{Newtons}}$$

As the "g-force" on a sphere is $\frac{4}{3}\pi\left(\frac{b}{2}\right)^3 (\rho_p - \rho_l)\, g$, the "g-force" on a particle at maximum speed (n = 3600 rpm) is

$$\text{max. "g-force"} = \frac{1.764 \times 3600^2 \times b^3}{7.68 \times 10^3\, b^3}$$

$$= \underline{2{,}976\ g}$$

With a minimum speed of 500 rpm and a maximum speed of 3,600 rpm, the respective minimum and maximum forces acting on a 20 μm diameter bead are $\underline{F_{c\ min} = 3.53nN}$ and $\underline{F_{c\ max} = 183nN.}$

# APPENDIX IV

## Adsorption of polyacrylamide onto glass surfaces

Slater (117) made an adsorption study of Separan AP30, an anionic polyacrylamide flocculant (similar to BTI A140) on fluorite. He used 1% w/v suspensions of chemically pure $CaF_2$ (8.5 sq. m/g) and determined the concentration of flocculant in solution 8 minutes after introduction. His results were

| | | | | | | | | |
|---|---|---|---|---|---|---|---|---|
| Amount of polymer adsorbed (p.p.m) | 2.0 | 4.4 | 5.4 | 5.7 | 7.2 | 7.7 | 9.2 | 11.4 |
| Polymer remaining in solution (p.p.m) | 0 | 0.6 | 0.7 | 1.9 | 2.8 | 5.2 | 10.8 | 13.6 |

An approximate estimate of the adsorption conditions of BTI A140 on the glass beads used in the present experiments can be made by calculating the adsorption density (p.p.m/sq.m) for each concentration of polymer remaining in solution and applying this to the conditions in the rotating concentric cylinder experiments.

The ratio of surface area to weight for perfectly smooth spherical glass beads of 10 $\mu$m diameter and 2.5 x $10^3 kg/m^3$ density is 0.24 sq.m/g. As 0.125% w/v suspensions were used, and making an allowance of 0.16 sq.m. for the surface area of the cylinders, the total area was 0.4 sq.m. in the 800ml volume of the annulus. The amount of polymer adsorbed can then be calculated to give

| | | | | | | | | |
|---|---|---|---|---|---|---|---|---|
| Amount of polymer adsorbed (p.p.m.) | 0.09 | 0.21 | 0.25 | 0.27 | 0.34 | 0.36 | 0.43 | 0.53 |
| Polymer remaining in solution (p.p.m) | 0 | 0.6 | 0.7 | 1.9 | 2.8 | 5.2 | 10.8 | 13.6 |

These results are plotted in figure 55 and show that above initial flocculant concentrations of 2.3 p.p.m. the amount

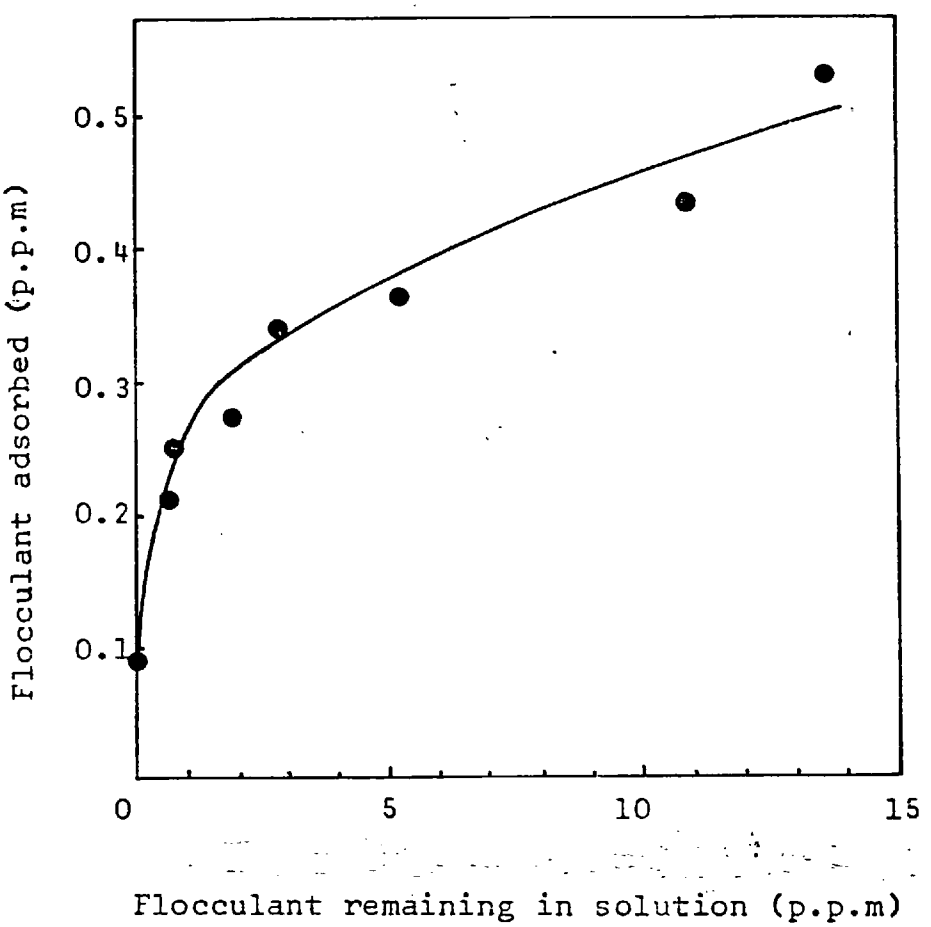



Figure 55

Adsorption of flocculant on glass beads. Estimated adsorption characteristics for rotating cylinder experiments

of flocculant adsorbed increases very slowly with increased flocculant concentration.

These are not equilibrium values. Slater stated that it took up to 24 hours for equilibrium to occur at the higher flocculant concentrations, however over the time interval at which the rotating cylinder experiments were carried out (3 - 30 minutes after initial contact) there would not be a marked increase in the amount of flocculant adsorbed.

# APPENDIX V
## Tables of Results

### a) Inversion Experiments

TABLE 2

Inversion experiments - adhesion of 10 μm diameter beads with $MgSO_4$ - no flocculant addition

| pH | $MgSO_4$ conc. (mM) | Propn. adhering (%) |
|---|---|---|
| 4 | 0.025 | 23 |
| 4 | 0.1 | 51 |
| 4 | 0.5 | 75 |
| 4 | 2.0 | 100 |
| 7 | 0.025 | 15 |
| 7 | 0.1 | 36 |
| 7 | 0.5 | 69 |
| 7 | 2.0 | 100 |
| 10 | 0.025 | 14.5 |
| 10 | 0.1 | 33 |
| 10 | 0.5 | 80 |
| 10 | 2.0 | 100 |

TABLE 3

Inversion experiments - adhesion of 30 μm diameter beads with $MgSO_4$ and BTI A140

| Flocculant conc (p.p.m) | $MgSO_4$ conc. (mM) | Propn. adhering (%) |
|---|---|---|
| 0 | 0.1 | 17 |
| 0 | 1.0 | 40 |
| 0 | 2.0 | 51 |
| 0.1 | 0.1 | 20 |
| 0.1 | 1.0 | 52 |
| 0.1 | 2.0 | 71 |
| 0.5 | 0.1 | 20 |
| 0.5 | 1.0 | 72 |
| 0.5 | 2.0 | 89 |
| 1.0 | 0.1 | 15 |
| 1.0 | 0.25 | 45 |
| 1.0 | 1.0 | 90 |
| 1.0 | 2.0 | 100 |

b) Flow-Through Experiments

TABLE 4

Flow-through experiments - the adhesion of 10 μm diameter beads.

i) 0.5mM $MgSO_4$, no flocculant, pH 7

| flow rate (ml/sec) | prop$^n$ adhering (%) |
|---|---|
| 0 | 100 |
| 0.032 | 100 |
| 0.094 | 81 |
| 0.218 | 62 |
| 0.404 | 49 |

50% adhesion at a flow rate of 0.4ml/sec

$F_H$ = 0.19nN

ii) 0.5mM $MgSO_4$, 1.0 p.p.m. BTI A140, pH 7

| flow rate (ml/sec) | prop$^n$ adhering (%) |
|---|---|
| 0 | 100 |
| 0.032 | 97 |
| 0.094 | 97 |
| 0.148 | 84 |
| 0.296 | 80 |
| 0.430 | 66 |

extrapolating, 50% adhesion at a flow rate of 0.575ml/sec

$F_H$ = 0.28nN

iii) 0.5mM $MgSO_4$, no flocculant, pH 10

| flow rate (ml/sec) | prop$^n$ adhering (%) |
|---|---|
| 0 | 100 |
| 0.071 | 96 |
| 0.144 | 88 |
| 0.284 | 50 |
| 0.355 | 50 |
| 0.406 | 42 |

50% adhesion at a flow rate of 0.35ml/sec

$F_H$ = 0.17nN

TABLE 4 Continued

iv) 0.5mM $MgSO_4$, 1.0 p.p.m. BTI A140, pH 10

| flow rate (ml/sec) | prop$^n$ adhering (%) |
|---|---|
| 0 | 100 |
| 0.030 | 98 |
| 0.051 | 95 |
| 0.190 | 91 |
| 0.236 | 89 |
| 0.365 | 89 |
| 0.437 | 89 |

TABLE 5

Flow-through experiments - the adhesion of 30 μm diameter beads

i) 0.5mM $MgSO_4$, no flocculant, pH 7

| flow rate (ml/sec) | prop$^n$ adhering (%) |
|---|---|
| 0 | 100 |
| 0.014 | 100 |
| 0.051 | 62 |
| 0.283 | 4 |

50% adhesion at a flow rate of 0.1ml/sec
$F_H$ = 0.43nN

ii) 0.5mM $MgSO_4$, 1.0 p.p.m. BTI A140, pH 7

| flow rate (ml/sec) | prop$^n$ adhering (%) |
|---|---|
| 0 | 100 |
| 0.057 | 77 |
| 0.157 | 63 |
| 0.236 | 53 |
| 0.353 | 20 |

50% adhesion at a flow rate of 0.25ml/sec
$F_H$ = 1.1nN

iii) 0.5mM $MgSO_4$, no flocculant, pH 10

| flow rate (ml/sec) | prop$^n$ adhering (%) |
|---|---|
| 0 | 100 |
| 0.083 | 79 |
| 0.177 | 54 |
| 0.272 | 42 |

50% adhesion at a flow rate of 0.2ml/sec
$F_H$ = 0.86nN

iv) 0.5mM $MgSO_4$, 0.5p.p.m. BTI A140, pH 10

| flow rate (ml/sec) | prop$^n$ adhering (%) |
|---|---|
| 0 | 100 |
| 0.028 | 100 |
| 0.042 | 91 |
| 0.158 | 84 |
| 0.284 | 80 |
| 0.388 | 69 |

extrapolating, 50% adhesion at a flow rate of 0.575ml/sec
$F_H$ = 2.5nN

TABLE 5 Continued

v) 0.5mM $MgSO_4$, 1.0 p.p.m. BTI A140, pH 10

| flow rate (ml/sec) | prop$^n$ adhering (%) |
|---|---|
| 0 | 100 |
| 0.071 | 100 |
| 0.150 | 100 |
| 0.237 | 100 |
| 0.406 | 100 |

TABLE 6

Flow-through experiments - the adhesion of beads with a cationic flocculant

i) Adhesion of 30 μm diameter beads with 0.5 p.p.m. Magnafloc 292 at pH 7

| flow rate (ml/sec) | prop$^{n}$ adhering (%) | flow rate (ml/sec) | prop$^{n}$ adhering (%) |
|---|---|---|---|
| 0 | 100 | 0 | 100 |
| 0.049 | 77 | 0.086 | 81 |
| 0.142 | 48 | 0.189 | 54 |
| 0.203 | 42 | 0.250 | 39 |
| 0.374 | 34 | 0.355 | 25 |

50% adhesion at a flow rate of 0.175ml/sec corresponding to $F_H$ = 0.76nN

ii) Adhesion of 10 μm diameter beads with 0.5 p.p.m. Magnafloc 292 at pH 7

| flow rate (ml/sec) | prop$^{n}$ adhering (%) | flow rate (ml/sec) | prop$^{n}$ adhering (%) |
|---|---|---|---|
| 0 | 100 | 0 | 100 |
| 0.032 | 28 | 0.071 | 23 |
| 0.236 | 19 | 0.203 | 12 |

50% adhesion at a flow rate of 0.025ml/sec corresponding to $F_H$ = 12pN

c) Centrifugal Experiments

TABLE 7

Centrifugal experiments - deposition in water, pH 10.

i) Flocculating medium: 8mM $MgSO_4$ and 10 p.p.m. BTI A140
Average bead diameter: 19.8 μm
Time since deposition: 2-6 hours

| Speed (rpm) | Force (nN) | Prop$^n$ adhering (%) |
|---|---|---|
| 500 | 3.43 | 92 |
| 1000 | 13.7 | 82 |
| 1500 | 30.8 | 52 |
| 2000 | 54.8 | 25 |

ii) Flocculating medium: 8mM $MgSO_4$ and 10 p.p.m. BTI A140
Average bead diameter: 20.1 μm
Time since deposition: 2-6 hours

| Speed (rpm) | Force (nN) | Prop$^n$ adhering (%) |
|---|---|---|
| 500 | 3.6 | 97 |
| 1000 | 14.3 | 82 |
| 1500 | 32.2 | 52 |
| 2000 | 57.3 | 20 |

iii) Flocculating medium: 8mM $MgSO_4$ and 20 p.p.m. BTI A140
Average bead diameter: 20.1 μm
Time since deposition: 2-6 hours

| Speed (rpm) | Force (nN) | Prop$^n$ adhering (%) |
|---|---|---|
| 500 | 3.6 | 100 |
| 1000 | 14.3 | 100 |
| 1500 | 32.2 | 87 |
| 2000 | 57.3 | 68 |
| 2500 | 89.4 | 43 |
| 3000 | 129 | 20 |

TABLE 7 Continued

iv) Flocculating medium: 8mM $MgSO_4$ and 10 p.p.m. BTI A140
Average bead diameter: 20.3 μm
Time since deposition: 22-30 hours

| Speed (rpm) | Force (nN) | Prop$^n$ adhering (%) |
|---|---|---|
| 500 | 3.69 | 98 |
| 1000 | 14.8 | 91 |
| 1500 | 33.2 | 61 |
| 2000 | 59.0 | 39 |
| 2500 | 92.4 | 25 |

v) Flocculating medium: 8mM $MgSO_4$ and 10 p.p.m. BTI A140
Average bead diameter: 19.8 μm
Time since deposition: 22-30 hours

| Speed (rpm) | Force (nN) | Prop$^n$ adhering (%) |
|---|---|---|
| 500 | 3.43 | 100 |
| 1000 | 13.7 | 98 |
| 1500 | 30.8 | 62 |
| 2000 | 54.8 | 43 |
| 2500 | 85.8 | 33 |

TABLE 8

Centrifugal experiments - deposition in 8mM $MgSO_4$, pH 10

i) Flocculating medium: 8mM $MgSO_4$ and 5 p.p.m. BTI A140
Average bead diameter: 20.1 μm
Time since deposition: 2-6 hours

| Speed (rpm) | Force (nN) | Prop$^n$ adhering (%) |
|---|---|---|
| 500 | 3.58 | 98 |
| 1000 | 14.3 | 90 |
| 1500 | 32.2 | 42 |
| 2000 | 57.3 | 4 |

ii) Flocculating medium: 8mM $MgSO_4$ and 10 p.p.m. BTI A140
Average bead diameter: 19.8 μm
Time since deposition: 2-6 hours

| Speed (rpm) | Force (nN) | Prop$^n$ adhering (%) |
|---|---|---|
| 1000 | 13.7 | 100 |
| 1500 | 30.8 | 90.5 |
| 2000 | 54.8 | 60 |
| 2500 | 85.8 | 21.5 |

iii) Flocculating medium: 8mM $MgSO_4$ and 10 p.p.m. BTI A140
Average bead diameter: 18.5 μm
Time since deposition: 2-6 hours

| Speed (rpm) | Force (nN) | Prop$^n$ adhering (%) |
|---|---|---|
| 500 | 2.79 | 99 |
| 1000 | 11.2 | 99 |
| 1500 | 25.1 | 90 |
| 2000 | 44.7 | 71 |
| 2500 | 69.6 | 42 |
| 3000 | 101 | 13 |

TABLE 8 Continued

iv) Flocculating medium: 8mM $MgSO_4$ and 10 p.p.m. BTI A140
Average bead diameter: 19.1 μm
Time since deposition: 2-6 hours

| Speed (rpm) | Force (nN) | Prop$^n$ adhering (%) |
|---|---|---|
| 1000 | 12.3 | 100 |
| 1500 | 27.7 | 90 |
| 2000 | 49.1 | 57 |
| 2500 | 76.8 | 35 |

v) Flocculating medium: 8mM $MgSO_4$ and 20 p.p.m. BTI A140
Average bead diameter: 21.0 μm
Time since deposition: 2-6 hours

| Speed (rpm) | Force (nN) | Prop$^n$ adhering (%) |
|---|---|---|
| 1500 | 36.8 | 100 |
| 2000 | 65.4 | 100 |
| 2500 | 102 | 75 |
| 2750 | 124 | 56 |
| 3000 | 147 | 55 |
| 3300 | 178 | 44 |

vi) Flocculating medium: 8mM $MgSO_4$ and 10 p.p.m. BTI A140
Average bead diameter: 19.8 μm
Time since deposition: 22-30 hours

| Speed (rpm) | Force (nN) | Prop$^n$ adhering (%) |
|---|---|---|
| 1000 | 13.7 | 100 |
| 1500 | 30.8 | 99.5 |
| 2000 | 54.8 | 90 |
| 2500 | 85.8 | 71 |
| 3000 | 123 | 59 |

TABLE 8 Continued

vii) Flocculating medium: 8mM $MgSO_4$ and 10 p.p.m. BTI A140
Average bead diameter: 20.6 μm
Time since deposition: 22-30 hours

| Speed (rpm) | Force (nN) | Prop$^n$ adhering (%) |
|---|---|---|
| 500 | 3.86 | 100 |
| 1000 | 15.4 | 99 |
| 1500 | 34.7 | 99 |
| 2000 | 61.8 | 81 |
| 2500 | 96.6 | 43 |
| 2750 | 116 | 39 |
| 3000 | 139 | 34 |

d) Rotating cylinder results

TABLE 9

Size distributions obtained during floc formation with 0.125% w/v suspensions of 5 - 40 μm diameter beads. Rotation at 80 rpm

i) 4 mM $MgSO_4$, 2.5 p.p.m. flocculant, pH 10

| | After 2 min | | After 3 min | | After 5 min | |
|---|---|---|---|---|---|---|
| floc size (mm) | No. (%) | Cum. % | No. (%) | Cum. % | No. (%) | Cum. % |
| 0.2 | 14.4 | 14.4 | 13.0 | 13.0 | 13.7 | 13.7 |
| 0.4 | 64.9 | 79.3 | 51.1 | 64.1 | 38.5 | 52.2 |
| 0.6 | 19.0 | 98.3 | 30.7 | 94.8 | 31.1 | 83.3 |
| 0.8 | 1.5 | 99.8 | 4.1 | 98.9 | 14.4 | 97.7 |
| 1.0 | 0.2 | 100.0 | 0.4 | 99.3 | 1.7 | 99.4 |
| 1.2 | | | 0.4 | 99.7 | 0.7 | 100.1 |
| 1.4 | | | 0.0 | 99.7 | | |
| 1.6 | | | 0.4 | 100.1 | | |
| | $\bar{x}$ = 0.417 | | $\bar{x}$ = 0.461 | | $\bar{x}$ = 0.508 | |
| | $\sigma$ = 0.128 | | $\sigma$ = 0.171 | | $\sigma$ = 0.199 | |

TABLE 9 Continued

ii) 4 mM $MgSO_4$, 5 p.p.m. flocculant, pH 10,

| | After 1 min | | After 2 min | | After 3 min | | After 5 min | |
|---|---|---|---|---|---|---|---|---|
| floc size (mm) | No. (%) | Cum. % | No. (%) | Cum. % | No. (%) | Cum. % | No. (%) | Cum. % |
| 0.2 | 5.8 | 5.8 | 3.1 | 3.1 | 1.5 | 1.5 | 5.6 | 5.6 |
| 0.4 | 19.2 | 25.0 | 11.2 | 14.3 | 3.1 | 4.6 | 4.2 | 9.8 |
| 0.6 | 39.2 | 64.2 | 30.6 | 44.9 | 27.7 | 32.3 | 11.3 | 21.1 |
| 0.8 | 23.3 | 87.5 | 31.6 | 76.5 | 24.6 | 56.9 | 19.7 | 40.8 |
| 1.0 | 7.5 | 95.0 | 14.3 | 90.8 | 20.0 | 76.9 | 28.2 | 69.0 |
| 1.2 | 4.2 | 99.2 | 7.1 | 97.9 | 15.4 | 92.3 | 15.5 | 84.5 |
| 1.4 | 0.8 | 100 | 1.0 | 98.9 | 0.0 | 92.3 | 2.8 | 87.3 |
| 1.6 | | | 1.0 | 99.9 | 7.7 | 100 | 7.0 | 94.3 |
| 1.8 | | | | | | | 2.8 | 97.1 |
| 2.0 | | | | | | | 1.4 | 98.5 |
| 2.2 | | | | | | | 0.0 | 98.5 |
| 2.4 | | | | | | | 1.4 | 99.9 |
| | $\bar{x}$ = 0.647 | | $\bar{x}$ = 0.749 | | $\bar{x}$ = 0.886 | | $\bar{x}$ = 0.986 | |
| | $\sigma$ = 0.239 | | $\sigma$ = 0.257 | | $\sigma$ = 0.312 | | $\sigma$ = 0.419 | |

TABLE 9 Continued

iii) 6 mM $MgSO_4$, 5 p.p.m. flocculant, pH 10

| | After 2 min | | After 3 min | | After 5 min | |
|---|---|---|---|---|---|---|
| floc size (mm) | No. (%) | Cum. % | No. (%) | Cum % | No. (%) | Cum. % |
| 0.4 | 41.7 | 41.7 | 21.0 | 21.0 | 9.4 | 9.4 |
| 0.6 | 8.3 | 49.0 | 12.7 | 33.7 | 7.8 | 17.2 |
| 0.8 | 10.4 | 60.4 | 13.8 | 47.5 | 21.9 | 39.1 |
| 1.0 | 22.9 | 83.3 | 7.5 | 55.0 | 7.8 | 46.9 |
| 1.2 | 8.3 | 91.6 | 17.5 | 72.5 | 14.1 | 61.0 |
| 1.4 | 4.2 | 95.8 | 8.7 | 81.2 | 6.3 | 67.3 |
| 1.6 | 4.2 | 100 | 6.9 | 88.1 | 15.6 | 82.9 |
| 1.8 | | | 4.4 | 92.5 | 6.3 | 89.2 |
| 2.0 | | | 5.0 | 97.5 | 3.1 | 92.3 |
| 2.2 | | | 2.5 | 100 | 1.6 | 93.9 |
| 2.4 | | | | | 1.6 | 95.5 |
| 2.6 | | | | | 3.1 | 98.6 |
| 2.8 | | | | | 1.6 | 100.2 |
| | $\bar{x}$ = 0.754 | | $\bar{x}$ = 1.022 | | $\bar{x}$ = 1.216 | |
| | $\sigma$ = 0.367 | | $\sigma$ = 0.513 | | $\sigma$ = 0.584 | |

TABLE 9 Continued

iv) 8 mM $MgSO_4$, 2.5 p.p.m. flocculant, pH 10

| | After 2 min | | After 3 min | | After 5 min | |
|---|---|---|---|---|---|---|
| floc size (mm) | No. (%) | Cum. % | No. (%) | Cum. % | No. (%) | Cum. % |
| 0.4 | 26.9 | 26.9 | 13.8 | 13.8 | 4.4 | 4.4 |
| 0.6 | 48.3 | 75.2 | 25.6 | 39.4 | 8.9 | 13.3 |
| 0.8 | 19.3 | 94.5 | 34.7 | 74.1 | 48.9 | 62.2 |
| 1.0 | 5.5 | 100 | 26.0 | 100.1 | 28.9 | 91.1 |
| 1.2 | | | | | 4.4 | 95.5 |
| 1.4 | | | | | 2.2 | 97.7 |
| 1.6 | | | | | 2.2 | 99.9 |
| | $\bar{x}$ = 0.607 | | $\bar{x}$ = 0.746 | | $\bar{x}$ = 0.870 | |
| | $\sigma$ = 0.166 | | $\sigma$ = 0.199 | | $\sigma$ = 0.218 | |

TABLE 9 Continued

v) 8 mM $MgSO_4$, 5 p.p.m. flocculant, pH 10

| | After 2 min | | After 3 min | | After 5 min | |
|---|---|---|---|---|---|---|
| floc size (mm) | No. (%) | Cum. % | No. (%) | Cum. % | No. (%) | Cum. % |
| 0.4 | 19.7 | 19.7 | 5.3 | 5.3 | 6.3 | 6.3 |
| 0.6 | 16.9 | 36.6 | 5.3 | 10.6 | 12.5 | 18.8 |
| 0.8 | 12.7 | 49.3 | 31.6 | 42.2 | 3.1 | 21.9 |
| 1.0 | 14.1 | 63.4 | 18.4 | 60.6 | 25.0 | 46.9 |
| 1.2 | 12.7 | 76.1 | 18.4 | 79.0 | 9.4 | 56.3 |
| 1.4 | 11.3 | 87.4 | 10.5 | 89.5 | 15.6 | 71.9 |
| 1.6 | 8.5 | 95.9 | 7.9 | 97.4 | 15.6 | 87.5 |
| 1.8 | 2.8 | 98.7 | 2.6 | 100 | 9.4 | 96.9 |
| 2.0 | 1.4 | 100.1 | | | 3.1 | 100 |
| | $\bar{x}$ = 0.946 | | $\bar{x}$ = 1.032 | | $\bar{x}$ = 1.188 | |
| | $\sigma$ = 0.434 | | $\sigma$ = 0.338 | | $\sigma$ = 0.436 | |

TABLE 9 Continued

vi) 16 mM $MgSO_4$, 2.5 p.p.m. flocculant, pH 10

| | After 2 min | | After 3 min | | After 5 min | |
|---|---|---|---|---|---|---|
| floc size (mm) | No. (%) | Cum. % | No. (%) | Cum. % | No. (%) | Cum. % |
| 0.4 | 21.5 | 21.5 | 6.5 | 6.5 | 4.2 | 4.2 |
| 0.6 | 11.6 | 33.1 | 15.4 | 21.9 | 12.3 | 16.5 |
| 0.8 | 15.7 | 48.8 | 16.9 | 38.8 | 14.1 | 30.6 |
| 1.0 | 16.3 | 65.1 | 18.7 | 57.7 | 17.5 | 48.1 |
| 1.2 | 14.5 | 79.6 | 18.3 | 75.8 | 17.1 | 65.2 |
| 1.4 | 11.3 | 90.9 | 13.6 | 89.4 | 14.8 | 80.0 |
| 1.6 | 9.1 | 100 | 10.6 | 100 | 13.2 | 93.2 |
| 1.8 | | | | | 4.3 | 97.5 |
| 2.0 | | | | | 2.5 | 100 |
| | $\bar{x}$ = 0.922 | | $\bar{x}$ = 1.020 | | $\bar{x}$ = 1.129 | |
| | $\sigma$ = 0.393 | | $\sigma$ = 0.350 | | $\sigma$ = 0.395 | |

TABLE 10

Rotating cylinder experiments - size distributions obtained during floc break-down with 0.125% suspensions of 5 - 40 μm diameter beads

i) 6 mM $MgSO_4$, 5 p.p.m. flocculant pH 10,

| | 80 rpm | | 150 rpm | | 200 rpm | | 300 rpm | |
|---|---|---|---|---|---|---|---|---|
| floc size (mm) | No. (%) | Cum. % | No. (%) | Cum. % | No. (%) | Cum. % | No. (%) | Cum. % |
| 0.4 | 9.4 | 9.4 | 25.0 | 25.0 | 22.4 | 22.4 | 18.1 | 18.1 |
| 0.6 | 7.8 | 17.2 | 11.4 | 36.4 | 6.1 | 28.5 | 19.7 | 37.8 |
| 0.8 | 21.9 | 39.1 | 11.4 | 47.8 | 26.5 | 55.0 | 24.2 | 62.0 |
| 1.0 | 7.8 | 46.9 | 2.3 | 50.1 | 16.3 | 71.3 | 18.1 | 80.1 |
| 1.2 | 14.1 | 61.0 | 34.1 | 84.2 | 12.2 | 83.5 | 7.6 | 87.7 |
| 1.4 | 6.3 | 67.3 | 6.8 | 91.0 | 2.0 | 85.5 | 3.0 | 90.7 |
| 1.6 | 15.6 | 82.9 | 0.0 | 91.0 | 4.1 | 89.6 | 1.5 | 92.2 |
| 1.8 | 6.3 | 89.2 | 2.3 | 93.3 | 2.0 | 91.6 | 3.0 | 95.2 |
| 2.0 | 3.1 | 92.3 | 4.5 | 97.8 | 8.2 | 99.8 | 4.5 | 99.7 |
| 2.2 | 1.6 | 93.9 | 0.0 | 97.8 | | | | |
| 2.4 | 1.6 | 95.5 | 2.3 | 100.1 | | | | |
| 2.6 | 3.1 | 98.6 | | | | | | |
| 2.8 | 1.6 | 100.2 | | | | | | |
| | $\bar{x}$ = 1.216 | | $\bar{x}$ = 0.972 | | $\bar{x}$ = 0.943 | | $\bar{x}$ = 0.870 | |
| | $\sigma$ = 0.584 | | $\sigma$ = 0.496 | | $\sigma$ = 0.469 | | $\sigma$ = 0.413 | |

TABLE 10 Continued

ii) 8 mM $MgSO_4$, 2.5 p.p.m. flocculant, pH 10

| | 80 rpm | | 150 rpm | | 250 rpm | | 300 rpm | |
|---|---|---|---|---|---|---|---|---|
| floc size (mm) | No. (%) | Cum. % | No. (%) | Cum. % | No. (%) | Cum. % | No. (%) | Cum. % |
| 0.4 | 4.4 | 4.4 | 18.3 | 18.3 | 33.0 | 33.0 | 41.3 | 41.3 |
| 0.6 | 8.9 | 13.3 | 33.3 | 51.6 | 34.0 | 67.0 | 32.6 | 73.9 |
| 0.8 | 48.9 | 62.2 | 28.3 | 79.9 | 16.0 | 83.0 | 15.2 | 89.1 |
| 1.0 | 28.9 | 91.1 | 11.7 | 91.6 | 5.3 | 88.3 | 4.3 | 93.4 |
| 1.2 | 4.4 | 95.5 | 5.0 | 96.6 | 8.5 | 96.8 | 4.3 | 97.7 |
| 1.4 | 2.2 | 97.7 | 1.7 | 98.3 | 0.0 | 96.8 | 0.0 | 97.7 |
| 1.6 | 2.2 | 99.9 | 1.7 | 100 | 3.2 | 100 | 2.2 | 99.9 |
| | $\bar{x}$ = 0.870 | | $\bar{x}$ = 0.727 | | $\bar{x}$ = 0.670 | | $\bar{x}$ = 0.612 | |
| | $\sigma$ = 0.218 | | $\sigma$ = 0.260 | | $\sigma$ = 0.295 | | $\sigma$ = 0.260 | |

TABLE 10 Continued

iii) 8 mM $MgSO_4$, 5 p.p.m. flocculant, pH 10

| | 80 rpm | | 150 rpm | | 200 rpm | |
|---|---|---|---|---|---|---|
| floc size (mm) | No. (%) | Cum. % | No. (%) | Cum. % | No. (%) | Cum. % |
| 0.4 | 6.3 | 6.3 | 27.0 | 27.0 | 11.6 | 11.6 |
| 0.6 | 12.5 | 18.8 | 0.0 | 27.0 | 14.0 | 25.6 |
| 0.8 | 3.1 | 21.9 | 10.8 | 37.8 | 16.3 | 41.9 |
| 1.0 | 25.0 | 46.9 | 10.8 | 48.6 | 9.3 | 51.2 |
| 1.2 | 9.4 | 56.3 | 21.6 | 70.2 | 11.6 | 62.8 |
| 1.4 | 15.6 | 71.9 | 2.7 | 72.9 | 2.3 | 65.1 |
| 1.6 | 15.6 | 87.5 | 10.8 | 83.7 | 23.2 | 88.3 |
| 1.8 | 9.4 | 96.9 | 16.2 | 99.9 | 11.6 | 99.9 |
| 2.0 | 3.1 | 100 | | | | |
| | $\bar{x}$ = 1.188 | | $\bar{x}$ = 1.107 | | $\bar{x}$ = 1.065 | |
| | $\sigma$ = 0.437 | | $\sigma$ = 0.480 | | $\sigma$ = 0.510 | |

TABLE 11

Rotating cylinder experiments - size distributions obtained during floc formation with 0.0625% suspensions of 5 - 40 μm diameter beads. Rotation at 80 rpm

i) 8 mM $MgSO_4$, 5 p.p.m. BTI A140, pH 10

| | After 2 min | | After 3 min | | After 5 min | |
|---|---|---|---|---|---|---|
| floc size (mm) | No. (%) | Cum. % | No. (%) | Cum. % | No. (%) | Cum. % |
| 0.4 | 66.7 | 66.7 | 67.7 | 67.7 | 78.6 | 78.6 |
| 0.6 | 9.5 | 76.2 | 19.4 | 87.1 | 9.5 | 88.1 |
| 0.8 | 4.8 | 81.0 | 0.0 | 87.1 | 0.0 | 88.1 |
| 1.0 | 9.5 | 90.5 | 6.5 | 93.6 | 2.4 | 90.5 |
| 1.2 | 4.8 | 95.3 | 0.0 | 93.6 | 0.0 | 90.5 |
| 1.4 | 0.0 | 95.3 | 3.2 | 96.8 | 0.0 | 90.5 |
| 1.6 | 4.8 | 100.1 | 0.0 | 96.8 | 2.4 | 92.9 |
| 1.8 | | | 3.2 | 100 | 4.8 | 97.7 |
| 2.0 | | | | | 2.4 | 100.1 |
| | $\bar{x}$ = 0.590 | | $\bar{x}$ = 0.555 | | $\bar{x}$ = 0.567 | |
| | $\sigma$ = 0.378 | | $\sigma$ = 0.325 | | $\sigma$ = 0.421 | |

TABLE 12

Rotating cylinder experiments - size distributions obtained during floc break-down with 8 mM $MgSO_4$ and 5 p.p.m. flocculant at pH 10. 0.125% w/v suspension of 13 μm (average) diameter beads.

| | 80 rpm | | 150 rpm | | 200 rpm | |
|---|---|---|---|---|---|---|
| floc size (mm) | No. (%) | Cum. % | No. (%) | Cum. % | No. (%) | Cum. % |
| 0.4 | 0 | 0.0 | 0 | 0.0 | 13.2 | 13.2 |
| 0.6 | 0 | 0.0 | 13.7 | 13.7 | 5.5 | 18.7 |
| 0.8 | 4.8 | 4.8 | 5.1 | 18.8 | 7.8 | 26.5 |
| 1.0 | 10.2 | 15.0 | 7.7 | 26.5 | 8.9 | 35.4 |
| 1.2 | 12.6 | 27.6 | 9.6 | 36.1 | 8.6 | 44.0 |
| 1.4 | 7.3 | 34.9 | 17.3 | 53.4 | 16.1 | 60.1 |
| 1.6 | 27.4 | 62.3 | 14.6 | 68.0 | 12.5 | 72.6 |
| 1.8 | 13.4 | 75.7 | 15.1 | 83.1 | 8.8 | 81.4 |
| 2.0 | 15.4 | 91.1 | 10.4 | 93.5 | 14.7 | 96.1 |
| 2.2 | 7.5 | 98.6 | 6.6 | 100.1 | 4.0 | 100.1 |
| 2.4 | 2.4 | 100.0 | | | | |
| | $\bar{x}$ = 1.604 | | $\bar{x}$ = 1.416 | | $\bar{x}$ = 1.306 | |
| | $\sigma$ = 0.372 | | $\sigma$ = 0.481 | | $\sigma$ = 0.476 | |

TABLE 13

Rotating cylinder experiments - size distributions obtained during floc break-down with 8 mM $MgSO_4$ and 5 p.p.m. flocculant at pH 10. 0.125% w/v suspension of 35 μm (average) diameter beads

| | 80 rpm | | 150 rpm | | 200 rpm | |
|---|---|---|---|---|---|---|
| floc size (mm) | No. (%) | Cum. % | No. (%) | Cum. % | No. (%) | Cum. % |
| 0.2 | 58.0 | 58.0 | 75.7 | 75.7 | 71.8 | 71.8 |
| 0.4 | 29.7 | 87.7 | 17.5 | 93.2 | 19.8 | 91.6 |
| 0.6 | 2.9 | 90.6 | 3.2 | 96.4 | 2.4 | 94.0 |
| 0.8 | 0.7 | 91.3 | 0.5 | 96.9 | 0.3 | 94.3 |
| 1.0 | 0.0 | 91.3 | 0.0 | 96.9 | 1.1 | 95.4 |
| 1.2 | 2.2 | 93.5 | 0.5 | 97.4 | 1.9 | 97.3 |
| 1.4 | 2.2 | 95.7 | 0.0 | 97.4 | 0.3 | 97.6 |
| 1.6 | 0.7 | 96.4 | 0.5 | 97.9 | 0.5 | 98.1 |
| 1.8 | 0.7 | 97.1 | 0.0 | 97.9 | 0.3 | 98.4 |
| 2.0 | 2.2 | 99.3 | 0.0 | 97.9 | 1.4 | 99.9 |
| 2.2 | 0.0 | 99.3 | 1.1 | 99.0 | 0.3 | 100.1 |
| 2.4 | 0.7 | 100.0 | 0.0 | 99.0 | | |
| 2.6 | | | 0.0 | 99.0 | | |
| 2.8 | | | 1.1 | 100.1 | | |
| | $\bar{x}$ = 0.400 | | $\bar{x}$ = 0.314 | | $\bar{x}$ = 0.336 | |
| | $\sigma$ = 0.414 | | $\sigma$ = 0.368 | | $\sigma$ = 0.321 | |

TABLE 14

Rotating cylinder experiments - size distributions obtained after floc formation at 80 rpm for 5 minutes using spherical beads and crushed glass particles

| floc size (mm) | 5-40 μm beads (%) | % | 5-40 μm glass av. 28 μm (%) | % | 0-40 μm glass av. 18 μm (%) | % |
|---|---|---|---|---|---|---|
| 0.4 | 6.3 | 6.3 | 9.8 | 9.8 | 7.0 | 7.0 |
| 0.6 | 12.5 | 18.8 | 12.7 | 22.5 | 6.9 | 13.9 |
| 0.8 | 3.1 | 21.9 | 8.1 | 30.6 | 9.9 | 23.8 |
| 1.0 | 25.0 | 46.9 | 13.5 | 44.1 | 6.2 | 30.0 |
| 1.2 | 9.4 | 56.3 | 15.9 | 60.0 | 12.5 | 42.5 |
| 1.4 | 15.6 | 71.9 | 6.5 | 66.5 | 17.5 | 50.0 |
| 1.6 | 15.6 | 87.5 | 14.1 | 80.6 | 13.8 | 63.8 |
| 1.8 | 9.4 | 96.9 | 6.9 | 87.5 | 8.4 | 72.2 |
| 2.0 | 3.1 | 100 | 8.3 | 95.8 | 11.9 | 84.1 |
| 2.2 | | | 4.3 | 100.1 | 5.3 | 89.4 |
| 2.4 | | | | | 6.7 | 96.1 |
| 2.6 | | | | | 3.8 | 99.9 |
| | $\bar{x}$ = 1.188 | | $\bar{x}$ = 1.113 | | $\bar{x}$ = 1.592 | |
| | $\sigma$ = 0.436 | | $\sigma$ = 0.640 | | $\sigma$ = 0.391 | |